

DESIGN OF SMART CONTROLLERS FOR HYBRID ELECTRIC VEHICLES

A THESIS SUBMITTED TO
THE GRADUATE SCHOOL OF NATURAL AND APPLIED SCIENCES
OF
MIDDLE EAST TECHNICAL UNIVERSITY

BY

ETKİN ÖZEN

IN PARTIAL FULFILLMENT OF THE REQUIREMENTS
FOR
THE DEGREE OF MASTER OF SCIENCE
IN
MECHANICAL ENGINEERING

AUGUST 2005

Approval of the Graduate School of Natural and Applied Sciences

Prof. Dr. Canan ÖZGEN
Director

I certify that this thesis satisfies all the requirements as a thesis for the degree of Master of Science.

Prof. Dr. Kemal İDER
Head of Department

This is to certify that we have read this thesis and that in our opinion it is fully adequate, in scope and quality, as a thesis for the degree of Master of Science.

Asst. Prof. Dr. Melik DÖLEN
Supervisor

Examining Committee Members

Prof. Dr. Y. Samim ÜNLÜSOY (METU, ME) _____

Asst. Prof. Dr. Melik DÖLEN (METU, ME) _____

Prof. Dr. Mehmet ÇALIŞKAN (METU, ME) _____

Asst. Prof. Dr. Buğra KOKU (METU, ME) _____

Asst. Prof. Dr. Ahmet HAVA (METU,EE) _____

I hereby declare that all information in this document has been obtained and presented in accordance with academic rules and ethical conduct. I also declare that, as required by these rules and conduct, I have fully cited and referenced all material and results that are not original to this work.

Name, Last name : Etkin ÖZEN

Signature :

ABSTRACT

DESIGN OF SMART CONTROLLERS FOR HYBRID ELECTRIC VEHICLES

Özen, Etkin

M.S., Department of Mechanical Engineering

Supervisor: Asst. Prof. Dr. Melik DÖLEN

August 2005, 203 pages

This thesis focuses on the feasibility of designing a commercial hybrid electric vehicle (HEV). In this work, relevant system models are developed for the vehicle including powertrain, braking system, electrical machines and battery. Based on these models ten different HEV configurations are assembled for detailed assessment of fuel consumption. This thesis also proposes a smart power management strategy which could be applied to any kind of HEV configuration. The suggested expert system deals with the external information about the driving conditions and modes of the driver as well as the internal states of the internal combustion engine efficiency and the state of charge of the battery, and decides on the power distribution between two different power supplies based on the predefined algorithms. The study illustrates the characteristics of the powertrain components for various HEV configurations. The work also shows the power flow of HEV configurations with the developed smart power management system and therefore, the effectiveness of power management strategies has been evaluated in detail.

Keywords: Hybrid Electric Vehicles, Vehicle Architectures, Power Management, Smart Controllers.

ÖZ

MELEZ ELEKTRİKLİ TAŞITLAR İÇİN AKILLI DENETLEYİCİLERİN TASARIMI

Özen, Etkin

Yüksek Lisans, Makina Mühendisliği Bölümü

Tez Yöneticisi: Yrd. Doç. Dr. Melik DÖLEN

Ağustos 2005, 203 sayfa

Bu tez çalışması, ticari melez elektrikli taşıt (MET) tasarımının uygulanabilirliğine odaklanmıştır. Bu çalışmada, taşıtın aktarım organlarını, frenleme sistemini, elektrikli makineleri ve aküyü içeren konu ile ilgili sistem modelleri geliştirilmiştir. Bu modellere dayanarak, on değişik hirit elektrikli taşıt şekli detaylı yakıt tüketimi değerlendirmesi için biraraya getirilmiştir. Ayrıca, bu tez çalışmasında, her türlü melez elektrikli taşıt tasarımına uygulanabilen akıllı bir denetleyici önerilmiştir. Önerilen uzman sistem sürüş şartları ve sürücü kipleri hakkındaki harici bilgilerin yanında içten yanmalı motorun verimliliği ve akünün yüklülük durumu gibi dahili durumlarla ilgilenir ve önceden belirtilmiş algoritmalara dayanarak iki farklı güç kaynağı arasındaki güç dağılımına karar verir. Çalışma, aktarım organlarının kendilerine has özelliklerini değişik MET tasarımları altındaki oluşumlarda görüntülemektedir. Tez ayrıca MET şekillerinin geliştirilen akıllı güç yönetimi sistemi ile güç yönetimini ve tork dağılımını da göstermektedir ki böylece güç yönetim stratejilerinin etkinliğini detaylı olarak değerlendirilmektedir.

Anahtar Kelimeler: Melez Elektrikli Taşıt, Taşıt Tasarımları, Güç Yönetimi, Akıllı Denetleyiciler.

To My Parents

ACKNOWLEDGMENTS

I express sincere appreciation to Asst. Prof. Dr. Melik Dölen for his perfect guidance, endless encouragement and support throughout this thesis. Also, I want to state special thanks to Prof. Dr. Samim Ünlüsoy for his guidance during the study.

I offer sincere thanks for my friends, Cenk E. Kükreler, E.Doruk Özdemir, Serkan Kasapoğlu and M. Ali Pişkin for their support, friendship and moral assistance. We were all in the same vehicle, and I am glad to see that, we all arrived our destination.

I am most grateful to my family for their extraordinary, never ending support, tolerance and understanding.

Finally, I want to thank Ford Otosan Co. and Gate Elektronik Co. for their financial and technical support in this thesis. My special thanks especially go to Mr. Evren Özatay and Dr. Murat Yıldırım for making this project possible. Consequently, I would like to express my gratitude to Prof. Dr. Mustafa İ. Gökler, director of METU-BILTİR Center, for his constant encouragement and guidance in the management of this project.

TABLE OF CONTENTS

PLAGIARISM	iii
ABSTRACT	iv
ÖZ	v
ACKNOWLEDGMENTS	vii
TABLE OF CONTENTS	viii
LIST OF FIGURES	xii
LIST OF TABLES	xvi
LIST OF SYMBOLS	xix
CHAPTERS	
1 INTRODUCTION	1
1.1 Introduction	1
1.2 Objective of this Thesis	4
1.3 Organization	5
2 LITERATURE REVIEW	6
2.1 Introduction	6
2.2 HEV Configurations	7
2.2.1 Series HEV Configuration	7
2.2.1.1 Characteristics of Series HEVs	7
2.2.1.2 Power Flow for Series HEVs	8
2.2.2 Parallel HEV Configuration	10
2.2.2.1 Characteristics of Parallel HEVs	10
2.2.2.2 Power Flow for Parallel HEVs	11
2.2.3 Series-parallel HEV Configuration	12
2.2.3.1 Characteristics of Series-parallel HEVs	12
2.2.3.2 Power Flow for Series-parallel HEVs	13
2.2.3.2.1 Power Flow for Engine Heavy Series-parallel HEVs	13
2.2.3.2.2 Power Flow for Electric Heavy Series-parallel HEVs	14

2.2.4	Complex HEV Configuration	15
2.2.4.1	Characteristics of Complex HEVs	15
2.2.4.2	Power Flow for Complex HEVs	16
2.2.5	Schematic Illustration of the HEV Configurations	18
2.3	Power Management Strategies for HEVs	19
2.3.1	Static Optimization Methods.....	20
2.3.1.1	Rule Based Algorithm.....	20
2.3.1.2	Baseline Static Control Strategy	22
2.3.2	Dynamic Optimization Methods	23
2.3.2.1	Dynamic Programming Based Algorithm.....	23
2.3.2.2	The Real-time Control Strategy	25
2.3.3	Fuzzy Logic Algorithm	27
2.4	Dynamic Modeling of HEV Powertrain Systems	29
2.4.1	Internal Combustion Engine Modeling.....	29
2.4.2	Transmission Systems Modeling	34
2.4.2.1	CVT Systems Modeling for HEVs	35
2.4.2.2	Automatic Transmission Systems Modeling for HEVs.....	36
2.4.2.3	Automated Manual Transmission Systems Modeling for HEVs.	36
2.5	Braking Systems Modeling.....	37
2.6	Electrical Systems Modeling.....	38
2.7	Closure	38
3	ELECTRICAL SYSTEMS MODELING	39
3.1	Introduction	39
3.2	Modeling of Electric Machines for HEVs	40
3.2.1	Permanent Magnet Synchronous Machines.....	43
3.3	Motor Drives for HEV Applications.....	45
3.4	Torque Modulation in Electric Machines	45
3.5	Modeling of Batteries for HEVs	48
3.6	Overall Electrical System Model	50
3.7	Closure	51
4	LONGITUDINAL VEHICLE DYNAMICS MODELING.....	52

4.1	Introduction	52
4.2	Vehicle Modeling and the Resistive Forces Acting On the Vehicle.....	53
4.3	Braking Systems Modeling for Hybrid Electric Vehicles.....	56
4.3.1	Braking Systems and Braking Dynamics.....	56
4.3.2	Regenerative Braking.....	61
4.3.2.1	Parallel Braking.....	63
4.3.2.2	Evaluation of the Regenerative Braking System Utilized in the Study	64
4.4.	Closure	68
5	VEHICLE DRIVETRAIN MODELING.....	69
5.1	Introduction.....	69
5.2	Internal Combustion Engine Modeling.....	70
5.2.1	Spark Ignition Engine Modeling.....	70
5.2.1.1	Throttle Characteristics	71
5.2.1.2	Intake Manifold Dynamics.....	73
5.2.1.3	Fuel Film Dynamics.....	74
5.2.1.4	Torque Production Model	75
5.2.1.5	Rotational Dynamics.....	77
5.2.1.6	Modifications on the Model.....	78
5.2.1.7	Evaluation of the Spark Ignition Engine Model	79
5.2.2	Map Based Diesel Engine Modeling.....	83
5.3	Transmission Systems Modeling	87
5.4	Closure	88
6	HYBRID ELECTRIC VEHICLE MODELING.....	89
6.1	Introduction.....	89
6.2	HEV Configurations with Elaborate Physical Models.....	89
6.3	Simplified HEV Model	102
6.4	Simulation Study.....	108
6.4.1	Simulation of HEV Configurations with Elaborate Physical models	109
6.4.1.1	Simulation Study in ECE Cycle.....	109
6.4.1.2	Simulation Results	113

6.4.1	Simulation of HEV Configurations with Simplified Model	119
6.5	Closure	126
7	SMART CONTROLLER DESIGN FOR HEVs	127
7.1	Introduction	127
7.2	HEV Smart Controller Topology	127
7.2.1	High-level Controller Design for HEVs	128
7.2.2	Power Manager	131
7.3	HEV Smart Controller Topology	135
7.4	Closure	149
8	CONCLUSION and FUTURE WORK	151
8.1	Conclusion	151
8.2	Future Work	153
	REFERENCES.....	154
	APPENDICES	
A	SIMULATION RESULTS.....	161
B	ELECTRICAL SYSTEMS MODELING FOR HYBRID ELECTRIC VEHICLES	181
B.1	Electric Machines in HEVs	181
B.1.1	Conventional DC Motors	183
B.1.2	Induction Motors	186
B.1.3	Synchronous Machines.....	190
B.1.3.1	Permanent Magnet Synchronous Machines (Trapezoidal Windings).....	191
B.1.3.2	Permanent Magnet Synchronous Machines (Sinusoidal Windings).....	191
B.2	Motor Drives for HEV Applications	192
B.3	Control of Electrical Machinery	194
B.3.1	Torque Control of DC Machines	194
B.3.2	Torque Control of Induction Machines	196
B.3.3	Torque Control of PMSM with Sinusoidal Windings.....	198
C	DRIVING CYCLES	201

LIST OF FIGURES

Fig. 2.1 Series HEV configuration.....	8
Fig. 2.2 Start-up or normal cruising of series HEVs.....	9
Fig. 2.3 Acceleration or battery charging during cruising of series HEVs.....	9
Fig. 2.4 Regenerative braking of series HEVs.....	9
Fig. 2.5 Parallel HEV configuration.....	10
Fig. 2.6 Start up and acceleration of Parallel HEVs.....	11
Fig. 2.7 Normal cruising of parallel HEVs.....	11
Fig. 2.8 Charging during interrupted cruising of Parallel HEVs.....	12
Fig. 2.9 Series-parallel HEV configuration.	12
Fig. 2.10 Start up of engine heavy series-parallel HEVs.....	13
Fig. 2.11 Normal cruising of engine heavy series-parallel HEVs.....	13
Fig. 2.12 Acceleration of engine heavy series-parallel HEVs.....	14
Fig. 2.13 Battery charging during normal cruising.....	14
Fig. 2.14 Start up of electric heavy series-parallel HEVs.....	15
Fig. 2.15 Normal cruising of electric heavy series-parallel HEVs.....	15
Fig. 2.16 Acceleration of electric heavy series-parallel HEVs.....	15
Fig. 2.17 Battery charging during normal cruising.....	15
Fig. 2.18 Complex HEV configuration.....	16
Fig. 2.19 Start up of complex HEVs.....	17
Fig. 2.20 Acceleration of complex HEVs.	17
Fig. 2.21 Normal driving and battery charging during cruising.....	17
Fig. 2.22 Interrupted cruising.....	17
Fig. 2.23 HEV configurations to be simulated.....	18
Fig. 2.24 Rule based power management [9].....	20
Fig. 2.25 BCS for high SOC [10].....	22
Fig. 2.26 BCS for low SOC [10].....	22
Fig. 2.27 Six steps of RTCS algorithm [10].....	26

Fig. 2.28 AFR control during intake stroke [19].....	30
Fig. 2.29 Block diagram of three state dynamic SI engine model [23].....	31
Fig. 2.30 Nonlinear mathematical model of ICE with secondary actuators[24]..	32
Fig. 2.31 Block diagram of engine model with F_c control [24].....	33
Fig. 2.32 Block diagram of engine model with θ_c control [24].....	33
Fig. 2.33 Block diagram of engine model with DBW control [24].....	34
Fig. 3.1 Block diagram of PMSM drive utilized in the current study.....	44
Fig. 3.2 Motor drive topology for HEVs.	45
Fig. 3.3 Torque modulation model for electrical machinery.....	46
Fig. 3.4 Torque-speed characteristics of electric motors.....	47
Fig. 3.5 Ideal battery block.....	49
Fig. 3.6 Electrical systems model used in the thesis.....	51
Fig. 4.1 Vehicle model with dynamic forces.....	53
Fig. 4.2 Simulink model of longitudinal vehicle dynamics.....	55
Fig. 4.3 Simulink model of resistant forces acting on the vehicle.....	55
Fig. 4.4 Resistance forces acting in urban cruising cycle.....	56
Fig. 4.5 Forces acting on a vehicle while braking.....	58
Fig. 4.6 Ideal braking forces proportioning.....	60
Fig. 4.7 Braking characteristics of C-3 in highway cycle.....	64
Fig. 4.8 Parallel braking of C-3 in highway cycle.....	65
Fig. 4.9 Braking characteristics of C-3 in EUDC cycle.....	66
Fig. 4.10 Parallel braking of C-3 in EUDC cycle.....	66
Fig. 4.11 Braking characteristics of P-4 in EUDC cycle.....	67
Fig. 4.12 Parallel braking of P-4 in EUDC cycle.....	67
Fig. 5.1 Spark ignition engine model.....	71
Fig. 5.2 Throttle Characteristics Subsystem in SI engine model.....	71
Fig. 5.3 Intake Manifold Dynamics Subsystem in SI engine model.....	73
Fig. 5.4 Fuel Film Dynamics Subsystem in SI engine model.....	74
Fig. 5.5 Torque Production Subsystem in SI engine model.....	76
Fig. 5.6 Rotational Dynamics Subsystem in SI engine model.....	77
Fig. 5.7 Vehicle speed characteristics in urban cruising cycle.....	79

Fig. 5.8 Air mass flow rate through throttle in urban cruising cycle.....	80
Fig. 5.9 Manifold pressure change in urban cruising cycle.....	80
Fig. 5.10 Air mass-flow rate into the manifold in urban cruising cycle.....	80
Fig. 5.11 Injected fuel rate in urban cruising cycle.....	81
Fig. 5.12 Change in the Lambda value in urban cruising cycle.....	81
Fig. 5.13 Friction torque in SI engine in urban cruising cycle.....	82
Fig 5.14 Engine speed variation in urban cruising cycle.....	82
Fig. 5.15 Diesel Engine Fuel Map supplied by Ford Otosan Co.....	83
Fig. 5.16 Specific Fuel Consumption Map of 1.8 [l], 75[PS], 175[Nm] diesel engine.....	84
Fig. 5.17 Desired engine operation regions of specific fuel consumption map...	84
Fig. 5.18 Vehicle speed characteristics of the urban cruising mode.....	85
Fig. 5.19 Injected fuel rate of the diesel engine.....	86
Fig. 5.20 Engine speed variation in the simulation.....	86
Fig 6.1 Simulink diagram of the conventional vehicle.....	91
Fig 6.2 Simulink diagram of the HEV configuration P-1.....	92
Fig 6.3 Simulink diagram of the HEV configuration P-2.....	93
Fig 6.4 Simulink diagram of the HEV configuration P-3.....	94
Fig 6.5 Simulink diagram of the HEV configuration P-4.....	95
Fig 6.6 Simulink diagram of the HEV configuration SP-1.....	96
Fig 6.7 Simulink diagram of the HEV configuration SP-2.....	97
Fig 6.8 Simulink diagram of the HEV configuration SP-3.....	98
Fig 6.9 Simulink diagram of the HEV configuration C-1.....	99
Fig 6.10 Simulink diagram of the HEV configuration C-2.....	100
Fig 6.11 Simulink diagram of the HEV configuration C-3.....	101
Fig 6.12 Generalized Vehicle Model.....	102
Fig. 6.13 Front axle of the generalized HEV (EM is behind the gearbox).....	103
Fig. 6.14 Rear axle of the generalized HEV.....	104
Fig. 6.15 Front axle of the generalized HEV (EM is between gearbox-clutch)...	106
Fig. 6.16 Nine Different Operating Modes.....	112
Fig. 6.17 Injected Fuel Rate of EM assisted urban cruising cycle.....	116

Fig. 6.18 Velocity Profile of EM assisted urban cruising cycle.....	116
Fig. 6.19 Engine Speed Variation in EM assisted urban cycle.....	117
Fig. 6.20 Demanded Power of EM in urban cruising cycle.....	117
Fig. 6.21 SOC of the Battery in urban cruising cycle.....	118
Fig. 7.1 Control system architecture for HEVs [12].....	129
Fig 7.2 Smart power management topology.....	130
Fig 7.3 Power Manager Algorithm.....	133
Fig. 7.4 Driving performance of conventional vehicle for urban cruising.....	136
Fig. 7.5 Driving performance of conventional vehicle for highway cruising.....	137
Fig. 7.6 Characteristics of conventional vehicle in EUDC.....	137
Fig. 7.7 Driving performance of configuration C-3 for urban cruising.....	141
Fig. 7.8 Driving performance of configuration C-3 for highway cruising.....	142
Fig. 7.9 Characteristics of configuration C-3 at EUDC.....	142
Fig. 7.10 Fuel consumption of HEV configuration C-3.....	144
Fig. 7.11 Driving performance of configuration P-4 for urban cruising.....	145
Fig. 7.12 Driving performance of configuration P-4 for highway cruising.....	145
Fig. 7.13 Fuel consumption of HEV configuration P-4.....	146
Fig. 7.14 Fuel consumption of HEV configuration P-4.....	147
Fig. B.1 Equivalent circuit of a separately excited DC motor.....	185
Fig. B.2 DC motor configurations.....	186
Fig. B.3 Per-phase equivalent circuit of an induction machine.....	188
Fig. B.4 Motor drive topology for HEVs.....	193
Fig. B.5 Typical motor driver topologies.....	193
Fig. B.6 Conventional DC servo motor drive.....	195
Fig. B.7 Block diagram of a conventional DC servo-motor drive.....	195
Fig. B.8 Indirect field oriented induction motor drive.....	198
Fig. B.9 Synchronous motor servo drive.....	199
Fig. B.10 Block diagram of a PM synchronous motor drive.....	200
Fig. C.1 ECE 15 Urban Cycle [52].....	201
Fig. C.2 Highway Driving Cycle.....	203
Fig. C.3 Speed of the vehicle in EUDC.....	203

LIST OF TABLES

Table 2.1 Load leveling strategies for a parallel HEV [13].....	28
Table 6.1 Injected Fuel Rate [g/s].....	114
Table 6.2 Fuel Consumption [l/100km].....	114
Table 6.3 State-of-Charge Change [%].....	115
Table 6.4 Critical results obtained in the simulation.....	116
Table 6.5 Power ratings of EMs.....	120
Table 6.6 Critical results related with urban cruising.....	121
Table 6.7 Critical results related with highway cruising.....	122
Table 6.8 Hybrid Ford Connect Evaluation Chart ($w_1 = w_2 = 0.5$ in (6.35)).....	125
Table 6.9 Hybrid Ford Connect Evaluation Chart ($w_1=0.7, w_2=0.3$ in (6.35))....	125
Table 7.1 Power Manager Algorithm for ECE.....	139
Table 7. 2 Power Manager Algorithm for Highway cycle.....	140
Table 7.3 Power Manager Algorithm for EUDC.....	140
Table 7.4 Average Fuel Consumption for the simulated cases.....	148
Table 7.5 Frequency of Utilization in Power Manager Algorithm for C-3 at EUDC.....	149
Table 7.6 Frequency of Utilization in Power Manager Algorithm for P-4 at EUDC.....	149
Table A.1 Urban cruising with EMA for configuration P-1.....	161
Table A.2 Generator mode operation of configuration P-1 for urban cruising....	162
Table A.3 Highway cruising with EMA for configuration P-1.....	162
Table A.4 Generator mode operation of configuration P-1 for highway cruising.....	162
Table A.5 Urban cruising with EMA for configuration P-2.....	163
Table A.6 Generator mode operation of configuration P-2 for urban cruising....	163
Table A.7 Highway cruising with EMA for configuration P-2.....	164
Table A.8 Generator mode operation of config. P-2 for highway cruising.....	164

Table A.9 Urban cruising with EMA for configuration P-3.....	165
Table A.10 Generator mode operation of configuration P-3 for urban cruising.	165
Table A.11 Highway cruising with EMA for configuration P-3.....	166
Table A.12 Generator mode operation of configuration P-3 for highway cruising.....	166
Table A.13 Urban cruising with EMA for configuration SP-1.....	167
Table A.14 Generator mode operation of configuration SP-1 for urban cruising.....	167
Table A.15 Highway cruising with EMA for configuration SP-1.....	168
Table A.16 Generator mode operation of configuration SP-1 for highway cruising.....	168
Table A.17 Urban cruising with EMA for configuration SP-2.....	169
Table A.18 Generator mode operation of configuration SP-2 for urban cruising.....	169
Table A.19 Highway cruising with EMA for configuration SP-2.....	170
Table A.20 Generator mode operation of configuration SP-2 for highway cruising.....	170
Table A.21 Urban cruising with EMA for configuration SP-3.....	171
Table A.22 Generator mode operation of configuration SP-3 for urban cruising.....	171
Table A.23 Highway cruising with EMA for configuration SP-3.....	172
Table A.24 Generator mode operation of configuration SP-3 for highway cruising.....	172
Table A.25 Urban cruising with EMA for configuration C-1.....	173
Table A.26 Generator mode operation of configuration C-1 for urban cruising.	173
Table A.27 Highway cruising with EMA for configuration C-1.....	174
Table A.28 Generator mode operation of configuration C-1 for highway cruising.....	174
Table A.29 Urban cruising with EMA for configuration C-2.....	175
Table A.30 Generator mode operation of configuration C-2 for urban cruising.	175
Table A.31 Highway cruising with EMA for configuration C-2.....	176

Table A.32 Generator mode operation of configuration C-2 for highway cruising.....	176
Table A.33 Urban cruising with EMA for configuration C-3.....	177
Table A.34 Generator mode operation of configuration C-3 for urban cruising.	177
Table A.35 Highway cruising with EMA for configuration C-3.....	178
Table A.36 Generator mode operation of configuration C-3 for highway cruising.....	178
Table A.37 Urban cruising with EMA for configuration P-4.....	179
Table A.38 Generator mode operation of configuration P-4 for urban cruising.	179
Table A.39 Highway cruising with EMA for configuration P-4.....	180
Table A.40 Generator mode operation of configuration P-4 for highway cruising.....	180

LIST OF SYMBOLS

a	experimental rolling resistance coefficient
A_f	frontal area of the vehicle
$(A/F)_s$	stoichiometric air-to-fuel ratio
A_{th}	cross-sectional area of throttle opening
b	experimental velocity coefficient
C_d	dimensionless drag coefficient
C_D	discharge coefficient
d	deceleration demand by the driver
f_b	break frequency of the current regulator
F_{br_f}, F_{br_r}	braking forces in the front and rear axles
FC_{min}	best fuel consumption among all HEV configurations
FC_{max}	worst fuel consumption among all HEV configurations
F_{drag}	aerodynamic drag force
F_f	front tractive force
F_g	gradient resistance force
F_r	rear tractive forces
F_{roll}	rolling resistance force
h	center of mass height
i	brake distribution factor
I_{batt}	current drawn from the battery
J_{eff}	effective inertia of the engine
L	wheelbase length
MA	maximum flow rate through a specific throttle
m_{ac}	air charge per stroke

\dot{m}_{ai}	air mass rate in the intake manifold
\dot{m}_{ap}	mass airflow rate out of the intake manifold
\dot{m}_{at}	air-flow rate through the throttle
MBT	optimal spark timing
\dot{m}_{jc}	actual flow rate entering the cylinder
m_{ff}	mass of fuel in the fuel film
\dot{m}_{fi}	injected fuel mass flow rate
\dot{m}_{fv}	mass flow rate of the fuel vapor
N	engine speed [rpm]
P_{CR}	critical pressure
P_{man}	manifold pressure
P_R	of pressure ratio
PRI	the normalized flow
Q_0	total capacity of the battery
R_{int}	effective internal resistance
SOC_{min}	best charge conservation among all HEV configurations
SOC_{max}	worst charge conservation among all HEV configurations
T_{br}	brake torque
TC	normalized flow as a function of the cross-sectional area
T_{dr}^*	desired driving torque
$T_{f/p}$	friction and pumping torque
T_{ic}	ICE torque
$(T_{ind})_{MBT, \lambda_s}$	indicated torque value of an engine at a fixed AFR and spark timing
T_m^*	demanded torque
T_{m_1}, T_{m_2}	electric motor assistance torques
T_{man}	manifold temperature
T_L	load torque exerted by the clutch

T_r	rated torque
v_{air}	cross wind velocity
V_{man}	manifold volume
V_{bstt}	battery voltage
V_{oc}	open circuit voltage
W_f, W_r	Normal loads acting on the front and rear axles

Abbreviations

ABS	anti-lock braking system
AFR	air-to-fuel ratio
CVT	continuously variable transmission
DOHC	dual-over head cam
ECE	european urban cycle
EM	electric motor
EMA	electric motor assistance
EUDC	extra urban driving cycle
ESR	equivalent series resistor
EV	electric vehicle
HEV	hybrid electric vehicle
ICE	Internal combustion engines
PMSM	permanent magnet synchronous machines
SOC	state of charge
ZEV	Zero emission vehicle

Greek Symbols

α	throttle angle
β	brake pedal angle
γ	clutch pedal angle
η_{con}	overall efficiency of the power converter
η_{conv}	efficiency of the DC-DC power converter
$\eta_{\Delta SA}$	spark timing efficiency
η_{vol}	volumetric efficiency of the ICE
θ	gradient angle
μ	adhesion coefficient
ρ	air density
τ_f	fuel evaporation time constant
ϕ_c	equivalence ratio
ω_{ic}	crank shaft speed
ω_r	Rated angular speed
ω_p	Maximum angular speed
ω_m	motor velocity
ω_e	rotational speed of the disc at the engine side.
ω_o	rotational speed of the disc at the engine side.

CHAPTER 1

INTRODUCTION

1.1 Introduction

Automobiles are the integral part of daily life as it provides freedom of mobility. Unfortunately, they consume nonrenewable resources of our planet and are one of the major sources for pollution and contamination of environment. Until encountering an oil crisis, the dependence of modern lives on fossil fuel such as petroleum will carry on unless alternative transportation ways and energy sources are taken into consideration. Automotive industries' solution to this problem is the **electric vehicles** (EVs), which are zero emission vehicles, and the **hybrid electric vehicles** (HEVs), which emit low amounts of environmentally harmful gases such as CO, CO₂ and NO_x. Especially, technology towards the zero emission vehicles has still great obstacles to be removed and hence, HEVs are more popular in investigation as it offers solutions to the EVs' problems. This thesis study also focuses on the feasibility of a hybridization of a commercial vehicle, namely Ford Tourneo Connect, as the commercial vehicles are widely utilized in daily life and hence, fuel efficiency has greater importance than the private cars. This research will be carried for different possible designs and component sizing via simulation of them in various driving cycles.

Until 1970s, the engineering efforts of the automotive industry were merely focused on the invention and design of faster, more comfortable and more reliable vehicles [1]. However, the considerable increase in the gasoline prices in 1973 due to the oil crisis in the world made the automobile industry realize the dependence on oil as the only source of energy. Therefore, simultaneously improving the acceleration

performance and fuel efficiency has become the main goal in modern automobile powertrain design as stated by Powel et al. [2], “The primary objective of automobile industry is the development of a vehicle for personal mobility with the specified performance criteria, including acceleration, braking, maneuverability, and comfort, all subjects to environmental, energy, safety and cost constraints”. Growing environmental concerns coupled with concerns about the global crude oil supplies speed up the researches aiming at new, fuel-efficient vehicle technologies.

The Public Law enacted by the USA Congress in 1976, the Electric and Hybrid Vehicle Research, Development and Demonstration Act (Public Law 94-113), gave momentum to the researchers on vehicles using alternative powerplant or power sources. EVs were the most researched and developed ones among them. However, due to the limitation of the batteries such as short driving range, high initial cost, long recharging for batteries and sluggish performance, the commercialization of the EVs were hampered dreadfully until 1990s. In 1990, California Air Resources Board (CARB) announced the legislation for **zero emission vehicles** (ZEVs). According to that legislation, by 1998 2% of vehicles of each automotive company, which sells more than 35000 vehicles a year, should be ZEVs (EVs). This legislation was the sign of the concerns about the environmental issues like urban pollution, emissions and global warming.

In the 1990s, the manufacturers of the EVs realized that their significant research and development efforts on ZEV technologies were obstructed by unsuitable, heavy and insufficient battery technologies. A number of automotive industries, especially automobile manufacturers like Toyota, Honda and Nissan, started developing HEVs to overcome the battery and range problem of pure electric vehicles. Hybridization of vehicles was a promising technology when compared with the conventional vehicles and EVs. It has the potential to outperform the barriers hindering the commercialization of electric vehicles with an auxiliary powerplant to drive the vehicle. Rapid refueling of batteries with regenerative braking and in consequence,

possibility of utilizing smaller batteries are the main advantages of hybrid electric vehicles (HEVs) over EVs and conventional vehicles.

Hybrid vehicles have more than one type of powerplant which supplies energy to the vehicle. These propulsion devices studied in hybrids are spark ignition (SI) engines, compression ignition (CI) engines, high output electric motors, fuel cells, gas turbines. The fuel energy is converted to the mechanical energy or electrical energy by coupling an EM to the output shaft of the engine when needed. In case of fuel cell powered vehicles, fuel energy can also be converted directly to electrical energy. Furthermore, the energy storage devices used in the HEVs are batteries, ultra-capacitors and flywheels.

HEVs have the potential of higher energy efficiency and reduced emissions when compared with conventional automobiles with proper design of powertrain components, such as downsizing the internal combustion engines and well-selected power management strategies for the vehicle like absorbing the kinetic energy lost during braking through EM or driving the vehicle with EM at the start-up of the trip where internal combustion engine are highly inefficient. Besides, they are designed to overcome the range limitations inherent in an EV with two distinct energy sources for propulsion. However, before commercialization of the HEVs, some design and implementation problems related with increased complexity has to be overcome as due to the usage of internal combustion engine, the zero emission concept is lost and the added powerplant (e.g. electric motor) increases the complexity in the management of the power/torque available from both sources. This management problem could be divided into two parts, the distribution of energy from the two different power sources and the management of this energy. These two problems could be shortly summarized as; the vehicle should decide how to meet the torque demand of the driver as well as considering the fuel-consumption and how to maintain the battery state of charge in an admissible level over a wide driving range as well as effectively assisting the prime power source.

To conclude, the gains in fuel economy associated with the introduction of HEVs are promising for the automotive industry. However, in order to utilize its benefits, major challenges in HEV design and operation, such as coordinating (managing) multiple energy sources, which are highly dependent on the configuration of drivetrain, components sizing, and other factors that affect the operation of HEVs, must be overcome. This increased complexity is the main drawback of the hybridization of vehicles which could be overcome by development of a proper and efficient control strategy for the usage of the powerplants.

1.2 Objective of this Thesis

The main objective of this thesis is to study both technical and economical feasibility of designing a commercial hybrid electric vehicle suitable for adaptation to a Ford Tourneo Connect. To accomplish that, a detailed simulation study is needed to be conducted with the utilization of proper models for vehicle components such as internal combustion engine, transmission system, braking system, electric motors and battery, etc. In addition this work also focuses on smart power management topology which could be applied to any kind of hybrid electric vehicle (HEV) configuration. The suggested expert system deals with the external information about the driving conditions and modes of the driver as well as the internal circumstances of the internal combustion engine efficiency and the state of charge of the battery. Additionally, it decides on the power flow among two different supplies based on the predefined algorithms.

Simulation of the two selected configurations with different smart power management algorithms will be performed in the urban cycle, highway cycle and mixed cruising cycle, and the results will be compared with each other and the conventional vehicle.

1.3 Organization

Following this introduction, Chapter 2 covers the current state of the Art for the HEVs. The stated HEV configurations with their proper power flow algorithms are discussed before the power management strategies offered for them are taken into consideration. Besides, the modeling of the powertrain components such as internal combustion engine and transmission systems is also evaluated.

Chapter 3 discusses the electrical system modelling in hybrid electric vehicles while Chapter 4 provides a general description of longitudinal vehicle dynamics. Especially, the proposed and developed regenerative braking system model is explained with simulations made for city and highway cycles.

Chapter 5 presents the powertrain models developed for this study. The Simulink models of the HEV configurations are presented in Chapter 6 in detail. The simulation results related with these models are also presented in this section. Apart from the elaborate physical models, simple HEV models are introduced with the simulation the designed configurations.

The designed expert power management system is explained and the key concept of this smart system is illustrated in Chapter 7. Furthermore, the implementation of high-level controller utilizing power distribution algorithms is discussed with the simulations demonstrated for two of the ten HEV configurations on urban and highway driving cycles.

Finally, concluding remarks of this study are summarized in Chapter 9.

CHAPTER 2

LITERATURE SURVEY

2.1. Introduction

In this chapter, various aspects of the hybrid electric vehicles, their components and their control architectures will be focused on and important scientific sources involving the mentioned subjects will be reviewed in order to lay out a background for this study.

Hybrid vehicles are the ones with more than one type of powerplant which supplies energy to the vehicle. These power supplies could be spark ignition engines, diesel/compress-ignition engines, gas turbines, electric motors, fuel-cells, batteries etc. Moreover, **hybrid electric vehicles** (HEVs), which are the main concern of this research, are the ones utilizing the **electric motor** (EM) as the second power plant.

The main reasons for conducting research on HEVs are to improve the fuel efficiency of the vehicles and to decrease the emissions in the urban areas, especially in cities with high population and traffic. Furthermore, the decrease in fuel consumption could be enhanced with proper design of powertrain components, such as downsizing the **internal combustion engines** (ICEs) and applying continuous variable transmission which could be optimized for better fuel consumption performance [3], and well-selected power management strategies for the vehicle like regaining the kinetic energy lost during braking through EM or driving the vehicle with EM at the start-up of the trip where ICE are known to be inefficient, etc. In fact, these power management strategies depending on the characteristics of the prime mover and the auxiliary powerplant used make the major improvement over the

desired performance of the vehicle as the increased complexity of these vehicles with the extra components on the drivetrain prevents the expected outcomes of the individual components to the total efficiency.

In the following sections; the HEV configuration types with their proper power management strategies will be discussed and power management strategies developed for HEVs will be covered in next section. Then, powertrain modeling of HEVs is discussed with two main subsections: ICE modeling and transmission systems modeling, and then regenerative braking systems used in HEVs and their modeling are investigated. Finally, electrical systems applications will be covered briefly.

2.2. HEV Configurations

There are two basic configurations of HEVs depending on the selection of the main propulsion power: series HEV and parallel HEV. However, with the improvements in the vehicle technologies, new HEVs are designed using the combinations of these two basic concepts and extended the classification of HEVs to four: series, parallel, series-parallel and complex. In the following sections, each of these four different configurations will be discussed in detail with their advantages and disadvantages [4] and the corresponding proper power management strategies [5]. At first, series HEV configuration will be covered.

2.2.1. Series HEV Configuration

2.2.1.1. Characteristics of Series HEVs

Among the four different designs, the series HEV configuration is the simplest one due to no mechanical connection between the ICE and the wheels and all the propulsion power comes from the EM while the ICE is only used to produce electricity through a generator. The converted electricity is either used to charge the

battery or to feed the motor directly. Fig 2.1 illustrates the power flow diagram of the mentioned configuration.

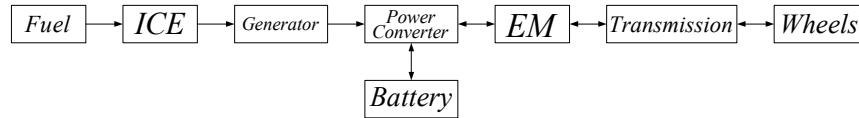


Fig 2.1 Series HEV configuration.

The most important advantage of series HEVs is simplicity of its drivetrain which is due to the absence of the clutches which allows the location of the ICE, generator and battery could flexibly be changed and also the decoupling between the ICE and the wheels permit the ICE to be operated in its most efficient operating region while maximizing fuel efficiency for generating power needed by the EM. Another advantage is its closeness to the zero emission when compared with the other HEV configurations. However, the requirement for a generator is an important disadvantage for this type. Furthermore, the electric motor to be chosen should be able sustain enough power for maximum gradeability, acceleration and highway cruising whereas during the battery selection, the rapid depletion due to high speed cruising and frequent acceleration demands should be taken into consideration as the running down of the battery results in increase in the fuel consumption due to highly usage of ICE during the high-speed cruising. Based upon these advantages and disadvantages, the series HEVs are best suited to low speed “stop-and-go” (interrupted) type driving. Besides, power flow characteristics of the mentioned HEV types are discussed in the following subsection.

2.2.1.2. Power Flow for Series HEVs

As the EM is the primary propulsion element, the vehicle is driven by the EM solely. Start-up and normal driving power flow characteristics is illustrated in Fig 2.2, in which the battery power is transmitted to the wheels via EM. However, ICE is used

as auxiliary power supply via generator for acceleration and battery charging in order to prevent the battery from depleting as seen from Fig 2.3. Also during interrupted driving, the ICE generates power in order to charge the battery.

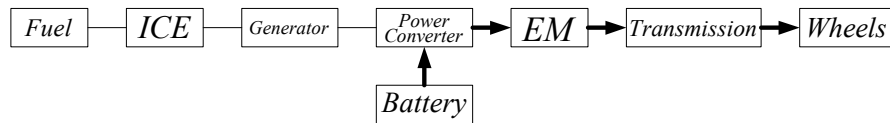


Fig 2.2 Start-up or normal cruising of series HEVs.

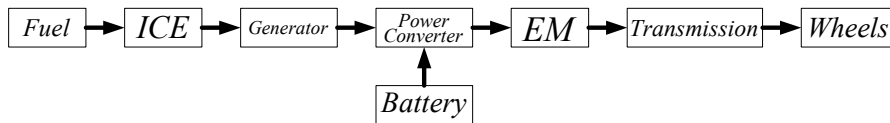


Fig 2.3 Acceleration or battery charging during cruising of series HEVs.

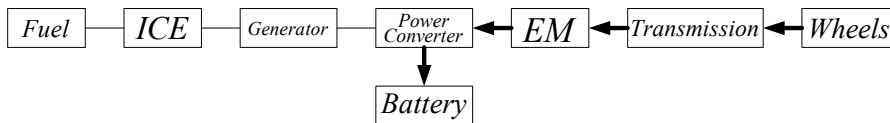


Fig 2.4 Regenerative braking of series HEVs.

As shown in Fig 2.4, during braking the electric motor acts as generator, which is referred to as “regenerative braking”. Therefore, the kinetic energy of the wheels is transformed into battery power through the EM and charges the battery [5].

Second type of the HEVs to be discussed among four different designs is the parallel HEV configuration and next section focuses on general aspects and the power flow characteristics of it.

2.2.2. Parallel HEV Configuration

2.2.2.1. Characteristics of Parallel HEVs

Unlike series HEVs, both power sources (ICE and electric motor) could be utilized for driving the vehicle with the help of two separate clutches which give opportunity of providing the desired power either solely from the prime mover or from both of the available sources. As illustrated in Fig 2.5, ICE and EM have independent connections from each other in order to deliver power to the wheels.

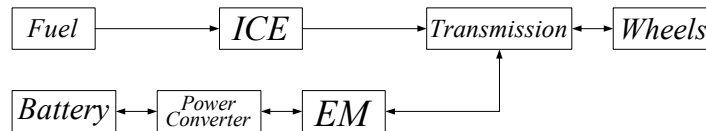


Fig 2.5 Parallel HEV configuration.

Different from the series HEVs, parallel HEVs have two propulsion systems: ICE and EM. The need for a generator is eliminated, which decreases the weight and the cost of the configuration, as the EM could be used for generating power. Also, as a result of the two clutches, both of the power sources could drive the vehicle alone, or together. Hence, both the motor and the engine designed could be smaller in order to get the same performance and according to the design considerations, either the ICE or the electric motor could be the prime mover and the other becomes the auxiliary power source. The disadvantages of a parallel HEV arises due to two different available power supplies which increases the complexity of the design and the necessity of more complex power management strategy, which is very much dependent upon the prime mover being selected and related power flow characteristics is discussed in the next section.

2.2.2.2. Power Flow for Parallel HEVs

Using the advantage of having two different propulsion systems in parallel HEVs, both the ICE and the electric motor provide the demanded power by the driver at the start-up and acceleration of the vehicle. As illustrated in Fig 2.6, energy from fuel tank and the battery is transmitted to the wheels via two separate ways.

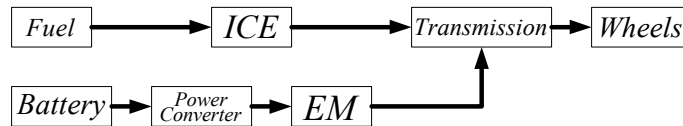


Fig 2.6 Start up or acceleration of parallel HEVs.

During normal cruising, only the selected prime mover is solely utilized for propulsion power and this is typically the ICE for parallel HEVs. In Fig 2.7, the ICE, which is the primary propulsion element, drives the vehicle.

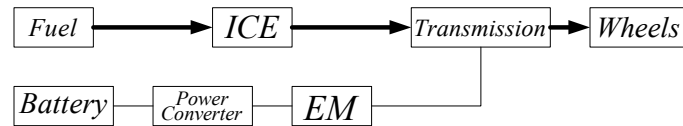


Fig 2.7 Normal cruising of parallel HEVs.

During interrupted cruising (Fig 2.8), ICE charges the battery through the transmission and EM, which eliminates the necessity for an extra component like a generator. As a general aspect of HEVs; at the deceleration or braking, the battery is charged via EM [5].

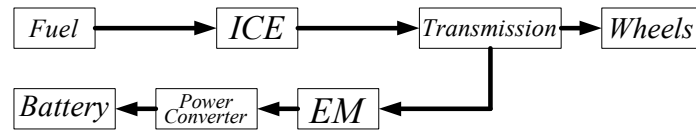


Fig 2.8 Charging during interrupted cruising of parallel HEVs.

Honda Insight uses this kind of power flow strategy with a 995 cc single overhead cam VTEC engine. The vehicle has a max. power of 76 HP at 5.700 [rpm] and a max. torque of 113 [Nm] at 1.500 [rpm] with the assist of an electric motor which produces 10 [kW] at 3000 [rpm]. It has an overall fuel consumption of 3.4 [l/100km] [6].

Third configuration to be mentioned is the series-parallel type of HEVs and the following section covers this kind of design in detail.

2.2.3. Series-parallel HEV Configuration

2.2.3.1. Characteristics of Series-parallel HEVs

Series-parallel HEV configuration is the combination of the features in the previously mentioned two configurations, series and parallel. As can be seen from Fig 2.9, it differs from the series HEVs due to the added power link between the ICE and the transmission. Similarly it deviates from the parallel HEVs significantly owing to the fact that a generator is located between the ICE and the electric motor.

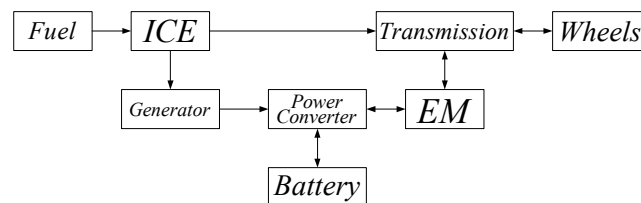


Fig 2.9 Series-parallel HEV configuration.

Although series-parallel HEVs inherit the advantageous features of series and parallel HEVs, increased complexity, weight, and cost are the main drawbacks of this system.

2.2.3.2. Power Flow for Series-parallel HEVs

Since this configuration takes advantage of the useful features of the series and parallel HEVs, it could be classified according to the primary propulsion source, which is heavily used than the other. That is, if the ICE engine is the primary power source, it is referred to as *Engine Heavy Series-Parallel HEV*. Similarly, if the electric motor is more active than the ICE, the resulting configuration is named as *Electric Heavy Series-Parallel HEV*. The following sections discuss the power flow strategies for the vehicles in these two sub-categories.

2.2.3.2.1. Power Flow for Engine Heavy Series-parallel HEVs

In engine heavy series-parallel HEVs, four modes of operation are taken into consideration for the control of power flow. As shown in Fig 2.10, the electric motor acts like the main propulsion source to drive the vehicle as the fuel consumption of the ICE is usually high at the startups. However, during normal driving (Fig 2.11), the ICE propels the vehicle alone at its optimum region for the fuel consumption.

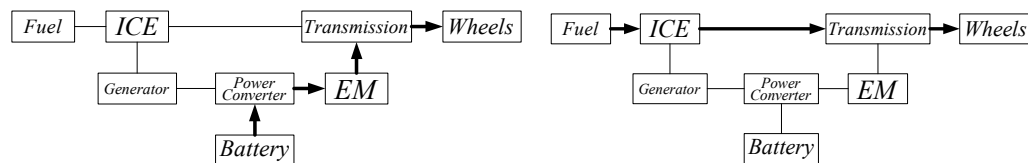


Fig 2.10 Start up of engine heavy series-parallel HEVs.

Fig 2.11 Normal cruising of engine heavy series-parallel HEVs.

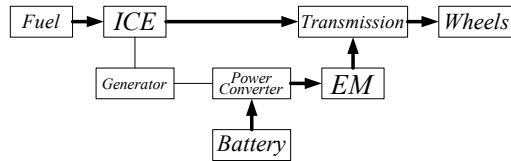


Fig 2.12 Acceleration of engine heavy series-parallel HEVs.

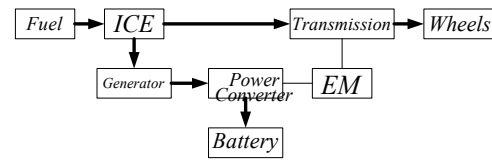


Fig 2.13 Battery charging during normal cruising.

During acceleration (Fig 2.12), the electric motor assists the ICE to supply the driver's demand power. As a unique characteristic of all HEVs, during deceleration EM acts like a generator to charge the battery by regenerative braking. If needed (e.g. the **state-of-charge** (SOC) of the battery goes below a certain level), ICE could charge the battery via generator and drive the vehicle as illustrated in Fig 2.13.

As an example, Nissan's mass-produced hybrid vehicle Tino uses a similar power flow strategy explained above. It constitutes a 1700 [ccm] ICE (74 kW) and a synchronous AC electric motor of 17 [kW] [5].

2.2.3.2.2. Power Flow for Electric Heavy Series-parallel HEVs

In electric heavy series-parallel HEVs, there are also four modes that should be taken into consideration for the control of power flow. At the startup (Fig 2.14), battery is the only propulsion source to drive the vehicle via EM as the fuel consumption of the ICE is high at the startups. During normal driving and acceleration (Figs 2.15-2.16), the ICE and the motor propel the vehicle together. The difference between these two modes is that in acceleration mode, the power coming to the electric motor is not only from fuel tank via generator but also from the battery. However, in normal driving mode fuel is the only energy source for the electric motor.

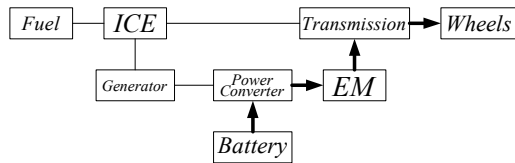


Fig 2.14 Start up of electric heavy series-parallel HEVs.

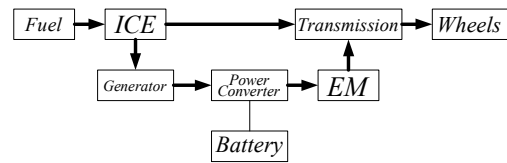


Fig 2.15 Normal cruising of electric heavy series-parallel HEVs.

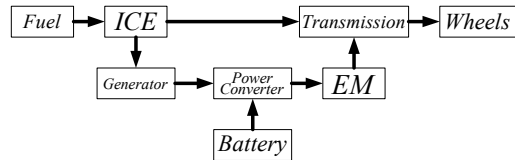


Fig 2.16 Acceleration of electric heavy series-parallel HEVs.

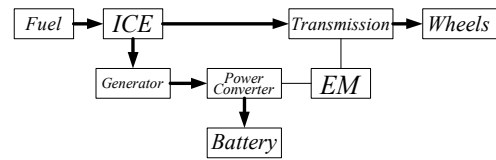


Fig 2.17 Battery charging during normal cruising.

During deceleration, EM acts as a generator in order to charge the battery by regenerative braking. If needed, the ICE could charge the battery via generator and also drive the vehicle.

Toyota Prius (Fig. 24) uses a similar power flow strategy in their hybrid synergy drive system. This system employs a 1497 [ccm] ICE with 76 [HP] at 5000 [rpm] and 50 [kW] permanent magnet AC synchronous motor [7].

Fourth and the last configuration of HEVs will be covered in the next section with the power flow aspects of them.

2.2.4. Complex HEV Configuration

2.2.4.1. Characteristics of Complex HEVs

Complex HEVs, which is illustrated in Fig 2.18, are different from the series-parallel HEVs due to the second electric motor included to the system instead of a generator.

In fact, the system has three propulsion components: two electric motors and an ICE. The motors are placed on to the different axles so as to have dual-axle propulsion.

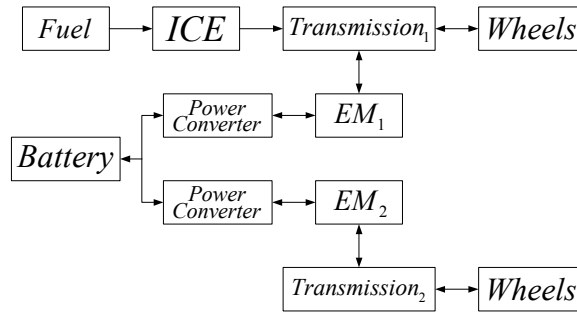


Fig 2.18 Complex HEV configuration.

According to the design considerations, either the ICE or the electric motors could be the prime mover while the others become the assistant power source. The disadvantages of complex HEVs are the increased complexity of the design, weight and the overall cost.

2.2.4.2. Power Flow for Complex HEVs

Complex HEV configuration is actually dual-axle propulsion system, i.e. front wheel axle and rear wheel axle is separately driven. ICE and one of the motors are placed on the front axle (EM_1) while the other motor is at the rear axle (EM_2). There is also no drive shaft connecting the axles which enables greater flexibility for the placement of the HEV components and besides, the drive train is lighter. Two motors enhance the effect of the regenerative braking while decreasing the fuel consumption of the vehicle.

Figures 2.19-2.22 illustrates the four different power flow mode of the corresponding HEV configuration. At the start up mode (Fig 2.19), the electric motors EM_1 and

EM_2 drive the vehicle as ICE has very poor fuel efficiency at the start up. During normal driving, which is shown in Fig 2.21, ICE propels the vehicle and charges the battery via the front motor which is coupled to the same drivetrain shaft as ICE if needed. During acceleration (Fig 2.20), all three propulsion devices are utilized simultaneously.

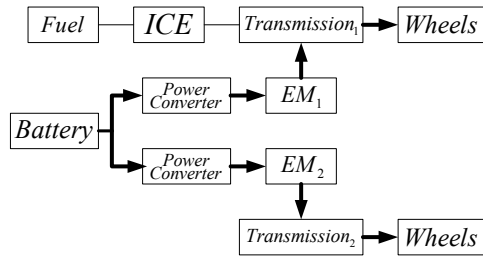


Fig 2.19 Start up of complex HEVs.

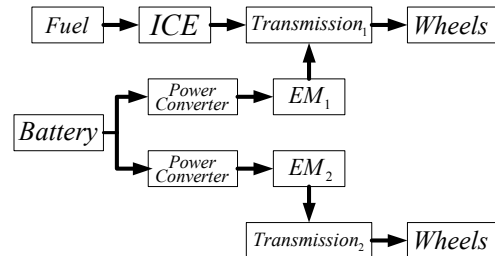


Fig 2.20 Acceleration of complex HEVs.

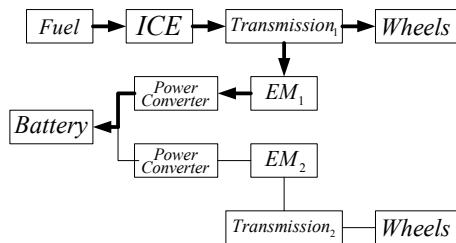


Fig 2.21 Normal driving and battery charging during cruising.

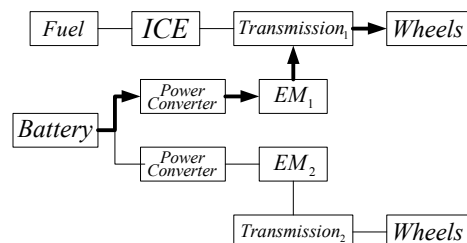


Fig 2.22 Interrupted cruising.

At low-speed cruise in city (Fig 2.22), only the front motor is used to propel the vehicle. At deceleration or braking mode, both electric motors act like generators and the overall efficiency of the regenerative braking increases [5].

GM Precept has adopted a similar power flow control strategy and uses the most aerodynamically efficient design in the world, with a drag coefficient (C_d) of 0.163. Its four-wheel drive, dual-axle features with a 35 [kW] EM at the front axle and a lean-burn compression-ignition direct-injection (CIDI) engine at the rear axle [8].

After covering all of the HEV configurations discussed in the scientific literature, the designs to be taken into consideration throughout the thesis will be stated in the next section.

2.2.5. Schematic Illustration of the HEV Configurations

All of the configurations mentioned before could be expanded into more sub-types by altering the driveline positioning of the HEV components as seen in Fig 2.23.

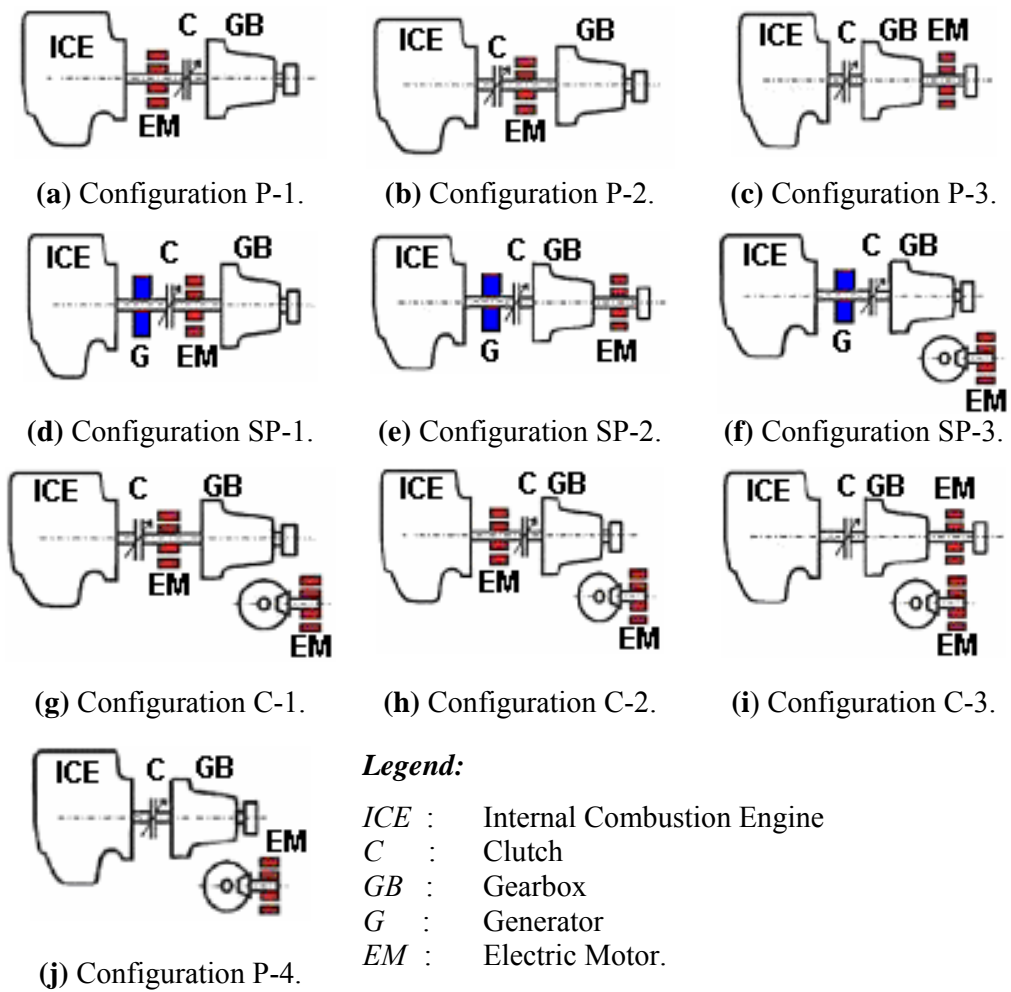


Fig. 2.23 HEV configurations to be simulated.

These ten different designs will be taken into consideration in this thesis study and some of them are adapted from [49]. Notice that, in Fig 2.23, P abbreviates for “Parallel” HEV configuration, whereas SP stands for “Series-Parallel” HEV configuration. For complex HEV designs, C is utilized. The terminology as well as the configurations introduced in this section will be used throughout this thesis.

After covering all of the HEV configurations with their power flow characteristics and the ones to be simulated in the thesis study, following section discusses the power management strategies developed for HEVs.

2.3. Power Management Strategies for HEVs

The HEVs give a tremendous flexibility in order to enhance the fuel consumption values as well as emissions of vehicles by offering four configurations which differ from each other just by the way they propel the vehicle. These main configurations could also be subdivided into more types according to the driveline placement and the power management strategy to be used. The driveline configuration of the HEV components is also an issue of this study which will be discussed in the later sections.

When compared, most of the power management strategies or algorithms for smart controllers developed HEVs could be summarized in three categories [9], namely static/rule based algorithms, dynamic programming strategies and algorithms using fuzzy logic and neural network control techniques. Static optimization methods or rule based algorithms [9-11] are utilizing point-wise optimizations which decide the proper power flow between different propulsion sources according to the optimization made for fuel efficiency and vehicle performance whereas in dynamic programming strategies, the optimizations could be made for dynamic system parameters changing with time [9-12]. Under transient conditions, these dynamic optimizations give more accurate results when compared with the fixed point optimization of steady-state parameters [10]. Finally, algorithms using fuzzy logic

and neural network control strategies are also investigated for HEV applications, however these are rare due to their complex nature and hard implementability to the vehicles [13-15].

At first, static optimization methods will be focused on in the following section with two different approaches: *rule based algorithm* and *baseline static control strategy*.

2.3.1. Static Optimization Methods

2.3.1.1. Rule Based Algorithm

The rule based power management strategy is based on determining the power flow of the HEV configuration depending on the predefined rules according to the component efficiencies and performances under steady-state conditions. As mentioned in reference [9], after interpreting the driver's power demand from the accelerator or brake pedal signals, P_{req} , the power management controller of a parallel HEV configuration decides on the power demand mode and executes the predetermined commands as shown in Fig 2.24 accordingly. These modes are described as follows.

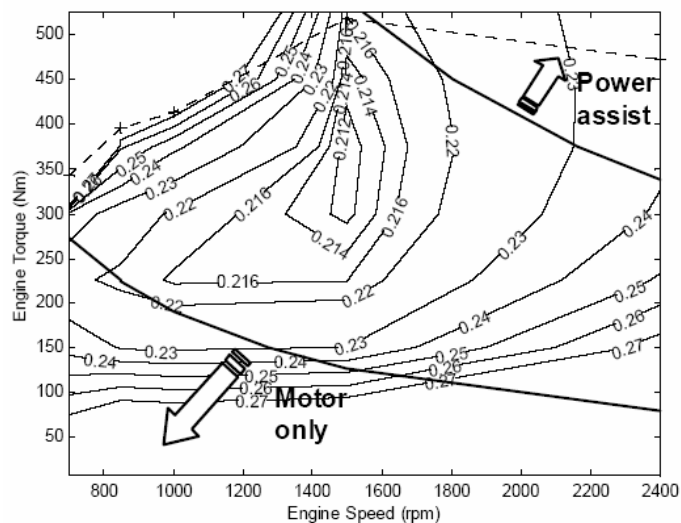


Fig 2.24 Rule based power management [9].

- Normal mode: ICE always runs between motor only region, which is below P_{e_on} , and power assist region, which is above P_{m_a} . These lines define the best efficiency region for the ICE and hence, EM is utilized for auxiliary power supply beyond P_{m_a} line and within motor only region EM is the only propulsion power. The algorithm rules could be summarized as:

$$\text{if } P_{tot} \leq P_{e_on} \rightarrow P_e = 0, P_m = P_{tot} \quad (2.1)$$

$$\text{if } P_{e_on} < P_{tot} \leq P_{m_a} \rightarrow P_e = P_{tot}, P_m = 0 \quad (2.2)$$

$$\text{if } P_{m_a} < P_{tot} \leq P_{m_a} + P_{m_max} \rightarrow P_e = P_{m_a}, P_m = P_{tot} - P_{m_a} \quad (2.3)$$

$$\text{if } P_{tot} > P_{m_a} + P_{m_max} \rightarrow P_e = P_{tot} - P_{m_max}, P_m = P_{m_max} \quad (2.4)$$

- Charging mode: When SOC drops below the SOC_{min} , the power management controller will switch to the charging mode which aims to keep the battery SOC within upper and lower bounds. In order to charge the battery while achieving the performance demanded by the driver, a predefined power, P_{ch} , is added to the driver power request, P_{req} , and this added power is converted by EM for the battery SOC. The algorithm rules of this mode are as follows:

$$\text{if } P_{tot} \leq P_{e_on} \rightarrow P_e = 0, P_m = P_{req} \quad (2.5)$$

$$\text{if } P_{e_on} < P_{tot} \leq P_{e_max} \rightarrow P_e = P_{tot}, P_m = -P_{ch} \quad (2.6)$$

$$\text{if } P_{tot} > P_{e_max} \rightarrow P_e = P_{e_max}, P_m = P_{req} - P_{e_max} \quad (2.7)$$

- Braking mode: The deceleration or braking demand of the driver is taken as a negative power request ($P_{req} < 0$) and regenerative braking is utilized up to the capacity of the EM or the battery. Parallel braking with friction brakes are employed if the capacity, P_{m_min} , is exceeded.

$$\text{if } P_{req} \geq P_{m_min} \rightarrow P_e = 0, P_m = P_{req}, P_b = 0 \quad (2.8)$$

$$\text{if } P_{req} < P_{m_min} \rightarrow P_e = 0, P_m = P_{m_min}, P_b = P_{req} - P_{m_min} \quad (2.9)$$

2.3.1.2. Baseline Static Control Strategy

The **Baseline static control strategy (BCS)** stated in reference [10] is also a static optimization technique which aims to minimize fuel consumption and keep the SOC of the battery between the desired limits by switching between the predetermined modes of vehicle operation without concerning the emissions or the EM torque variations due to battery SOC change. This strategy is also defined for parallel HEV configuration and the ICE is selected as the prime mover whereas EM is utilized for supporting power supply. According to the SOC level of the battery, EM is operated in various ways:

- The EM supplies all demanded torque by the driver below a certain minimum vehicle speed, which is mentioned by electric launch speed in Fig 2.25.

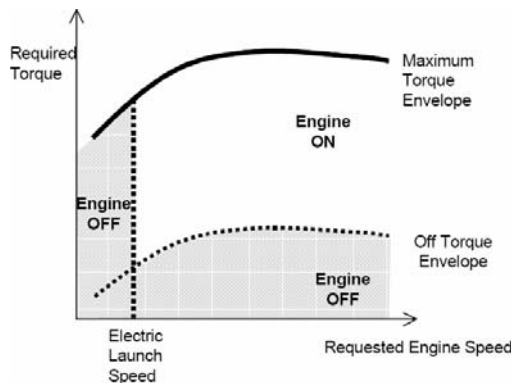


Fig 2.25 BCS for high SOC [10].

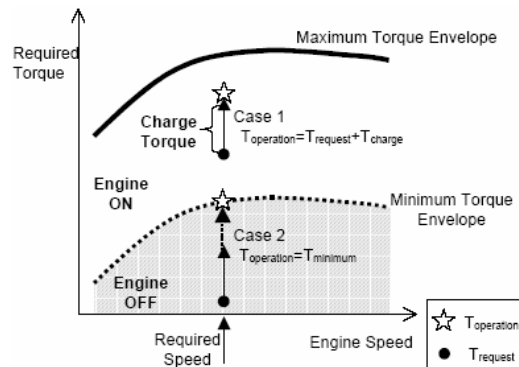


Fig 2.26 BCS for low SOC [10].

- If the required torque exceeds the maximum available ICE torque, which is shown as maximum torque envelope in Fig 2.25, EM is utilized as the supplementary power.
- Regenerative braking is also a responsibility of EM.
- Below the “off torque envelope”, ICE is shut off.

- If the SOC is low, the engine provides the power demanded by the driver and the excess power needed to charge the battery, which is illustrated as Case 1 in Fig 2.26. However, ICE could not produce a torque below the off torque envelope line (Case 2).

These static optimization control strategies based on assisting ICE at predetermined case are commonly used in the HEV power management systems due to their easy application and less computation requirement when compared with other strategies. For instance, Toyota Prius utilizes this basic control strategy of EM assistance when needed and the battery is chosen to be the peak power supply of the vehicle. Hence, EM power is provided exclusively on takeoff and low speeds. As another example, the Honda Insight uses the IC engine as the primary propulsion device while the EM is used to assist the ICE on startup and acceleration.

Dynamic optimization methods which are different from the above mentioned static optimization methods by utilizing time dependent dynamic computations are discussed in the next section with two different algorithms stated in the literature: *dynamic programming based algorithm* and *the real-time control strategy*.

2.3.2. Dynamic Optimization Methods

2.3.2.1. Dynamic Programming Based Algorithm

The dynamic programming based algorithms mentioned in references [9] and [12] usually depend on a model with optimization schemes aiming to minimize a cost function in order to compute the best control strategy. In [9], the cost function to be minimized has the following form:

$$J = fuel [kg] = \sum_{k=0}^{N-1} L(x(k), u(k)) \quad (2.10)$$

where the only term that L function depended upon is the instantaneous fuel consumption rate of the ICE. With the proper inequality constraints, the engine speed, SOC, fuel consumption and motor torque are bounded within predetermined limits and with the equality constraints, the vehicle is guaranteed to follow the specified driving cycle with the suitable speed and acceleration values. Also in reference [12], the aim of the dynamic optimization is to minimize a cost function, whose sum is the fuel consumption of the HEV for a defined driving cycle in order by utilizing a sequence of control achievements for the ICE torque, EM torque, and gear selection of the HEV:

$$\min J = \min_{\{T_{e,k}, T_{m,k}, g_k\}, k=0,1,\dots,N-1} \sum_{k=0}^{N-1} W_{fuel,k} \quad (2.11)$$

where k : time index,

N : is the total number of steps of the driving cycle

$W_{fuel,k}$: the engine fuel flow rate.

The torque balance equation to be satisfied is:

$$T_{wh,k} (T_{e,k} + T_{m,k} \cdot g_k \cdot \omega_{wh,req,k}) + T_{brake,k} = T_{wh,req,k} \quad (2.12)$$

where $T_{wh,k}$: the wheel torque,

$T_{e,k}$: engine torque,

$T_{m,k}$: motor torque,

g_k : the transmission gear number

$T_{brake,k}$: the friction braking torque.

The SOC of the battery is computed as follows:

$$SOC_{k+1} = SOC_k + f(SOC_k, T_{m,k}, \omega_{m,k}) \quad (2.13)$$

With the proper inequality constraints; the engine speed, SOC, fuel consumption and motor torque are bounded within predetermined limits. The augmented cost function to be minimized for fuel efficiency improvement then becomes:

$$\min J = \min_{\{T_{e,k}, shift_k\}, k=0,1,\dots,N-1} \left\{ \sum_{k=0}^{N-1} [W_{fuel,k} + L_k] + G_N \right\} \quad (2.14)$$

where $shift_k$: gear shifting command,

L_k : gear change penalty function,

G_N : SOC terminal penalty.

2.3.2.2. The Real-time Control Strategy

The **real-time control strategy** (RTCS) stated in reference [10] aims to improve the fuel consumption and emission of a parallel HEV by calculating the replacement energy which would restore the battery's SOC to its initial level and optimizing the efficiency with the determination of the ideal operation points of ICE and EM in the entire trip. An overall impact function made up of the weightings of mean fuel consumption value and emission performance is established in order to compute the ideal operation points, which is calculated by minimization of this function. As this function is time dependent, the computation of this operation points are continuous and adjusted according to the driving conditions. In Fig 2.27 six steps of RTCS is outlined briefly.

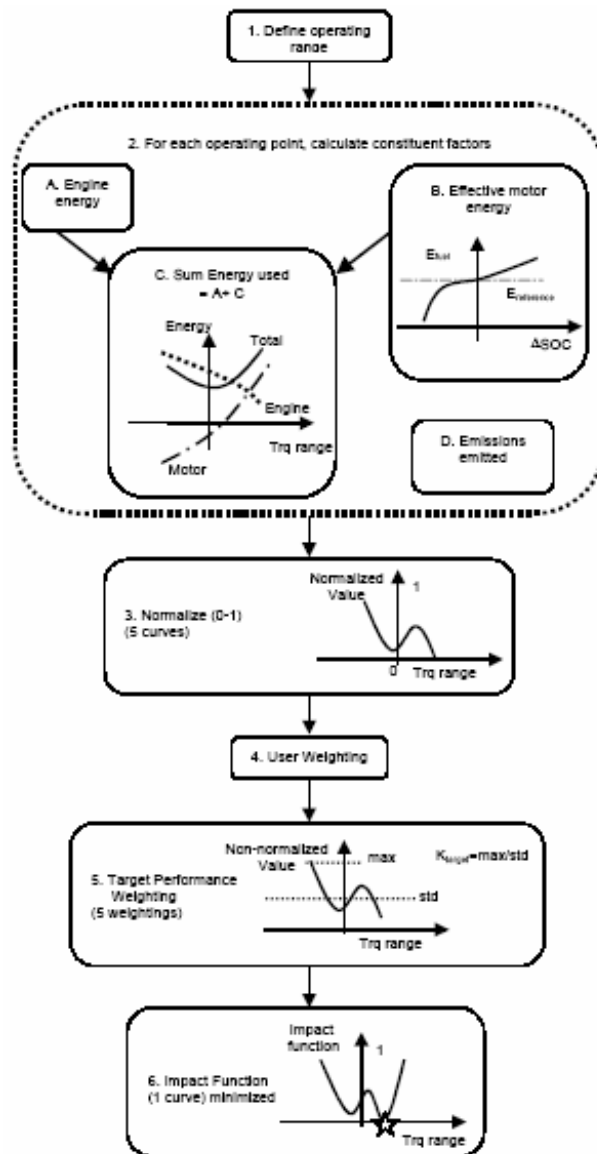


Fig 2.27 Six steps of RTCS algorithm [10].

In the first step, the range of operating points denoted by the range of acceptable motor torques demanded is defined and after that, for each of the candidate operating points the fuel energy to be consumed by ICE, emissions and the total energy to be consumed by the vehicle is computed. In the third step, these computed factors are normalized before the user weightings and target performance weightings are

applied. As the final step, overall impact function is computed for the operating point of that time step.

Finally, fuzzy logic algorithm, which is the third way of power management in the HEVs, is focused on in the following section.

2.3.3. Fuzzy Logic Algorithm

The intention of using rules/fuzzy logic control technique for HEV power management is to utilize the concept of “load-leveling”, which attempts to run the irreversible energy machines like ICE only in an efficient region while compensating the power demanded from the reversible energy device, i.e. EM is used for leveling the load [12]. Due to the unknown nature of future power demand, a charge sustaining strategy is also needed to keep the SOC level between preset bounds [11].

A **fuzzy logic controller** (FLC) application is presented in reference [13] in order to display the potential of an advanced operation strategy for HEVs. The targeted advanced controller utilizes the EM in a parallel HEV to force the ICE to operate at or near its peak point of efficiency or at or near its best fuel economy. In the reference, two control strategies, which optimize the efficiency of the ICE and the fuel consumption respectively, are investigated. Efficient load leveling in an HEV where the ICE is the prime mover aims to move the actual operating point of the ICE as close to the point of best efficiency for every time step in the driving cycle. The resulting power difference will be leveled by the electrical machine and when the SOC capacity of the battery is filled up to the upper bound, the EM dominates the automobile’s operation.

In reference [13], four different scenarios for locating actual operating point of ICE relative to the best efficiency point which is represented in Table 2.1 are as follows:

Table 2.1 Load leveling strategies for a parallel HEV [13].

CASE	ω_{ICE}	T_{ICE}	$\Delta\alpha$	T_{EM}
I	LOW	LOW	>0	<0
II	LOW	HIGH	<0	>0
III	HIGH	LOW	>0	<0
IV	HIGH	HIGH	<0	>0

where ω_{ICE} : engine speed,

T_{ICE} : engine torque,

$\Delta\alpha$: change in throttle command

T_{EM} : electrical machinery torque

and the above mentioned cases are:

- *Case1*: When engine speed and engine torque output are too low, until the ICE reach the best efficiency point, throttle command is increased while EM is operated as generator in order to maintain the overall powertrain output at a constant level and to prevent undesirable acceleration.
- *Case2*: When engine speed is too low while the engine output torque is too high, the throttle command is decreased to have the ICE approach the point of best efficiency while EM is utilized to adjust for the decrease in the ICE power output and maintain the overall powertrain output at a constant level.
- *Case3*: When engine speed is too high while the engine torque is too low, increasing the throttle command make the ICE approach the point of best efficiency and the excessive ICE power output is leveled by EM running as a generator.
- *Case4*: When both engine speed and engine torque outputs are too high, the throttle command is decreased. The EM must operate to compensate for the reduction in ICE power output and maintain the overall powertrain output at a constant level.

After discussing the power management strategies mentioned in the scientific literature, powertrain system modeling of the HEVs are stated in the next section.

2.4. Dynamic Modeling of HEV Powertrain Systems

The drivetrains of HEVs are nonlinear dynamic integrated systems of electrical, mechanical and chemical devices whose primary goal is to supply the needed power for cruising. In order to simulate the performances of these vehicles, their dynamic powertrain components must also be modeled.

2.4.1. Internal Combustion Engine Modeling

Due to more strict environmental regulations, the improvements in the control of ICE performance in transient regions appear to be an important issue and researches are made in order to improve the vehicle emissions and fuel economy by controlling the **air-to-fuel ratio** (AFR) very precisely as deviations from the stoichiometric AFR strongly influence the cylinder air charging process, mixture formation and transient performance of the engine. Utilization of feed-forward controllers parallel to the oxygen sensor is common in most of the conventional engines although the algorithms of them are not suitable for compensation of the external disturbances and deviations of the variables of the engine due to the fact that during design of these control algorithms, steady-state maps of the engines are taken into account by adding relevant open-loop correction terms. Hence, in order to solve these problems, many researches have been achieved on development of control-oriented dynamic engine models and model based control of ICEs [16-18].

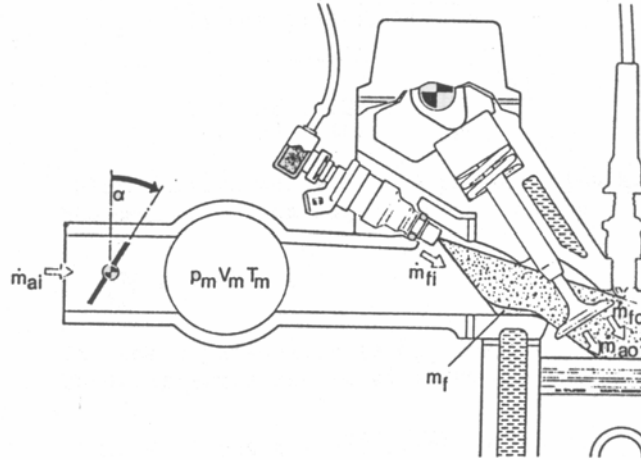


Fig 2.28 AFR control during intake stroke [19].

According to reference [19], in order to reduce tail-pipe emissions using a three-way catalytic converter, the air-to-fuel ratio (AFR) should be controlled very precisely in both steady state and transient engine operations. Therefore, a new fuel injection technique is presented in [19] and founded on a simultaneous control of air and fuel by changing the throttle angle simultaneously via an electronic throttle control and the injection time of the different cylinders.

In reference [20], a nonlinear dynamic model of a port fuel-injected engine is developed which predicts the mean engine brake torque as a function of the engine controls (i.e. throttle angle, spark advance, fuel flow rate, and exhaust gas recirculation (EGR) flow rate).

A very accurate mean value engine models are presented in [21] and [22]. Their accuracy is due to the fact that engine states are defined as mean instead of instantaneous values and mean engine states are the independent variables of nonlinear differential equations the ICE. In [21] engine model developed is based on engine power which is found to be quite different as engine torque is thought to be more acceptable in describing the dynamic engine behaviors. Reference [22] aims to derive a modified manifold pressure state equation which is simpler and more

accurate since this equation can be used to predict the instantaneous mean air mass flow to the cylinders by taking into account of the effect of the filling or emptying of the intake manifold with air during throttle opening or closing.

The study in [23] introduces a nonlinear dynamic engine model shown in Fig 2.29 which is valid in very wide SI operations as it covers the engine operation regimes that is away from the stoichiometric AFR and takes the AFR related spark advance into account. The dynamic mathematical model of the spark ignition engine is supported with the test data taken at steady and transient engine regimes.

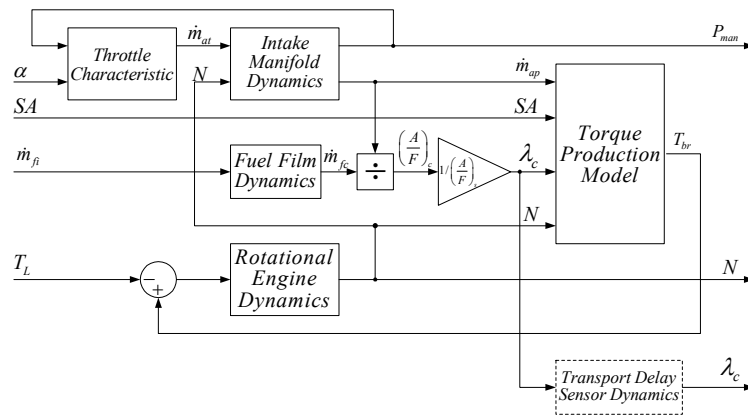


Fig 2.29 Block diagram of three state dynamic SI engine model [23].

The engine model consists of three input variables, which are the throttle angle, fuel flow rate, and spark advance, and utilizes three state variables as intake manifold pressure, engine speed, and fuel mass in the fuel film. The only disturbance on to the ICE is the load torque.

The objective of [24] is to investigate the effects of the secondary actuators at the inlet port of the cylinders used in coordination with the fuel injectors for stringent AFR control and better tracking of demanded torque. The presented nonlinear

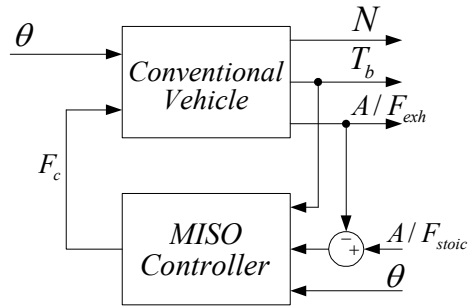


Fig 2.31 Block diagram of engine model with F_c control [24].

- F_c model: The fuel adjustment made by multiple-input, single-output controllers (MISO) is based on AFR, torque, and throttle position measurements. Fuel command is used to minimize AFR deviations caused by the rapid changes in the throttle position, θ , made by the driver during acceleration or deceleration.

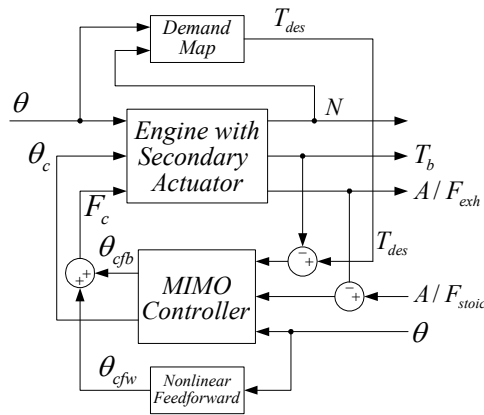


Fig 2.32 Block diagram of engine model with θ_c control [24].

- θ_c model: The fuel adjustment of this model is made by multiple-input, multi-output controllers (MIMO) and also based on AFR, torque, and throttle position measurements. Fuel command and θ_c are calculated derived from

the nonlinear feedforward term and the linear feedback term by the MIMO controller in order to minimize AFR deviations occurred during acceleration or deceleration.

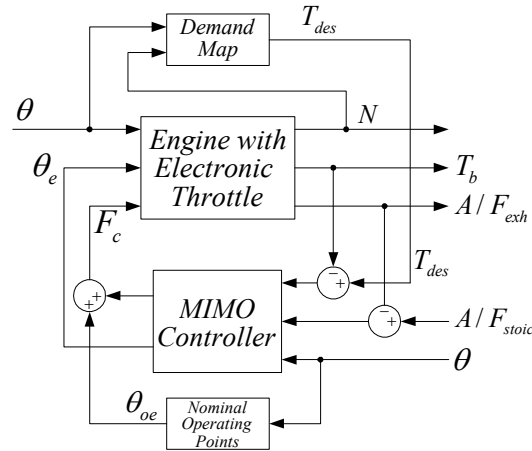


Fig 2.33 Block diagram of engine model with *DBW* control [24]

- *DWB model*: The fuel adjustment of this model is again made by multiple-input, multi-output controllers (MIMO) and also based on AFR, torque, and throttle position measurements. However, in this model, the driver controls the pedal position while the controller regulates the throttle position and the fuel command (F_c) according to the torque demanded by the driver (T_{des}) and AFR computed for best efficiency [24].

After discussing about the internal combustion engine modeling, next section deals with another significant element of the powertrain: *transmission systems*.

2.4.2. Transmission Systems Modeling

Development of HEVs has encouraged the research and development of advanced transmissions which are capable of transmitting torque from two or more power

sources in order to supply the driver demand while decreasing the fuel consumption of the vehicle. For that purpose, different types of transmission systems are investigated: **continuously variable transmission** (CVT), automatic transmission and manual transmission.

2.4.2.1. CVT Systems Modeling for HEVs

Due to providing continuously changing ratio between the power source of the vehicle and its wheels, CVTs promise to improve the performance and drivability of vehicles. Different from the manual and automatic gearbox systems, CVT uses belt or chain systems which alleviate having variable (infinite) gear ratios that are selected according to the power management strategy of improving fuel economy while supplying the demanded power by the driver [3]. However, power limitations of the belts systems used in the CVTs and increased complexity of the control architectures that are needed to be utilized for superior power management are the main problem of utilizing CVT in vehicles. In reference [25], a CVT system with power split design is presented in order to minimize the loading of the belt while increasing the power transmitted through the transmission.

Two new control algorithms are presented in [26] and [27]. In [26], a control system configuration, which determines the CVT ratio from the target drive torque and vehicle speed, is stated. This integrated SI engine/CVT control system is based on the steady-state relationship between the demanded drive torque and the vehicle speed, gear ratio, engine torque and fuel economy. The other research, [27], is on diesel engine integrated with CVT and the control system improvement in order to obtain better acceleration performance while considering the fuel efficiency of the vehicle. Apart from these two studies, [3] deals with the performance optimization of a CVT equipped vehicle without sacrificing from the fuel economy.

Due to its beneficial properties for fuel efficiency and emission reduction, CVT is the first choice of the car companies for their target HEV to be mass produced. Toyota

Prius I, Toyota Prius II, Honda Insight, Honda Civic IMA and Honda Hybrid Accord offer CVT as standard transmission system while some of them has the opportunity of selecting automatic transmission instead of CVT. As mentioned in references [28-31]; with proper control system algorithms, the overall system efficiency could be maximized while meeting the desired performances. Reference [31] presents also another advantage of utilizing CVT for HEVs. Employing CVT in order to operate the engine at its best efficiency range provides achieving the needed driving power with a smaller EM, inverter and battery which helps to decrease the cost of a HEV system applied to medium-to-large vehicles.

2.4.2.2. Automatic Transmission Systems Modeling for HEVs

The quasi-static powertrain model composed of one-dimensional torque formulation including torque and angular velocity transmitted through the engine, the torque converter, automatic transmission gearbox and differential is presented in [32] with the automatic shift logic map, torque converter capacity factor and torque ratio data for the automatic transmission of 1994 Ford Taurus. Moreover, the applications of automatic transmissions to the HEVs are presented in [33] where a novel parallel hybrid electric transmission is described. The developed transmission system is a two degree-of-freedom automatic transmission which could transmit torque from two distinct power sources and thus it could be easily applicable for HEV systems where EM is utilized as an auxiliary power supply.

2.4.2.3. Automated Manual Transmission Systems Modeling for HEVs

Automation of a manual transmission combined with the proper choice of shift points and elimination of the torque converter can improve fuel economy and the driver interaction with the clutch and the gear shift required in standard manual transmission/clutch combination, while providing near automatic transmission performance. Therefore, the driveline efficiency of the conventional powertrain portion of the HEV system can be improved by the inclusion of an automatic manual

transmission/dry clutch driveline combination. However, such combinations of components, with an array of energy and power levels yield a potentially difficult ensemble dynamic control problem, which is the issue of the reference [2]. Also in [34], an automatic transmission is replaced with a five-speed electro-hydraulically controlled manual transmission due to its light design and programmable attribute with programmable logic controller according to the engines best efficiency regions.

One of the main aspects of HEVs is its characteristic regenerative braking system and the following section investigates the modeling of this feature by discussing the frictional braking systems as well.

2.5. Braking Systems Modeling

One of the most important features of HEVs is the regenerative braking ability that could be described as converting the kinetic energy of the vehicle, which is lost while braking, back to the electrical form that could be stored in the batteries via electric motors and inverters. The capability of the bidirectional energy flow of the electric motors makes it possible to recover the dissipated energy as heat on the friction brake pairs and allow the vehicle to drive the vehicle with the regenerated energy later. Hence, the overall fuel efficiency of the vehicle is improved significantly with the utilization of the recaptured energy of the vehicle.

Studies made on regenerative braking of the HEVs are mainly on increasing the effectiveness of regenerative braking by developing proper electronic control algorithms, in [35] and [36], and enhancing the components' efficiencies. For instance, reference [37] investigates the line and pad pressures for the front and rear brakes, capacity of EM utilization as generator mode according to the deceleration demand and a wheel lock-up algorithm in a Matlab/Simulink environment while in [38], three different braking patterns, which are braking with optimal feel, braking with optimal energy recovery and parallel braking, are investigated without changing the braking systems of the conventional vehicles very much. [39] discusses the

demands on the regenerative braking system in which the regenerative braking and the frictional braking is used in tandem and a hybrid heavy truck is simulated on a heavy-braking cycle with different charge acceptance capabilities of the energy store device in order to visualize the demands of the frictional braking system and the regenerative braking one.

2.6. Electrical Systems Modeling

HEVs utilize three types of electrical system components:

- Electrical Machinery
- Battery
- Power Converter.

All of these three elements are well studied in the literature and are comprehensively discussed in [4], [50] and [51]. Hence, it is not going to be repeated here. However, for self-containment, a brief overview of electrical systems is given in Appendix B.

2.7. Closure

In this chapter, brief information about the HEV was given and then the HEV configurations with their proper power management strategies were investigated. Power management strategies investigated for the HEVs were discussed afterwards. Before dealing with detailed mathematical powertrain models in the following chapters, concise survey of powertrain modeling of HEVs was presented. Finally, regenerative braking modeling and electrical systems modeling was covered.

CHAPTER 3

ELECTRICAL SYSTEMS MODELING

3.1 Introduction

The main difference between HEVs and the conventional vehicles is apparently the extra electrical systems added. Although the complexity of the power management and the control of power increases due to the additional electrical machinery, the vital effects on fuel efficiency and reduced emissions makes the electric machines attractive for consumer. Hence, this chapter deals with simple and effective electrical systems models, which are electrical machines and batteries.

In this chapter, the electromechanical components used in power conversion and the batteries will be elaborated. These components include conventional motors/generators as well as their corresponding DC/DC and DC/AC power converters. Once useful models for these elements are presented, the thesis focuses on putting them together to obtain practical electrical system models to simulate conveniently the electromechanical power conversion taking place in the HEV under development.

From the perspective of systems engineering; the above mentioned systems constitute a number of discontinuities. Unfortunately, the detailed mathematical models trying to capture all known physical features of such systems often times lead to numerical instabilities during the simulation phase. To rectify this effect, the simulation-time steps must be reduced dramatically, which in turn increases the computation time by 1000 folds. Note that to assess the dynamic performance of a HEV (acceleration / deceleration, braking, fuel consumption, gas emissions etc.); one

need to take a look at a driving cycle for at least a period of 5 to 30 minutes. Thus, the resulting simulation session, of which employs inherently nonlinear models, would easily result in an extensive computation period of a few hours up to a day on a fast personal computer (PC).

To overcome these stated difficulties, various simplifying assumptions, which are essentially based on the capabilities of modern power conversion systems at the leading-edge of the power electronics technology, have to be made along the way in this study to come up with manageable mathematical models. Hence, in this study, a special emphasis is placed on the fact that no oversimplifications on the developed models are made and that the resulting models do capture accurately the vital attributes of these systems under investigation.

The organization of this chapter of the study is as follows: The first section gives concise information about the electrical machinery utilized in HEVs. The next section discusses the motor drives of HEV applications and then, the brushless DC motor model is presented. A compact modulator model is reviewed in the next section. Finally, the battery model utilized in the simulation study of the HEV configurations is covered.

3.2 Modeling of Electric Machines for HEVs

The electric machines play a critical role in the fuel economy of a HEV. The main functions performed by an electric machine in a typical HEV configuration are propulsion of the vehicle, regenerating energy during braking and improving fuel efficiency of the ICE by boosting or sinking (some portion of) the engine power in order to operate the engine at its peak efficiency.

The overall power conversion efficiency of a generic electric machine (70 % to 90 %) is much higher if compared to that of an internal combustion (e.g. diesel or spark ignition) engine, which ranges in between 10-30 %. Furthermore, an electric

machine operated as a motor can provide full torque at low speeds while its instantaneous power rating can be two or three times the nominal (rated) one. As a key propulsion system element, an electric motor conveniently assists the engine during acceleration- and start-up regime of the vehicle. In such cases, the internal combustion engine (ICE) is known to consume notable amount of extra fuel.

During braking, the kinetic energy of a conventional vehicle is ordinarily wasted over the brakes in terms of heat generated. Thus, the fuel efficiency of such vehicles become poor in the city cruising, where the vehicles have to decelerate to full stop and then to accelerate to resume their course for many times. When used in generator (a.k.a. regenerative braking) mode, the electric machine in a HEV can help recover most of that energy by generating electric energy and then pumping it to the battery pack of the vehicle. Consequently, the overall fuel efficiency of the HEV in the city would be dramatically improved. In city where the average speed of the vehicle is usually less than 30 km/h; the HEV may actually switch off the inefficient ICE and could effectively rely on the electric motor as the prime-mover.

Whether it is a diesel or spark-ignition engine, an ICE, by design, operates at the peak fuel efficiency along a certain trajectory in its operating space (torque vs. speed). If coupled to the engine, the electric machine could be used to operate the engine at its peak efficiency by boosting or sinking (some portion of) the engine power when needed during the operation. Consequently, the fuel efficiency of the HEV can be increased dramatically by 20-50%.

Due to the redundancy in the architecture of a HEV, the electrical machinery could improve the reliability of the vehicle. In case the vehicle is out-of-fuel or the engine malfunctions, the electric machine can be safely used to drive the vehicle to the nearest service station.

At the expense of added complexity and cost; the electric machines make significant contributions to the performance of the HEV that manifest themselves in terms of

improved mileage (fuel efficiency), lowered harmful gas emissions, lower noise, and enhanced reliability. The desired properties of an electric motor within the context of HEV can be summarized as follows [4]:

- Ruggedness and low maintenance
- High torque-to-inertia ratio
- High power-to-weight ratio
- High efficiency
- High maximum torque generation capability at extended periods
- High speed operation
- Extended constant power region
- Low acoustic noise emission
- Low electromagnetic interference (EMI)
- Low cost
- Ease of control and flexibility

Unfortunately, none of the contemporary electrical machinery does possess these listed features all together. Hence, a compromise should be made to select a machinery to satisfy only the most essential properties of a HEV application. Not surprisingly, a wide variety of electric motors/generators are employed in HEV technology including

- Conventional (brush type) DC motors
 - Separately excited DC motor
 - Series DC motors (a.k.a. universal motors)
 - DC shunt motors
 - Compound motors (differential and integral)
- Permanent magnet synchronous motors
 - Trapezoidal winding (a.k.a. brushless DC motor)
 - Sinusoidal winding (a.k.a. AC-servomotor)
- Induction (asynchronous) motors
- Switched reluctance motors.

The detailed information about the working principles and the related mathematical models are presented in reference [4] and [50] for each of these EMs. In the current

study, due to its high efficiency benefits, a brushless DC motor is taken into consideration for the targeted HEV configurations.

3.2.1 Permanent Magnet Synchronous Machines

Synchronous machines are commonly used in servo-drive applications such as computer peripheral equipment, robotics, CNC machine tools, home appliances, medical equipment etc. For low power applications up to a few kW, **permanent magnet synchronous machines** (PMSM) are on their way to replace all conventional DC motors. Synchronous motors with wound rotor field are suitable candidates for some HEV applications.

A PMSM with wound rotor constitutes two windings: rotor and stator windings. The three-phase stator windings of a synchronous machine have a sinusoidal distribution in the stator slots. When the stator is supplied with a set of balanced three phase currents, whose frequency is to be controlled by electronic means; a constant amplitude flux rotating at the synchronous speed is produced in the air gap. On the other hand, the field winding on the rotor produces a field flux. Thus, the torque is produced as an interaction between the magneto-motive-forces created by these two windings. The developed torque is maximized when the magnetic axis of the rotor field and the corresponding axis of the stator field are mutually orthogonal.

The reason behind the popularity of these machines is the simplicity of control. Only six discrete rotor positions per (electrical) revolution are needed in a three-phase machine to lock the phase of stator currents to those of the back EMF voltage waveforms for effective torque modulation. A set of three Hall-effect sensors, which are placed on the stator 120° apart, face the magnet wheel attached onto the rotor. Hence, they provide information on the orientation of the rotor's magnetic field. Thus, the controller excites the stator windings so that both magnetic fields are mutually orthogonal to each other to produce the highest torque possible. Since the motor, which is controlled via this "electronic commutation" scheme, resembles a

conventional DC motor turned inside out, the motor system is also known as brushless DC motor in industry. Note that this control scheme eliminates the need for high-resolution encoder or a position sensor. But, the penalty paid in return is in performance. For HEV applications, a high resolution encoder may be necessary for phase advancing at high speeds.

The PMSM driver, not surprisingly, resembles a conventional DC servomotor system and in Fig 3.1, the EM block developed for the simulation study of the designed HEV configurations is presented.

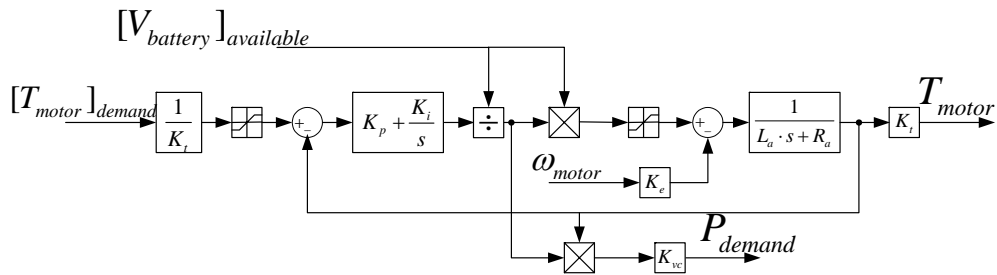


Fig. 3.1 Block diagram of PMSM drive utilized in the current study.

According to the demanded torque from the high-level controller, the voltage needed for that torque is computed and this voltage is compared with the available voltage that the battery could supply at that instant according to its state of the charge value. Finally, the available torque is transmitted to the drivetrain.

After considering the modeling of the electric motors, especially the PMSMs, next section deals with the motor drives applied in the HEVs.

3.3 Motor Drives for HEV Applications

A motor drive consists of a power electronics converter and its controller as illustrated in Fig. 3.2. The converter is composed of fast-acting solid-state switching devices and handles the power flow between the battery and the motor. The digital controller processes the command input and the feedback information to generate the switching signals for the power converter switches.

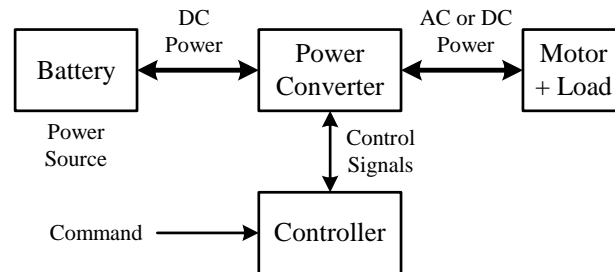


Fig. 3.2 Motor drive topology for HEVs.

A modern power converter often times employs a DC voltage source to generate the power (AC or DC) required by the motor. The solid-state devices in a certain converter topology basically function as on/off electronic switches to convert this fixed DC supply voltage (or so called DC bus voltage) to a variable voltage and variable frequency supply. All switching devices have a control terminal so that they can be turned on and off at will according to the command generated by the controller.

3.4 Torque Modulation in Electric Machines

High bandwidth and accurate current control plays a key role in dynamics of modern electrical motor drives. Such drivers employ a cascaded control strategy to achieve high performance in motion control. Current controlled voltage source inverters are often times utilized in such systems. The bandwidth of a typical current regulator

used is on the order of a few kHz. Furthermore, the modern motor drivers mostly employ vector control techniques to regulate the phase currents of the motors to achieve effective torque modulation. Thus, in torque command mode, the motor along with its driver can be envisioned as a torque modulator as shown in Fig. 3.3.

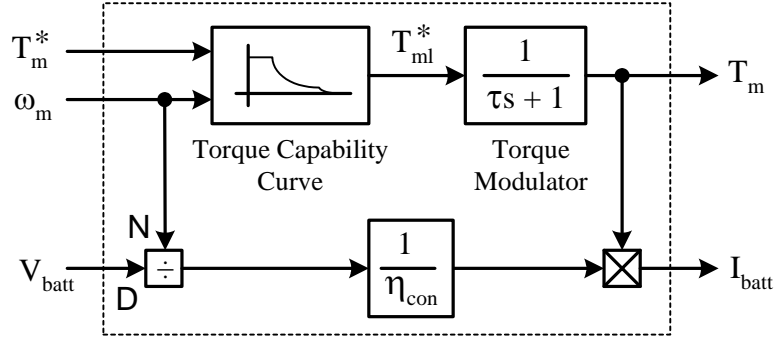


Fig. 3.3 Torque modulation model for electrical machinery.

In this model, the torque modulator is modeled as a first-order linear system with a time constant τ . Assuming that the current regulator dominates the dynamics of the system, one can determine the time constant as

$$\tau = 1 / 2\pi f_b \quad (3.1)$$

where f_b is the break frequency of the current regulator that which ranges between 1 kHz to 5 kHz. On the other hand, the torque generation capability of a particular type of motor has to be taken into consideration so as to model the dynamic behavior of the system accurately. To do that, the motor velocity (ω_m) is used to calculate the upper bound of the torque curve. If the demanded torque (T_m^*) is higher than what the system can generate; the torque command is saturated to the corresponding upper limit.

Note that electric motors/generators have three distinct regions in their torque-curve: **i)** constant torque region; **ii)** constant power region; **iii)** natural mode region. The envelope of the torque speed curve for an electric motor is illustrated in Fig. 3.4. The

motor can deliver the rated torque (T_r) up to its base speed or rated speed (ω_r). Beyond that point, electric motors operate in constant power region where the torque inversely proportional to the speed. Electric motors can operate in high speeds via field weakening in the constant power region. There exists a third region for high speed motors where the torque is inversely proportional to the square of the speed. Note that for most cases, HEV's maximum speed (ω_p) is considered to be at the end of the constant power region [43] and [44].

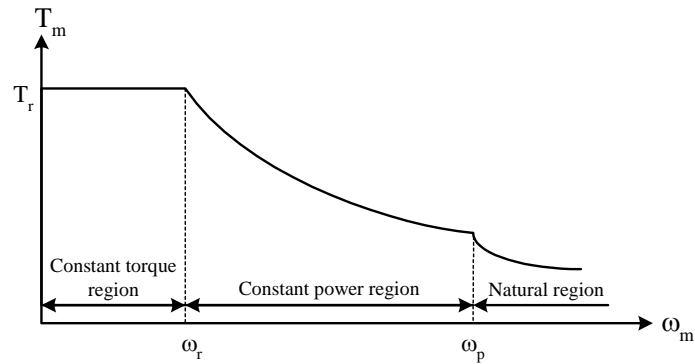


Fig. 3.4 Torque-speed characteristics of electric motors.

For the model given in Fig. 3.3, the envelope of the torque capability curve (T_{max}) is calculated using three non-negative parameters (T_r , ω_r , and ω_p):

$$T_{max} = \begin{cases} T_r, & |\omega_m| \leq \omega_r \\ \frac{T_r \omega_r}{|\omega_m|}, & \omega_r < |\omega_m| \leq \omega_p \\ 0, & else \end{cases} \quad (3.2)$$

Thus, the modified reference of the modulator, T_{ml}^* , becomes

$$T_{ml}^* = \begin{cases} \text{sgn}(T_m^*) T_{max}, & |T_m^*| \geq T_{max} \\ T_m^*, & else \end{cases} \quad (3.3)$$

Note that (3.2) and (3.3) also cover the generator capability regions as well. Once the developed torque is calculated, the current drawn (I_{batt}) from the battery is calculated with the utilization of the output power of the motor:

$$I_{batt} = \frac{T_m \omega_m}{\eta_{con} V_{batt}} \quad (3.4)$$

where η_{con} corresponds to the overall efficiency of the power converter (0.85 – 0.95). For the simplified HEV model, the above mentioned torque modulation model is used for EM applications of the related HEV configurations. The base speed for the selected EMs is taken as 100 [rad/s] while the rated torque values of 8, 12 and 16 [Nm] are selected for the simulation study.

As the modeling of the electrical machines is accomplished, the next section explains the battery model utilized in the thesis study.

3.5 Modeling of Batteries for HEVs

Batteries provide alternative power source for the HEVs. Not surprisingly battery modeling is of major concern in this thesis as the power management strategies must take into account the current SOC at a particular driving regime and should try to conserve the electrical charge throughout that entire driving cycle. Therefore, in the simulation study conducted in this thesis, overall HEV model must incorporate a relatively simple but complete battery model for the purpose of monitoring the SOC accurately.

Electrical energy needed by the EMs is mostly obtained from the batteries by the conversion of the chemical energy stored in the battery. Due to their complex nature (as outlined by [45-47]), the modeling of the batteries is quiet challenging. Therefore, in the simulation study, two different simplified battery models are utilized. The first one is a simplified version of 25 [Ah] with 318 [V] lead-acid battery pack which was presented in ADVISOR [48] and shown in Fig 3.5.

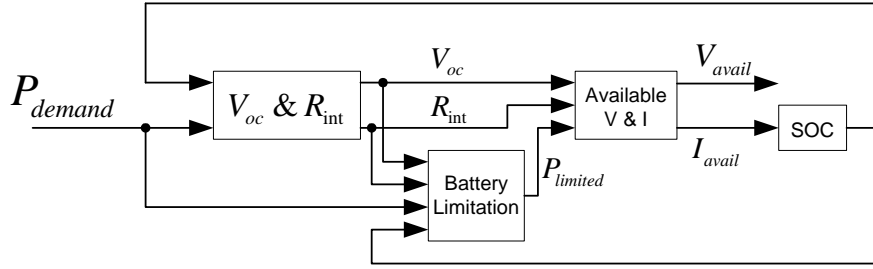


Fig. 3.5 Ideal battery block.

In this model, the battery is assumed ideal, i.e. it has 100% electrical efficiency, and the change in the temperature does not affect the battery performance. In Fig 3.5, the power demand from the EMs is the input to this system. The demanded battery power and the instantaneous SOC are used to calculate the effective internal resistance (R_{int}) and the open circuit voltage (V_{oc}) of the battery. In subsystem labeled “*Battery Limitation*”, maximum available battery power is mainly computed according to its minimum allowable voltage level of the battery. Also, battery is prevented from being overcharged and depleted. The available current and voltage values are calculated and sent as an output of the block. Finally, instantaneous SOC of the battery is computed by integrating the battery current.

A simplified battery model is also utilized in the simulation studies. The model which essentially corresponds to a large capacitor with low **equivalent series resistor** (ESR), is assumed to be charged to a large extent. Hence, the voltage change in the terminal of the battery pack does not change that much while sourcing or sinking the battery current:

$$I_{batt} = \frac{P_{batt}}{V_{batt} \eta_{conv}} \quad (3.5)$$

where η_{conv} is the efficiency of the DC-DC power converter managing the battery current (charge) as well as the DC link voltage. SOC is calculated by using the following expressions:

$$q = \int_0^t I_{batt} \cdot dt \quad (3.6)$$

$$SOC = 1 - \frac{q}{Q_0} \quad (3.7)$$

where Q_0 refers to the total capacity of the ideal battery being used.

3.6 Overall Electrical System Model

The overall electrical system of the HEV considered in this study is illustrated in Fig 3.6. Note that the system is adapted from that of a Toyota Prius hybrid electric vehicle. Here, a number of battery cells are connected in parallel to yield an overall DC voltage of (standard) 42 Volts. The total capacity of the battery pack is assumed to be 1300-Watthours, i.e. Q_0 is $300 \times 3600 = 4.68$ [MJ] (same as the battery pack used in Toyota Prius).

Hence, a DC/DC power converter (buck and boost) enabling bidirectional power flow between its input and output is utilized to boost the voltage from 42 volts to 200 volts. The output of the converter is essentially coupled to DC link capacitor bank for intermediate power storage. Thus, the drive of each electrical machine shares the same DC bus. Note that in this configuration, the drives are to be operated in torque control mode to provide the electromagnetic torque demanded by the high level controller of the hybrid electric vehicle.

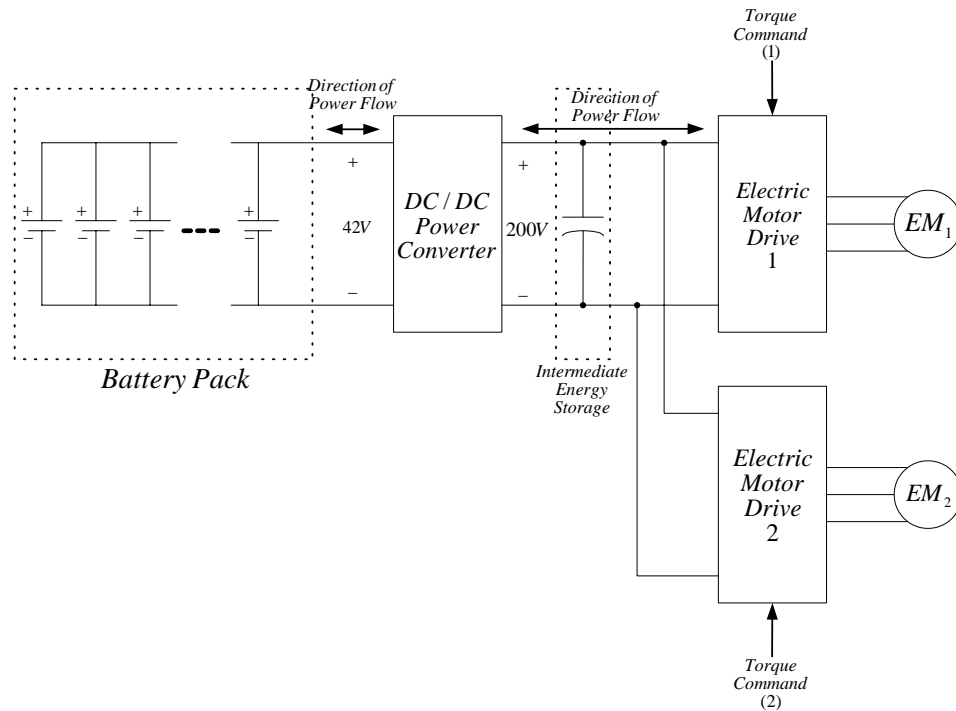


Fig. 3.6 Electrical systems model used in the thesis.

3.7 Closure

Following the introduction of the electrical systems utilized in the HEV applications; the electrical machinery utilized in HEVs and information related to various aspects of these elements was discussed. Due to their broad application field, only permanent magnet synchronous machines were discussed and the block diagram of the relevant EM model used in the simulations was presented. However, a complete discussion of all other electrical system elements was included in the appendix for the sake of self containment of this work. This chapter briefly discussed the torque modulation in the EMs. For the sake of convenience, the motor drives used in the current study could be modeled as ideal torque modulators. The battery model utilized in the HEV configurations was then presented. Consequently, the final section presented a general electrical system model suitable for generic HEV applications.

CHAPTER 4

LONGITUDINAL VEHICLE DYNAMICS MODELING

4.1 Introduction

Resistant forces acting on the vehicle and the braking system have significant effect on the vehicle performance and the fuel efficiency which is the central theme for utilizing hybrid electric vehicles. Hence, in this chapter, a simple but effective single dimensional vehicle model of the target vehicle, Ford Tourneo Connect, is developed for the purpose of assessing the feasibility of the realizing such a hybrid vehicle.

Longitudinal vehicle dynamics is mostly based on Newton's second law of motion. The object (concentrated mass) could accelerate when the resultant force of tractive force and the resistive forces acting on the vehicle on it is nonzero. Therefore, the acceleration of a vehicle depends on force generated by the vehicle's propulsion unit, aerodynamic drag, effective mass of the vehicle and tire-road interactions.

Vehicles are in fact composed of many complex mechanical parts that are distributed over entire vehicle body. For the longitudinal motion studies, assuming the vehicle as a lumped mass concentrated at the mass center (center of gravity) yields reasonable results with tolerable errors while taking into account the vehicle power trains in the longitudinal cruising. Consequently, the vehicle considered in this study is modeled as unit total mass located at the center of mass.

In the following sections, the resistive forces on the vehicle are first investigated. Then, then the braking dynamics of the conventional vehicles are discussed in detail. Since regenerative braking in HEVs plays a key role in regaining the kinetic energy

of the vehicle (during deceleration) which may be otherwise wasted as heat, the regenerative braking systems are elaborated in the next section. Finally, the simulation results of the corresponding regenerative braking system are presented in order to visualize its capabilities.

4.2 Vehicle Modeling and the Resistive Forces Acting On the Vehicle

Rolling resistance force (F_{roll}), aerodynamic drag force (F_{drag}) and gradient resistance force (F_g) are the main resistance forces which are taken into account in this study and are shown in Fig 4.1 with the front and rear tractive forces (F_f & F_r).

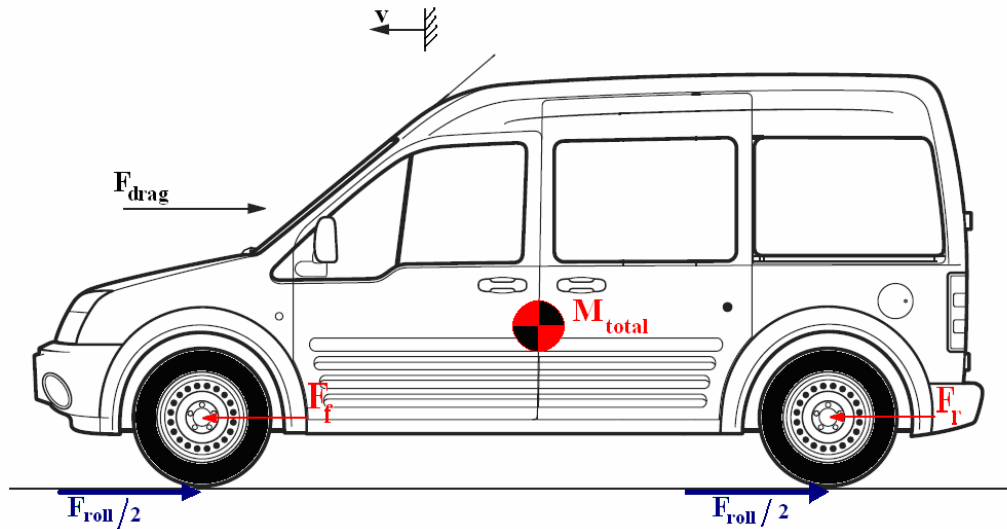


Fig. 4.1 Vehicle model with dynamic forces.

During cruising, the tire deforms due to the tire inflation pressure, vehicle speed, tire type and weight of the vehicle exerted on the tire. Rolling resistance occurs as some part of the energy is dissipated because of this tire-road interaction and the deformation of the tire surface and could be calculated as [40]:

$$F_{roll} = (a + bv)Mg \quad (4.1)$$

where a is the experimental rolling resistance coefficient which depends on the tire inflation pressure, load distributed on the tire and the tire designation and taken as 0.014371, while b is another experimental velocity coefficient with a value of 1.5×10^{-5} for radial type tires.

Aerodynamic drag force, which is mainly due to the normal pressure drag around the vehicle, could be defined as the resistant force exerted on to the vehicle while moving through air and is proportional to the vehicle frontal area, vehicle speed and aerodynamic drag coefficient as follows:

$$F_{drag} = \frac{1}{2} \rho C_d A_f (v + v_{air})^2 \quad (4.2)$$

where C_d is the dimensionless drag coefficient, A_f is the frontal area of the vehicle in m^2 , v_{air} is the cross wind velocity in m/s and ρ is the air density in kg/m^3 .

Gradient resistance force is due to the downward component of the vehicle weight which is parallel to the road during climbing up a gradient. Its effect depends on the inclination of the climb and the vehicle mass as follows:

$$F_g = Mg \sin \theta \quad (4.3)$$

where θ is the gradient angle in radians.

Armed with this information, one can develop a simple, yet effective model for a conventional vehicle. Fig. 4.2 and 4.3 illustrate the block diagram of such a model. These mathematical models are exclusively used in simulations conducted via Simulink.

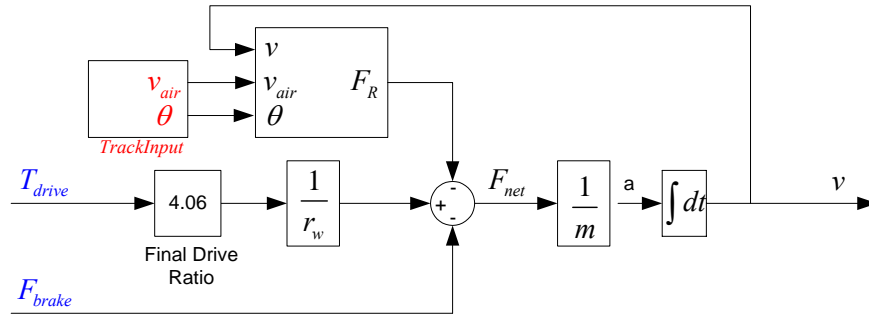


Fig. 4.2 Simulink model of longitudinal vehicle dynamics.

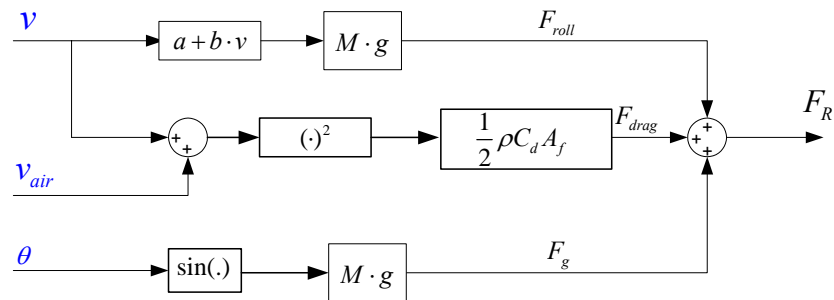


Fig. 4.3 Simulink model of resistant forces acting on the vehicle.

As can be seen from Fig 4.2, the resultant force of resistive forces, traction force and the braking force, which will be elaborated in the following section, leads to the acceleration or the deceleration of the vehicle. Fig 4.4 presents the magnitude of resistance forces acting on the vehicle during cruising in the urban driving cycle. Please refer Appendix C for the details about this standard driving cycle.

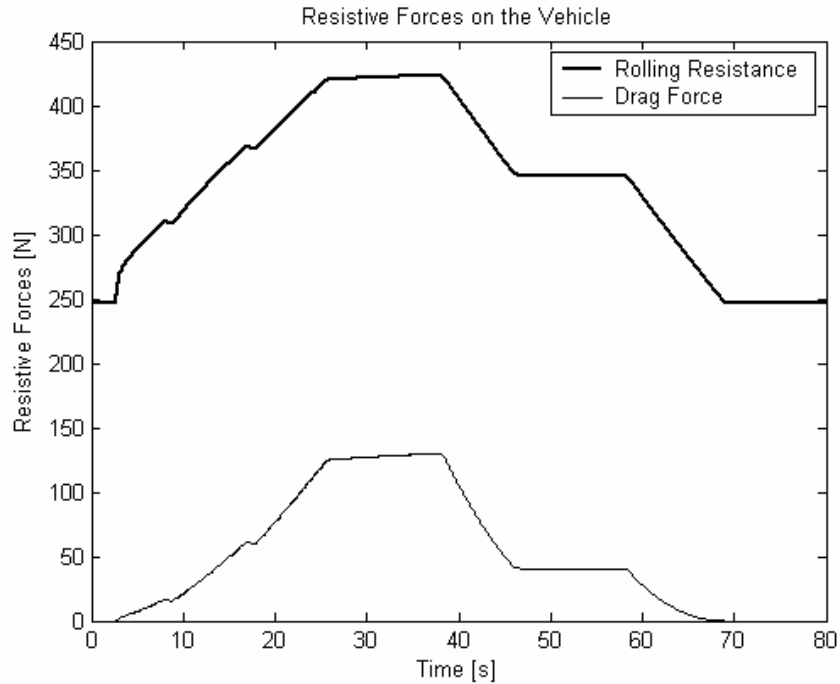


Fig. 4.4 Resistance forces acting in urban cruising cycle.

4.3 Braking Systems Modeling for Hybrid Electric Vehicles

One of the main advantages of the HEVs is the regenerative braking capability, which increases the fuel efficiency of the vehicle by regaining the kinetic energy of the vehicle during braking via electrical power generation. The following sections are related with aspects of the regenerative braking. First, braking systems for conventional vehicles will be discussed.

4.3.1 Braking Systems and Braking Dynamics

The continuous adjustment of the vehicle speed according to the driver's demand and the traffic conditions yielding safe driving is the main issue of the braking system in the vehicles. These speed and distance adjustments could be classified as:

1. Deceleration of a vehicle in a controlled manner or stopping it when necessary.
2. Maintaining a constant speed during downhill driving.
3. Holding a vehicle stationary at a particular spot.

Service brakes fulfill the first and second functions of vehicle braking system while the parking brake, which shares the main components of the service brake, is particularly used to hold the vehicle stationary on a gradient or straight road.

The effectiveness of any braking system depends on the friction, which is between the tire contact patch and the road surface which is actually affected by the road conditions, tire inflation pressure, normal tire load and the tire specification. In order to improve the braking performance and the maneuverability of the vehicles, electronically controlled braking systems are used in the current vehicle applications. For instance, an **anti-lock braking system** (ABS) is an electronic feedback control system which greatly enhances steering control and the stopping distance by controlling the tire-ground contact slip-ratio and, hence, preventing the wheels to be locked completely.

The friction between the tire and road depends on the load exerted to the road through the tire which changes with the deceleration of the vehicle. The vertical loads carried by the front and rear wheels are not equal as a result of the center of mass being away from the midpoint of the vehicle, hence this inequality affects the available tire-road adhesion for each wheel differently. When a vehicle experiences braking, these loads also vary with the deceleration of the vehicle. In order to use the braking system effectively, the braking effort has to be apportioned between the front and rear axles according to the loads being carried by these axles, in Fig 4.5, dynamic effects of braking is shown with the related forces. The maximum braking stability could only be maintained by distributing these braking forces and keeping their values within reasonable limits.

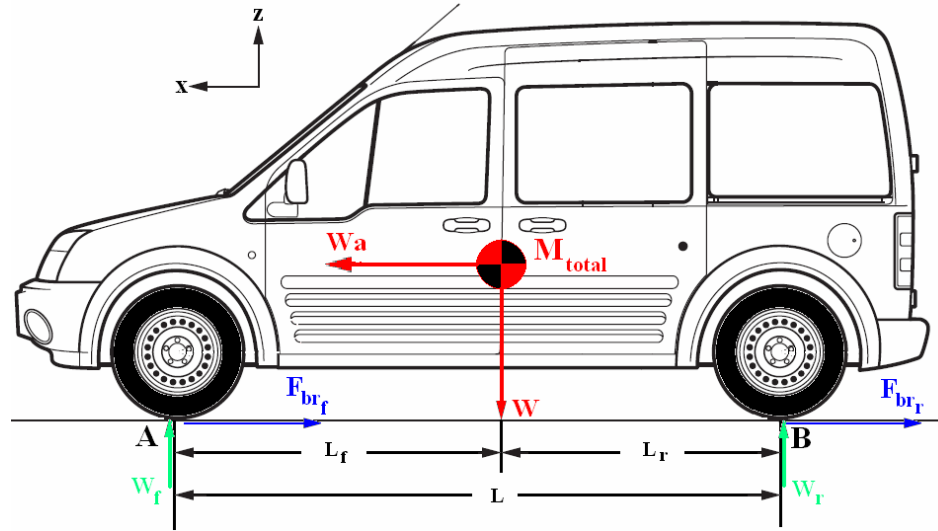


Fig. 4.5 Forces acting on a vehicle while braking.

Normal loads acting on the front and rear axles (W_f and W_r) could be computed by using the balance of forces and moments [40]:

$$W_f = W \left(\frac{L_r}{L} + \frac{h}{L} a \right) \quad (4.4)$$

$$W_r = W \left(\frac{L_f}{L} - \frac{h}{L} a \right) \quad (4.5)$$

- where W: total vehicle weight [kgm/s²],
L: wheelbase length [m],
L_r: distance between the front wheel and the center of mass [m],
L_h: distance between the rear wheel and the center of mass [m],
h: center of mass height [m],
d: deceleration demand by the driver [m/s²],
a: the non dimensional deceleration value.

Here, the non-dimensional deceleration is defined as:

$$a = -\frac{\ddot{x}}{g} = \frac{d}{g} \quad (4.6)$$

As mentioned above, in order to use the braking system effectively, the braking forces (F_{br_f} and F_{br_r}) in the front and rear axles must be in proportion according to the loads being carried by these axles (W_f and W_r). Therefore, a relationship of braking forces governing the maximum deceleration available by utilizing the full adhesion possible between the tires and the road surface ($\mu = \mu_f = \mu_r$) could be verified as:

$$\frac{F_{br_f}}{W} = \left(\frac{L_r + ah}{L_f - ah} \right) \frac{F_{br_r}}{W} \quad (4.7)$$

$$\frac{F_{br_f}}{W} = a - \frac{F_{br_r}}{W} \quad (4.8)$$

By submitting (4.8) into (4.7), ideal brake distribution on the front and the rear axles become:

$$\frac{F_{br_f}}{W} = a \left(\frac{L_r + h d}{L} \right) \quad (4.9)$$

$$\frac{F_{br_r}}{W} = a \left(\frac{L_f - h d}{L} \right) \quad (4.10)$$

If a “brake distribution factor” is defined as the ratio of the front braking force to the total braking force [40]:

$$i = \frac{F_{br_f}}{F_{br_f} + F_{br_r}} = \frac{F_{br_f}}{W a} \quad (4.11)$$

then

$$\frac{F_f}{W} = i a \quad (4.12)$$

$$\frac{F_r}{W} = (1-i) a \quad (4.13)$$

From the (4.12), brake distribution factor for ideal braking could be presented as

$$i = \frac{L_r}{L} + \frac{h}{L} \frac{d}{g} \quad (4.14)$$

The ideal distribution of braking force for the rear and the front axles is shown in Fig 4.6 by a exponential curve for an complex HEV configuration with 2400 kg total mass, and the adhesive capability between the road and the tires could be fully utilized, when the ideal distribution curve is being followed during braking. Changes in load transfer between the front and the rear axles and the changes in the center of mass position of the vehicle necessitate a variable braking distribution factor in order to utilize this ideal braking.

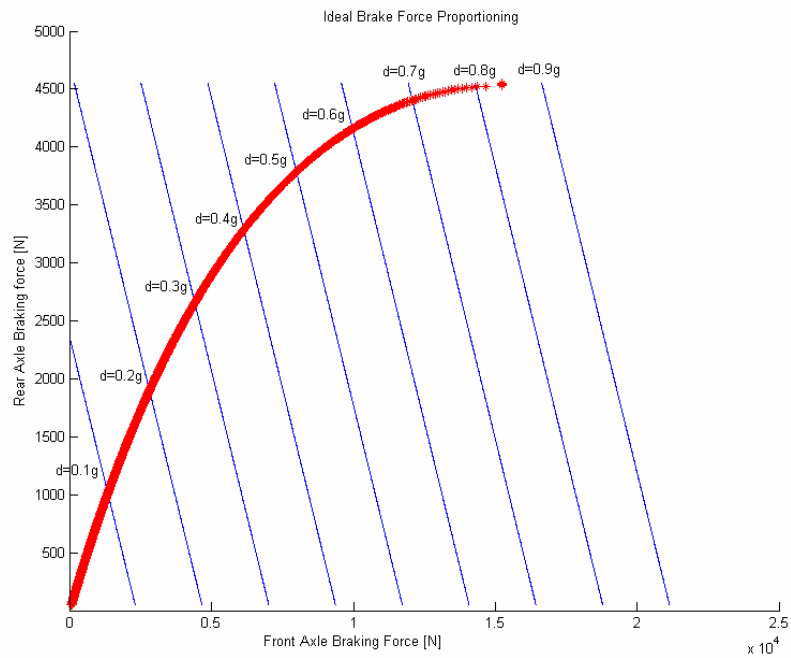


Fig. 4.6 Ideal braking forces proportioning.

By following the ideal braking forces proportioning curve, the front and rear axles could be locked simultaneously when the braking forces reach the adhesive limitation between the road and the tires [38]. However, locking the axles simultaneously, which is really very difficult to sustain, gives the best braking performance for the driver and the vehicle. Up to the point at which the axle being locked is an issue of braking system design by deciding that critical value. At decelerations less than that value, front axle is locked before the rear axle and vice versa. It is desirable, from a safety point of view, for the front axle to lock in preference to rear as during front axle locking, the vehicle cannot be steered but will carry on moving forward without spinning which allows the driver to regain directional control of the vehicle simply by releasing the brakes. If the rear axle has locked and the vehicle has begun to spin, the driver reaction must be rapid if the control of the situation is to be regained, which is really difficult with passenger cars with small moment of inertia [40]. As a result of this vehicle instability problem while braking, in the design of the braking systems European standards require that the front wheels must lock-up first for decelerations up to 0.8 irrespective of the brake force magnitude. Therefore it is feasible to apply a fixed brake ratio that will consistently lead to the front axle lock which is commonly applied to the design of the brake system found on passenger vehicles.

After considering the dynamics of the braking systems for conventional vehicles, following sections cover the regenerative braking which is the braking system application in HEVs.

4.3.2 Regenerative Braking

One of the most important features of HEVs is the regenerative braking that could be described as converting the kinetic energy of the vehicle back to the electrical form that could be stored in the batteries through the use of electric machinery and their power converters. The capability of the bidirectional energy flow of the electric motors makes it possible to recover the dissipated energy as heat on the friction

brake pairs and allow the vehicle to drive the vehicle with the regenerated energy later. Hence, the overall fuel efficiency of the vehicle is improved significantly with the utilization of the recaptured energy of the vehicle.

The effectiveness of the energy generation while braking depends on the capacity and the efficiency of the electric machines operated (i.e. electric motors or generators) and the power capacity of the energy storage devices associated with these electrical machines (see Section 3.1.3). Hence, the available regenerative braking torque is determined by the electrical components' power restrictions (i.e. ratings). As can be seen from the Fig 3.4, at speeds more than their rated/base speed (ω_r), the electric motors could only supply and absorb (or sink in) constant power which means available regenerative braking torque will decrease at high speeds.

At low speed cruising, regenerative braking may solely supply the required braking force as the electric motors could produce constant rated torque at speeds less than its rated one and the required braking torques will be relatively smaller if compared to those at higher cruising speeds. However at high speeds, the required braking forces demanded by the driver could only be covered with parallel operation of the frictional (conventional) braking and regenerative braking systems. Although it has less torque production capability at high speeds, regenerative braking should be used to increase the SOC of the battery. The braking system of a HEV could be improved by applying appropriate control algorithm which realizes braking with ideal front and rear braking force distribution and development of highly efficient electrical machines and energy storage devices.

The next section discusses the parallel braking system which utilizes both friction braking and regenerative braking according to the commands sent by the HEV controller.

4.3.2.1 Parallel braking

Regenerative braking capability depends on many factors:

- the torque-speed characteristics of the EMs,
- on the deceleration demanded by the driver,
- vehicle speed,
- the adhesion between the tire and the ground,
- HEV configuration, i.e. only the EM driven axle could be effective for regenerative braking.

A controller is needed to check these variables and to adjust the braking torques of the front and rear axles in order to follow the ideal braking force distribution curve. Determining the priority between the two braking systems and regulating the frictional brake forces independently are other functional requirements on the controllers.

The brake controller's first function is the safety of the driver by supplying maximum adhesive capability for the tire-ground contact. Following the ideal braking force distribution curve by controlling the front and rear axle braking forces of the both braking systems enhances the braking performance and stability of the vehicle. The second function of the controller is to recover as much energy as the electrical components capability permits and hence the regenerative braking system should be used whenever possible. Therefore, at first, the deceleration demand by the driver and the vertical loads for each axle is computed by the brake controller and then the capability of the EM(s) is checked whether they could be enough to generate the required braking torque or not. If not, the distribution between the front/rear axle braking torques and regenerative/friction braking system is determined by the brake controller.

Final section deals with the evaluation of the developed regenerative braking system by simulating the commercial HEV in urban and highway cycles.

4.3.2.2 Evaluation of the Regenerative Braking System Utilized in the Study

The brake controller system is evaluated for two different HEV configurations (C-3 and P-4, see Section 2.2.5) respectively using two different cycles. The selection of the target HEV configurations is made according to their powertrain placement of the electrical machinery and the available EMs in the design. Hence, configuration C-3, which has one EM on each axle, and configuration P-4, which has an EM at the rear axle, are preferred for the monitoring the capability of the regenerative braking system developed for the study. In order to visualize the limitations of the proposed system, both configurations are simulated in two different cycles: a highway cycle with high acceleration/deceleration demands plus EUDC, which is mentioned in detail in Appendix C. The results of the above mentioned simulations are presented in Figs 4.7-4.12.

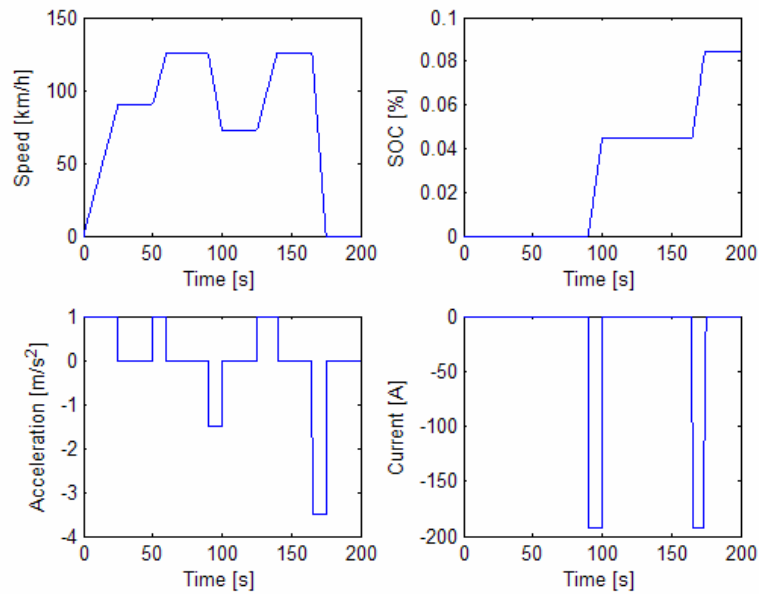


Fig. 4.7 Braking characteristics of C-3 in highway cycle.

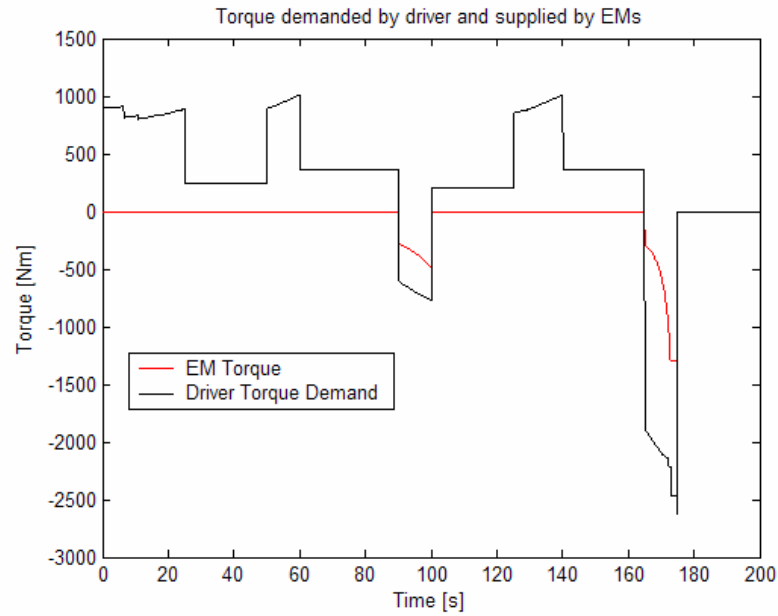


Fig. 4.8 Parallel braking of C-3 in highway cycle.

As can be seen from Fig 4.8, EMs could not supply the demanded torques to yield the desired deceleration and the friction brakes are used in parallel for producing the required braking forces. With the utilization of regenerative braking, part of the kinetic energy to be lost is converted into electrical energy and the battery is charged, which is presented by the increase of the SOC during braking. After checking the utilization of the parallel braking, C-3 and P-4 configuration is simulated through EUDC cycle, which will be elaborated in the eighth chapter, and the results are shown in Figs 4.9 & 4.12:

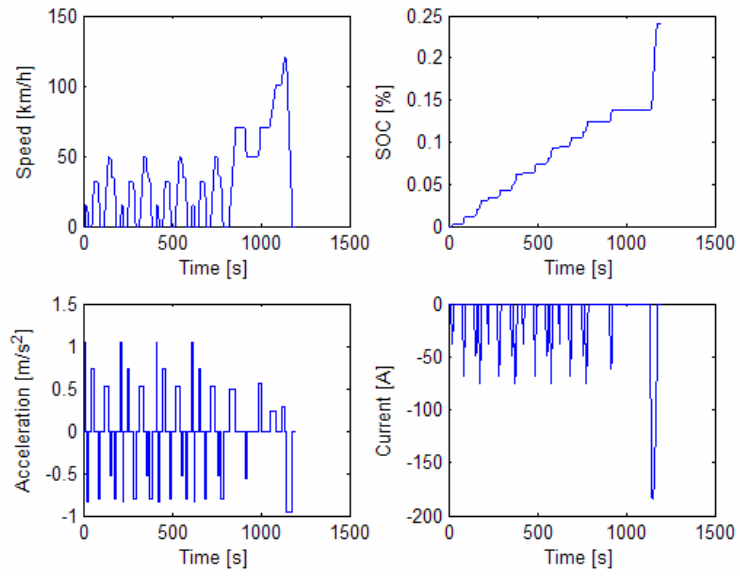


Fig. 4.9 Braking characteristics of C-3 in EUDC cycle.

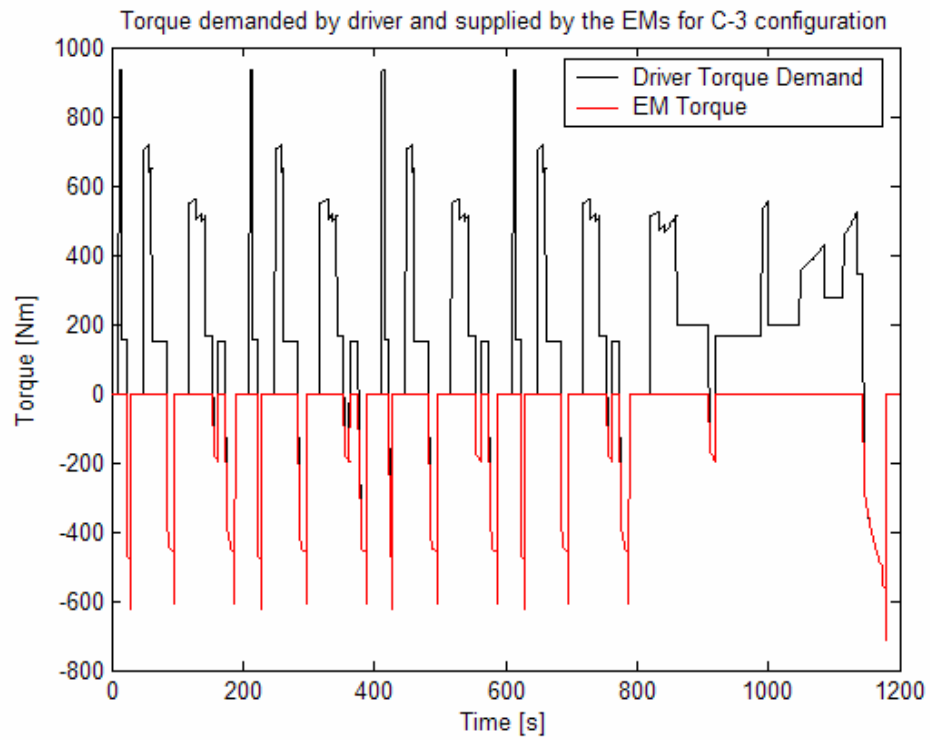


Fig. 4.10 Parallel braking of C-3 in EUDC cycle.

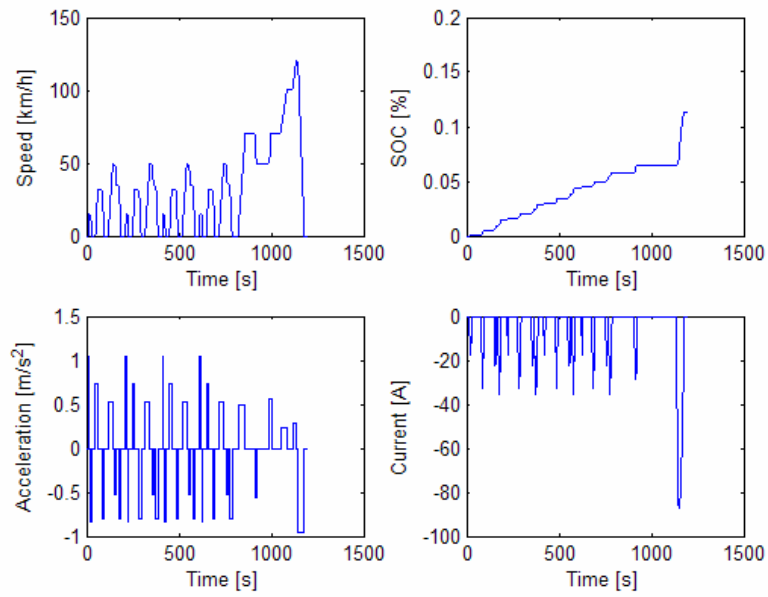


Fig. 4.11 Braking characteristics of P-4 in EUDC cycle.

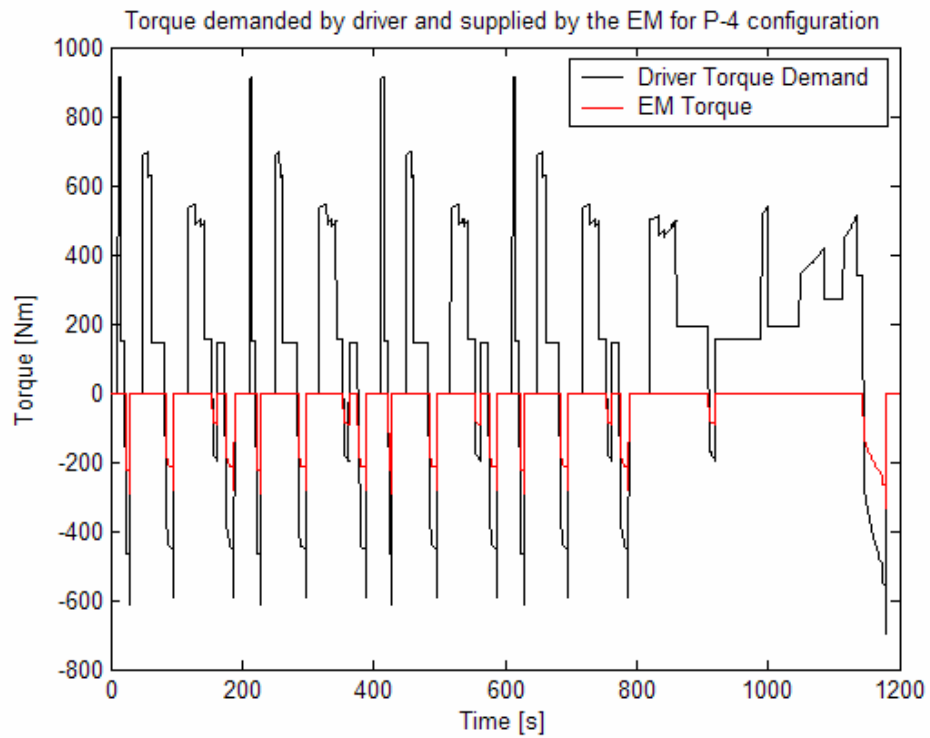


Fig. 4.12 Parallel braking of P-4 in EUDC cycle.

When compared to P-4, the C-3 configuration has an extra EM attached to the front axle which obviously affects the effectiveness of the regenerative braking as can be observed from the SOC values. Similarly, the parallel braking capability of each configuration can be seen in Figs. 4.12 and 4.10. Note that the SOC value of C-3 is two times higher than that of the P-4's due to its extra EM. It is obvious from Fig 4.12 that the regenerative braking system could supply the needed braking alone while P-4 needs friction brakes as only the EM driven axle could be effective for regenerative braking.

4.4 Closure

In this chapter, longitudinal vehicle dynamics including the braking system used in the thesis were investigated. At the first section, vehicle dynamics with the resistive forces acting on was taken into consideration. Then, the braking dynamics of the conventional vehicles were discussed in detail in order to have an opinion about the aspects of the braking system of the HEVs in this study. The regenerative braking systems proposed for HEVs were presented afterwards. Finally, the simulation results of the corresponding regenerative braking system used in the study was presented in order to evaluate its capabilities.

The simulation results have shown that regenerative braking system could supply the needed braking alone for deceleration demands of around $1 \text{ [m/s}^2\text{]}$ and is effective only in the EM driven axle which is an important issue for HEV configuration type selection.

CHAPTER 5

VEHICLE DRIVETRAIN MODELING

5.1 Introduction

The main reason for investigating HEVs is to improve the fuel efficiency of the vehicles and decrease the emissions in the urban areas, especially in cities with high population and traffic. Moreover, the decrease in fuel consumption could be enhanced with proper design of powertrain components which could be optimized for better fuel consumption performance. Hence, proper internal combustion engine and transmission systems model is needed for the evaluation of the fuel efficiency performance of the HEVs.

In fact, internal combustion engine model having almost the same fuel consumption and maximum power with the one utilized in the Ford Tourneo Connect is to be modeled in the thesis and the first part of the chapter involves the related model. Nonlinear dynamic model of a spark ignition engine and a map based diesel engine model are presented in the mentioned sections with the relevant differential equations. Besides, the transmission system used in the same type of vehicle is modeled for having nearly the same performance stated in its catalog. As only available option in transmission of the Ford Tourneo Connect is the manual transmission, proper transmission system including the clutch dynamics is discussed in the related sections.

The drivetrains of HEVs are nonlinear dynamic systems composed of electrical, mechanical and chemical devices whose primary goal is to supply the needed power for cruising. In order to simulate the performances of these vehicles, their dynamic

powertrain components must also be modeled. Therefore, in the following sections; internal combustion engine modeling and transmission system modeling for HEVs will be presented. Nonlinear dynamic spark ignition engine model and diesel engine model based on steady-state fuel-torque map will be discussed respectively in the ICE modeling section. Owing to the desire of the Ford Otosan Co. manual transmission and clutch model is covered in the final section.

5.2 Internal Combustion Engine Modeling

Due to more strict environmental regulations, the improvements on the control of ICE performance in transient regions appear to be an important issue and significant research efforts are made to improve the vehicle emissions and fuel economy by controlling the **air-to-fuel-ratio** (AFR) very precisely as deviations from the stoichiometric AFR strongly influence the cylinder air charging process, mixture formation and transient performance of the engine. Hence, to solve these problems, many research efforts have been concentrated on development of control-oriented dynamic engine models and model-reference based control schemes.

5.2.1 Spark Ignition Engine Modeling

The mathematical model of **spark ignition** (SI) engine is here developed rather than employing steady-state engine fuel map. Thus, the nonlinear engine model of [23] could be adapted to a wide operating range of SI engines operations as it covers the engine operation regimes away from the stoichiometric AFR. The model, which also takes into account the AFR related spark advance, is quite suitable for assessing the vehicle's fuel consumption accurately while observing the effect of nonlinearities in transient regimes. The overall mathematical model of the engine is illustrated in Fig 5.1.

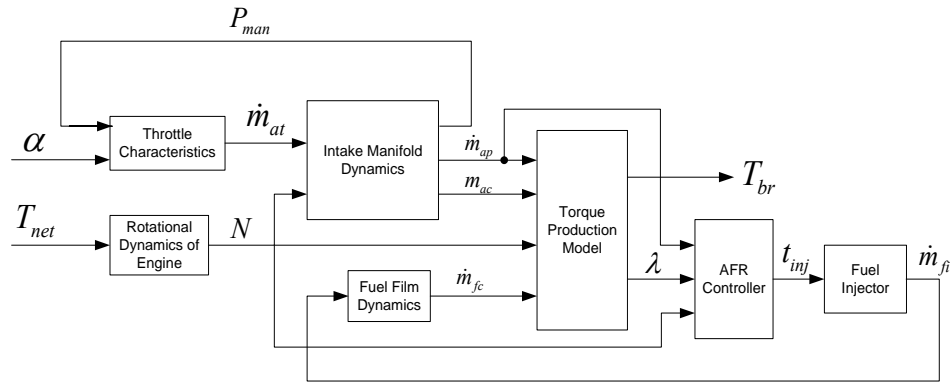


Fig. 5.1 Spark ignition engine model.

The engine model consists of two input variables, which are the throttle angle (α) and net torque produced to drive the vehicle and utilizes four state variables as intake manifold pressure, engine speed, fuel mass in the fuel film and injection frequency of the fuel. As can be seen from Fig. 5.1, the SI engine model is composed of mainly six sub-models: *throttle characteristics*, *intake manifold dynamics*, *rotational dynamics*, *fuel film dynamics*, *torque production model* and *AFR controller*. Brake torque (T_{br}) is the output of the ICE system in order to drive the vehicle. Following sections focus on the mentioned sub-systems respectively.

5.2.1.1 Throttle Characteristics

Throttle characteristics subsystem deals with the air rate coming into the manifold through the throttle valve as seen in Fig 5.2. The air flow through the throttle valve is modeled as isentropic flow of compressible fluid and the inputs to this sub-model are alpha (α) and the manifold pressure (P_{man}).

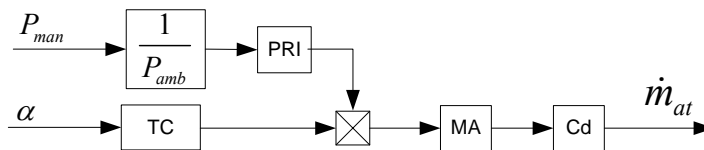


Fig. 5.2 Throttle Characteristics Subsystem in SI engine model.

The air-flow rate through the throttle (\dot{m}_{at}), is calculated as follows [23]:

$$\dot{m}_{at} = C_D \cdot MA \cdot TC \cdot PRI \quad (5.1)$$

where C_D is the discharge coefficient. In (5.1), the maximum flow rate through a specific throttle (MA) can be expressed as

$$MA = \frac{P_{amb} \cdot A_{th}(\alpha_{max})}{\sqrt{RT_{amb}}} \quad (5.2)$$

Similarly, the normalized flow as a function of the cross-sectional area (TC) is

$$TC = \frac{A_{th}(\alpha)}{A_{th}(\alpha_{max})} \quad (5.3)$$

When the cross-sectional area of throttle opening (A_{th}) is inserted in (5.3), the simplified function of MA presented by [23] is:

$$TC(\alpha) = 1 - \cos\left(\frac{\pi}{180} \cdot (-1.1549 \cdot \alpha - 0.00225)\right) \quad (5.4)$$

Finally, the normalized flow (PRI) as a function of pressure ratio (P_R) is:

$$PRI = P_R^{1/\gamma} \left(\frac{2}{\gamma+1}\right)^{(\gamma+1)/2(1-\gamma)} \sqrt{\left(\frac{2}{\gamma-1} [1 - P_R^{(\gamma-1)/\gamma}]\right)} \text{ if } P_R \geq P_{CR} \quad (5.5a)$$

$$PRI = 1.0 \quad \text{otherwise} \quad (5.5b)$$

where intake manifold pressure ratio and critical pressure are defined as:

$$P_R = \frac{P_T}{P_0} \approx \frac{P_{man}}{P_{amb}} = \frac{P_{man}}{1.01325} \quad (5.6)$$

$$P_{CR} = \left(\frac{2}{\gamma+1}\right)^{\gamma/(\gamma-1)} = 0.5283 \quad (5.7)$$

As shown in (5.5), if the pressure ratio at the intake manifold (P_R) is below the critical pressure (P_{CR}), the mass of the air flow rate through the throttle is independent of engine speed and manifold pressure and taken as 1.

5.2.1.2 Intake Manifold Dynamics

Intake manifold dynamics subsystem deals with the calculation of the intake manifold pressure, air flow rate into the intake port and the cylinder air charge per stroke. Fig 5.3 presents the intake manifold dynamics model block diagram.

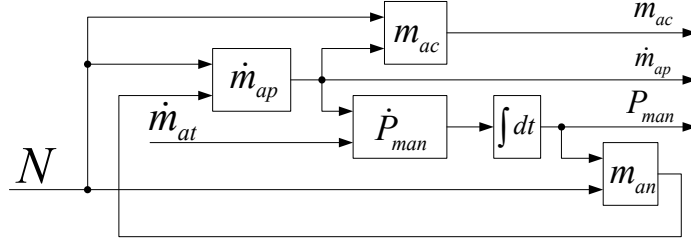


Fig. 5.3 Intake Manifold Dynamics Subsystem in SI engine model.

The conservation of the air mass in the intake manifold and ideal gas law are used for calculating the manifold pressure for which (5.8) and (5.9) are used:

$$\dot{m}_{ai} = \dot{m}_{at} - \dot{m}_{ap} \quad (5.8)$$

$$\dot{m}_{ai} = \frac{d}{dt} \left(\frac{P_{man} V_{man}}{RT_{man}} \right) \quad (5.9)$$

where \dot{m}_{at} : air mass rate in the intake manifold.

\dot{m}_{ap} : air mass flow rate into the intake port.

$P_{man}, V_{man}, T_{man}$: Manifold pressure, volume and temperature.

By substituting (5.9) into (5.8), the manifold pressure state equation, (5.10), is obtained [23]:

$$\dot{P}_{man} \approx \frac{RT_{man}}{V_{man}} (\dot{m}_{at} - \dot{m}_{ap}) \approx \frac{RT_{man}}{V_{man}} \cdot (\dot{m}_{at} - \dot{m}_{ap}) \quad (5.10)$$

The mass airflow rate out of the intake manifold (\dot{m}_{ap}) is represented by a speed-density algorithm:

$$\dot{m}_{ap} = \frac{V_D}{120RT_{man}} \eta_{vol} P_{man} N \quad (5.11)$$

where η_{vol} is the volumetric efficiency of the SI engine. In [23], $\eta_{vol} P_{man}$ is called the normalized air charge and its approximated equation is presented as

$$m_{ap} = \eta_{vol} P_{man} = f_1(n) + f_2(n) P_{man} \quad (5.12)$$

where f_1 and f_2 are two polynomials depending upon engine speed [krpm]. The air charge per stroke (m_{ac}) plays an important role rather than the normalized air charge during the development of the SI engine model as the SI engine operation is based on the engine events. Therefore the air charge per stroke is calculated by the integration of the air mass flow into the intake port between intake events. This integration simply leads to

$$m_{ac} = \frac{30 \cdot \dot{m}_{ap}}{N} \quad (5.13)$$

5.2.1.3 Fuel Film Dynamics

Fuel film dynamics subsystem, which is shown in Fig 5.4, deals with the fuel delivery process from the injector to the inside of the cylinder.

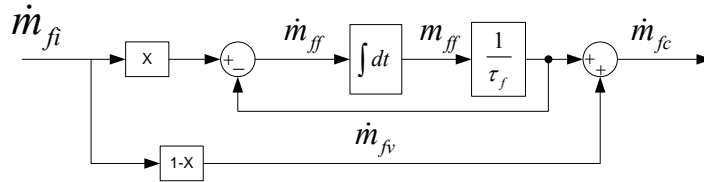


Fig. 5.4 Fuel Film Dynamics Subsystem in SI engine model.

In this model, the fuel to be injected is assumed to be proportional to the airflow and that some fraction (X) of injected fuel hits the intake manifold walls and forms a fuel puddle on the walls. Another assumption made in this model is that the film thickness is proportional to the amount fuel in the film. The film dynamics continuity equation, which is represented in Fig 5.4, could be expressed as [23]:

$$\dot{m}_{ff} = -\frac{1}{\tau_f} m_{ff} + X \cdot \dot{m}_{fi} \quad (5.14)$$

where m_{ff} : mass of fuel in the fuel film.

\dot{m}_{fi} : injected fuel mass flow rate.

τ_f : fuel evaporation time constant.

The fraction of the fuel, which does not form fuel film, directly enters the cylinder with airflow:

$$\dot{m}_{fv} = (1 - X) \dot{m}_{fi} \quad (5.15)$$

where \dot{m}_{fv} is the mass flow rate of the fuel vapor. As a result, the actual flow rate entering the cylinder (\dot{m}_{fc}) is the sum of the mass flow rate of fuel vapor and the evaporated fuel from the film with time constant τ_f .

$$\dot{m}_{fc} = \dot{m}_{fv} + \frac{1}{\tau_f} m_{ff} \quad (5.16)$$

5.2.1.4 Torque Production Model

Torque production subsystem deals with the calculation of the indicated torque, the friction torque and the brake torque at optimal spark timing and the torque production in the engine is a relatively complicated process that depends on many physical parameters as illustrated in Fig 5.5. At first, the actual AFR in the cylinder ($\dot{m}_{ap} / \dot{m}_{fc}$) is calculated by an equivalence ratio:

$$\phi_c = 1 / \lambda = (A / F)_s \frac{\dot{m}_{fc}}{\dot{m}_{ap}} \quad (5.17)$$

where $(A/F)_s$ is the stoichiometric air-to-fuel ratio.

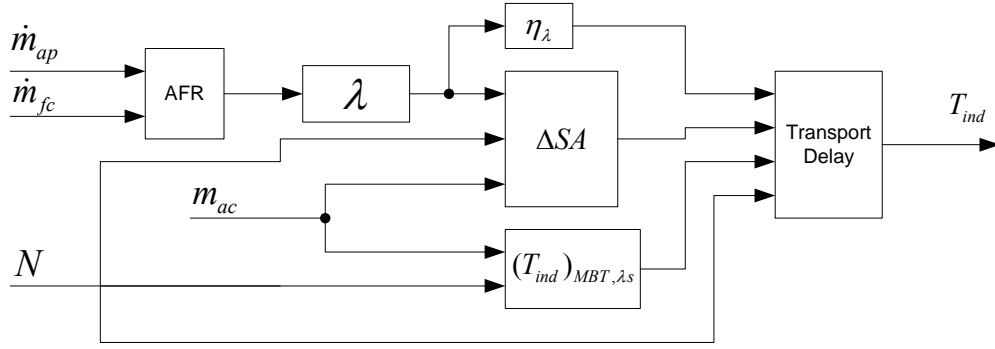


Fig. 5.5 Torque Production Subsystem in SI engine model.

The engine torque is the product of the combustion process in the cylinder which is mainly influenced by the AFR of the mixture in the cylinder, spark timing, and the combustion efficiency; whereas transport delay gives the dynamic characteristics to the torque production subsystem.

The **optimal spark timing** (MBT) at the stoichiometric AFR is computed at first. Then, the MBT at various engine operating conditions is calculated by indicating the difference between them as:

$$(MBT)_\lambda = (MBT)_{\lambda_s} + \Delta MBT(\lambda) \quad (5.18)$$

Here, $(MBT)_{\lambda_s}$ is the optimal spark timing at the stoichiometric AFR while $(MBT)_\lambda$ represents the optimal spark timing at the arbitrary AFR. By least-square regression utilization on the steady-state engine test data gives the approximated polynomials for $(MBT)_{\lambda_s}$ and $\Delta MBT(\lambda)$. These are respectively:

$$(MBT)_{\lambda_s} = f(m_{ac}, n) = f_3(n) + f_4(n, m_{ac}) \quad (5.19)$$

$$\Delta MBT(\lambda) = d_0 + d_1\lambda + d_2\lambda^2 \quad (5.20)$$

The indicated torque at the MBT and the stoichiometric AFR could be written as:

$$T_{ind}(n, m_{ac}, \eta_{\Delta SA}, \eta_\lambda) = (T_{ind})_{MBT, \lambda_s} \cdot \eta_\lambda \cdot \eta_{\Delta SA} \quad (5.19)$$

where $(T_{ind})_{MBT,\lambda_s}$ is the indicated torque value of an engine at a fixed AFR and spark timing which is also an approximated polynomial obtained from the steady-state engine test data. In order to reflect the effects of these values, efficiency terms are multiplied with the indicated torque. $\eta_{\Delta SA}$ represents the spark timing efficiency which is a function of the difference of spark timing between MBT at an arbitrary AFR and spark timing at the current operation:

$$\Delta SA = (MBT)_\lambda - SA \quad (5.20)$$

Note that η_λ in (5.19) denotes the influence of the AFR to the indicated torque. The corresponding approximated polynomials of the steady-state engine test data are as follows:

$$(T_{ind})_{MBT,\lambda_s} = f_3(n) + f_4(n, m_{ac}) \quad (5.21)$$

$$\eta_\lambda = l_0 + l_1\lambda + l_2\lambda^2 \quad (5.22)$$

$$\eta_{\Delta SA} = s_0 + s_1(\Delta SA) + s_2(\Delta SA)^2 \quad (5.23)$$

In order to synchronize the sample times of the model with the intake events of the SI engine occurred during the combustion cycle, transport delays for the torque production is computed for the parameters shown in Fig 5.5.

5.2.1.5 Rotational Dynamics

Rotational subsystem deals with the engine rotational effects as seen from Fig 5.6:

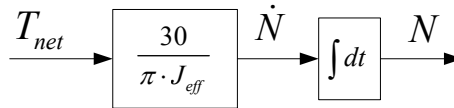


Fig. 5.6 Rotational Dynamics Subsystem in SI engine model.

The assumption of a lumped parameter system with constant inertia is used during the modeling of the SI engine. Engine friction and pumping losses decreases the indicated torque produced by the SI engine and subtracted from the indicated torque. The net torque is called the “brake torque” and used for the computations of the rotational speed of the engine drive shaft by using Newton’s second law of motion:

$$J_{eff} \frac{dN(t)}{dt} = \frac{30}{\pi} (T_{ind}(t) - T_{f/p}(t) - T_L(t)) \quad (5.24)$$

where $T_{f/p}(t)$: the friction and pumping torque,

$T_L(t)$: the load torque exerted by the clutch,

J_{eff} : effective inertia of the engine,

$N(t)$: engine speed [rpm].

5.2.1.6 Modifications on the Model

The engine model explained briefly was originally developed for a 2000 [ccm], four-cylinder SI engine. However, it must be downsized to 1800 [ccm] (giving a maximum power of 85 [kW] at 5300 rpm) in order to have the same ICE characteristics of Ford Tourneo Connect with 1800 [ccm] gasoline engine by changing two variable used in the model. The first one is the cylinder volume parameter and the other one is the air mass flow rate into the intake port. The original engine model has the performance of around 180 [PS] at 5700 [rpm] with 2000 [ccm] dual-over head cam (DOHC) engine. The change in the cylinder volume was not sufficient to have an 85 [kW] power at the given engine speed. Therefore, by reducing the air mass entering the cylinder, the lambda sensor reduces the relevant fuel rate in order to have the air-to-fuel ratio be nearly at the stoichiometric value. As a result, the needed maximum power that the spark ignition engine supplies could be achieved by tuning of the air mass rate into the intake port and in order to decrease from 112 [kW] to 85 [kW], 20 % reduction is made in the air mass rate.

5.2.1.7 Evaluation of the Spark Ignition Engine Model

In order to visualize the performance of the above stated spark ignition engine model, a simulation was carried out in which the vehicle was being monitored in an urban cruising mode presented in Fig 5.7. The details on the driving cycle are presented in Appendix C.

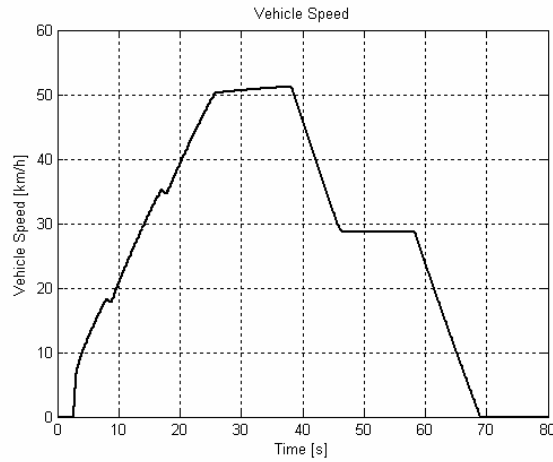


Fig. 5.7 Vehicle speed characteristics in urban cruising cycle.

As presented in 5.2.1.1 and 5.2.1.2, the air mass flow rate passing through the throttle is computed for calculation of the change in the manifold pressure, which in turn affects the air mass flow rate into the manifolds' intake port. These features of the modeled spark ignition engine are demonstrated in Figs 5.8-5.10 through the simulation case.

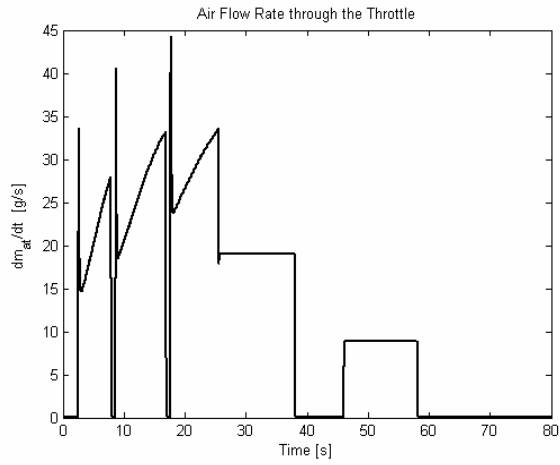


Fig. 5.8 Air mass flow rate through throttle in urban cruising cycle.

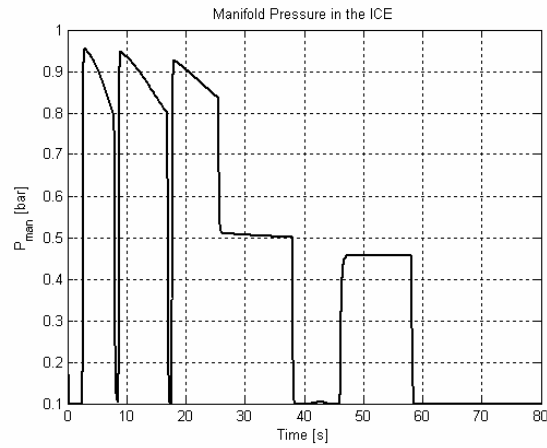


Fig. 5.9 Manifold pressure change in urban cruising cycle.

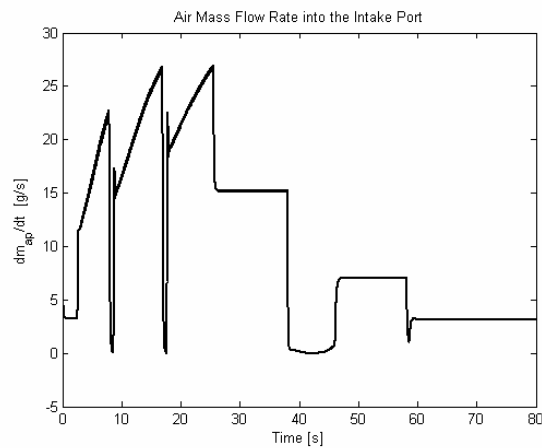


Fig. 5.10 Air mass-flow rate into the manifold in urban cruising cycle.

Moreover, the fuel injection characteristics of the SI engine model are observed in the simulation case as seen in Fig 5.11.

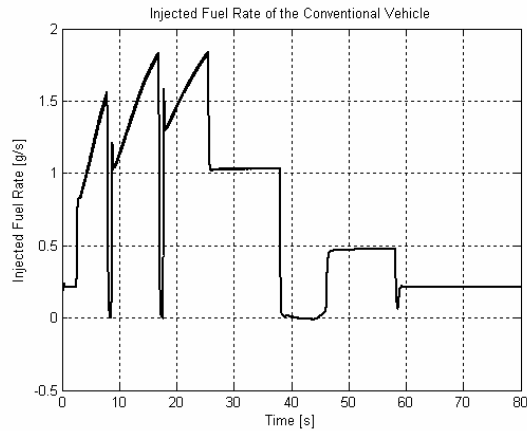


Fig. 5.11 Injected fuel rate in urban cruising cycle.

Notice that the injected fuel rate is changing according to the air mass flow rate entering into the intake port as could be observed in Figs 5.10 and 5.11. This value is controlled by the AFR controller according to the lambda parameter which happens to be the AFR deviation of the engine from the stoichiometric AFR value. The lambda value of the SI engine in the simulation case is also presented in Fig 5.12.

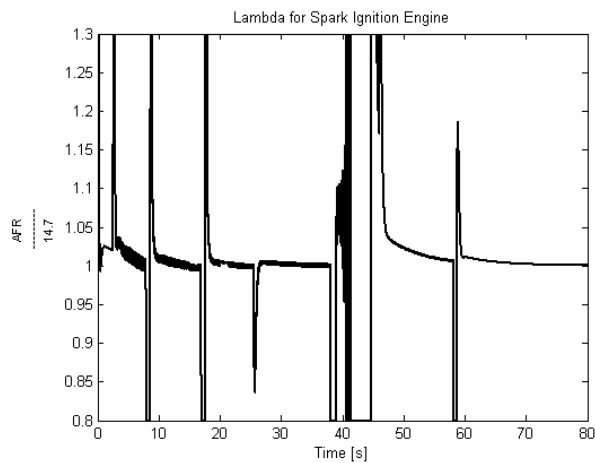


Fig. 5.12 Change in the Lambda value in urban cruising cycle.

Finally, the frictional losses of the SI engine was evaluated which affects the brake torque of the engine as well as the engine speed. Figs 5.13 and 5.14 presents the frictional torque occurred and the engine speed change according to it respectively.

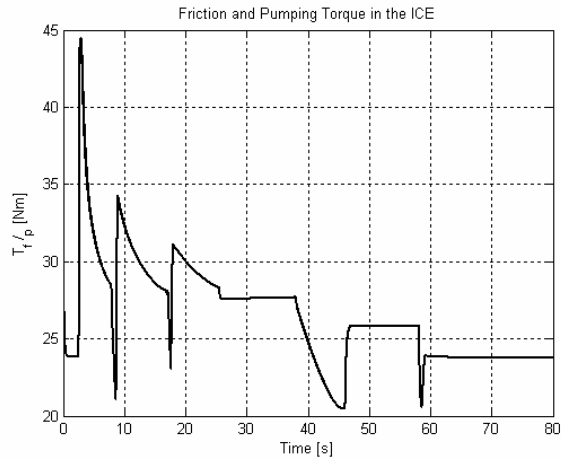


Fig. 5.13 Friction torque in SI engine in urban cruising cycle.

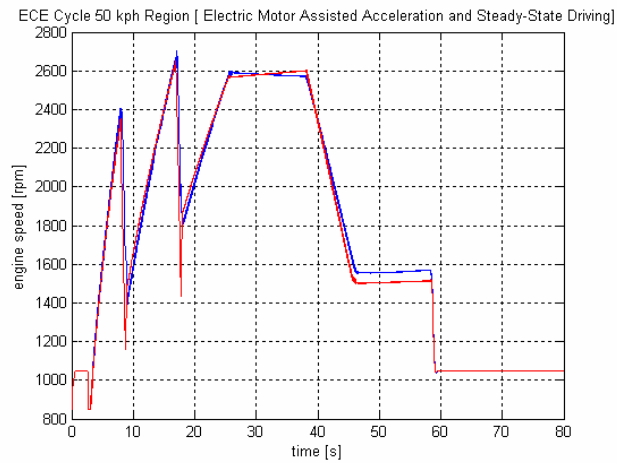


Fig 5.14 Engine speed variation in urban cruising cycle.

5.2.2 Map Based Diesel Engine Modeling

Map based engine modelling is widely utilized in technical literature owing to the fact that the model yields acceptable results for steady state regimes and that the implementation of the model is straightforward. Therefore, in this thesis, a simple model, which is based on the power requirement of the target vehicle, will be developed. In fact, Ford Otosan intends to develop a hybrid vehicle utilizing a diesel engine rather than spark ignition which was the focus of the study. The corresponding model is implemented as an efficient MATLAB code which in turn enables faster simulation when compared with the previously developed HEV model utilizing SI engine.

At this stage, the fuel map of 1.8 [l] Ford Transit Connect (75[PS], 175[Nm]) diesel engine (Fig. 5.15) provided by Ford Otosan Co., is to be utilized to accomplish this goal and is based on the injected fuel rates of the diesel engine operating at the steady-state. Hence, it easily lends itself for a computational method which solely takes advantage of the quasi-static power balance of the target vehicle. The fuel map of the above mentioned engine is illustrated in Fig 5.15.

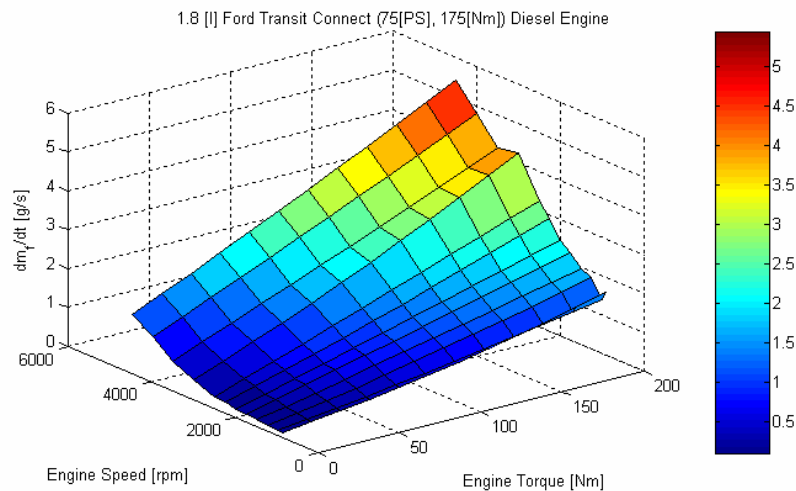


Fig. 5.15 Diesel Engine Fuel Map supplied by Ford Otosan Co.

A 2D look-up table is created to determine the fuel consumption at the specified operating point. Consequently, when the engine torque and the speed (i.e. engine output power) are specified, the fuel consumption is directly determined using this lookup table. Note that, specific fuel consumption of this engine, which is measured in terms of [g/kWh], is of interest to determine its most efficient operating regimes. Figs. 5.16-5.17 demonstrate the specific fuel consumption maps of the related diesel engine.

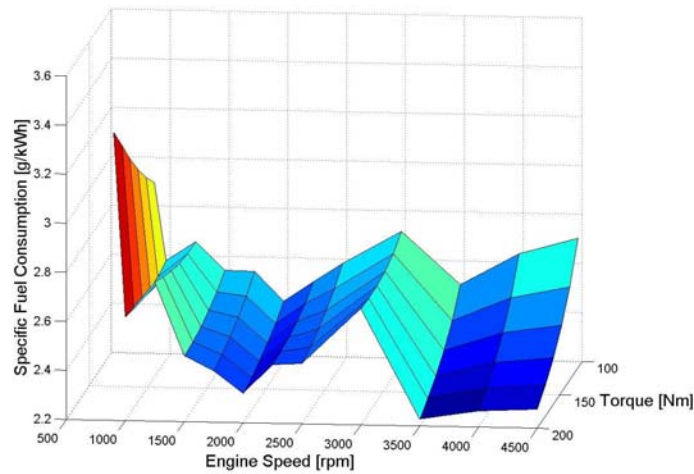


Fig. 5.16 Specific Fuel Consumption Map of 1.8 [l], 75[PS], 175[Nm] diesel engine

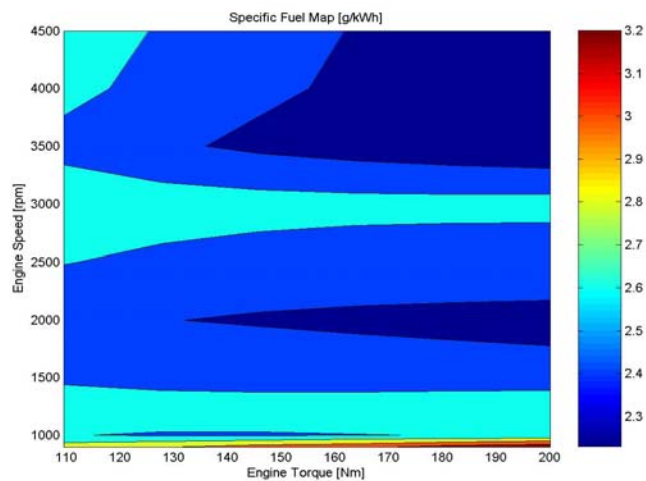


Fig. 5.17 Desired engine operation regions of specific fuel consumption map.

As can be seen from the figures, the engine runs efficiently at two distinct engine speeds: 2000 [rpm] and 3500 [rpm]. Hence, to design optimal power management strategies for HEV designs, these efficient regions will be taken into consideration during the optimization of the engine fuel efficiency.

Moreover, in order to visualize the performance of the above stated diesel engine model, a simulation was carried out in which the vehicle was being monitored in the same urban cruising mode, which is shown in Fig 5.18, as the SI engine was being tested.

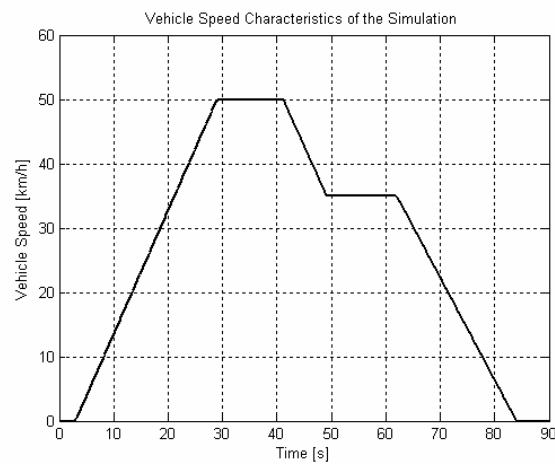


Fig. 5.18 Vehicle speed characteristics of the urban cruising mode.

As the diesel engine model is mainly a fuel map based, the parameters like intake manifold pressure, mass flow rate entering into the intake port, etc. cannot be estimated. However, injected fuel rate during the trip and the engine speed variation are calculated as illustrated in Figs. 5.19 and 5.20 respectively for the purpose of comparing qualitatively the outputs of this model to those of the spark ignition engine model presented in Art. 5.2.1.

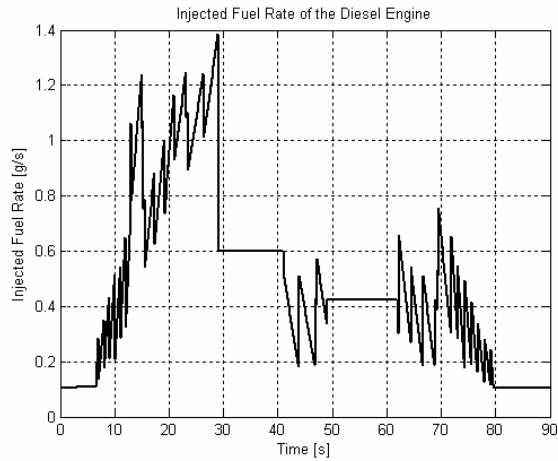


Fig. 5.19 Injected fuel rate of the diesel engine.

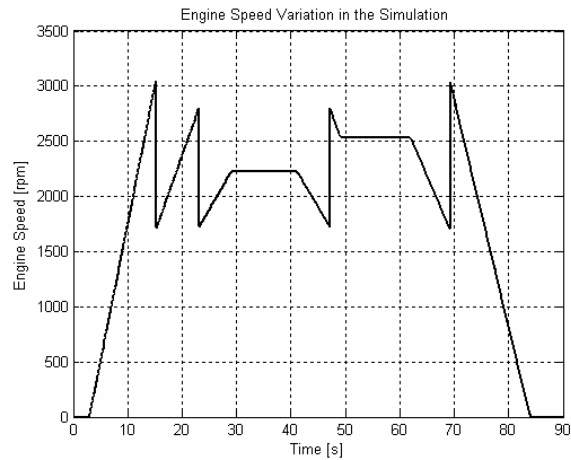


Fig. 5.20 Engine speed variation in the simulation.

When Fig 5.19 is compared with Fig 5.11, it is obviously seen that the behavior of both engines has almost the same trend. Besides, the engine speed alterations, which are presented in Figs 5.20 and 5.14; both models yields the similar characteristics.

As the appropriate internal combustion engine models are constructed, the transmission system of the Ford Tourneo Connect also need to be modeled in order

to have the nearly the same performance of the target vehicle. Final section of the chapter covers the transmission system modeling of the vehicle.

5.3 Transmission Systems Modeling

Development of HEVs has initiated significant research and development efforts on the advanced transmissions which are capable of transmitting torque from two or more power sources in order to supply the driver's torque demand while decreasing the fuel consumption of the vehicle. For that purpose, different types of transmission systems are investigated in the literature: CVT, automatic transmission and manual transmission. However, only manual transmission model is taken into consideration as the target vehicle Ford Tourneo Connect has only manual transmission option and the HEV to be developed by Ford Otosan will also use manual transmission in its powertrain.

The torque transmitted through the transmission system depends on the gear rate of the selected gear by the driver and the slippage rate between the clutch discs. Hence, a dynamic clutch model is adapted from [41-42]. In the developed model, the torque transmitted from the disc on the ICE side to the disc on the wheel side is:

$$T_f = 2\mu NR \text{sgn}(\omega_e - \omega_o) \quad (5.25)$$

where N : the clamp (normal) load on to the discs.

R : average friction radius.

ω_e : rotational speed of the disc at the engine side.

ω_o : rotational speed of the disc at the engine side.

According to the exerted normal force on the discs, which is the clutch pedal input, the transmitted torque can be calculated. The coefficient of friction for the clutch discs and the average friction radius could be computed as:

$$\mu = \text{sgn}(\omega_e - \omega_o) \left(0.2 + 0.1e^{-0.3|\omega_e - \omega_o|} \right) + 10^{-4(\omega_e - \omega_o)} \quad (5.26)$$

$$R = \frac{2}{3} \left(\frac{R_o^3 - R_i^3}{R_o^2 - R_i^2} \right) \quad (5.27)$$

where R_o : outer radius of the discs.

R_i : inner radius of the discs.

5.4 Closure

This chapter focused on powertrain modeling for HEVs and began with constructing the appropriate models for the internal combustion engines to be utilized in the Ford Tourneo Connect. In the study, it was initially decided to utilize a spark ignition engine for the proposed HEV configurations. Hence, a nonlinear dynamic SI engine model was developed with the personal assistance of Dr. Yoon (see [23]). The parameters and data used in the reference paper were also supplied by him, and the SI engine model was achieved. However, due to the fact that Ford Otosan Co. intends to develop a hybrid vehicle utilizing a diesel engine rather than spark ignition, another ICE model, which is based on steady-state diesel engine fuel map, was developed for further research. Finally, the manual transmission model with a clutch was explained. For the computation of the drive torque, the clutch model needs the clutch pedal input; hence the driver model has to be improved by adding the relevant inputs.

CHAPTER 6

HYBRID ELECTRIC VEHICLE MODELLING

6.1 Introduction

HEVs are nonlinear integrated systems composed of electrical, mechanical and electro-chemical devices. Modeling each component should be achieved before constructing a HEV model for the assessment of its overall performance. In the previous chapters, modeling of internal combustion engine, transmission system, braking system, electric motor and battery were discussed in detail. For the feasibility study of a commercial HEV, the proposed configurations, which are mentioned in section 2.2.5, should be constructed and simulated in various driving cycles. This chapter deals with the putting these individual components together to come up with a generalized models for various hybrid Ford Tourneo Connect configurations.

6.2 HEV Configurations with Elaborate Physical Models

At the earlier stages of this work, the vehicle model of a conventional Ford Tourneo Connect with spark-ignition engine was developed. The appropriate electric motor drivers along with a suitable battery model were obtained for the purpose of modeling an entire family (configurations) of hybrid Ford Tourneo Connect vehicles. These models are presented in Fig 6.1-6.10. The vehicle model constitutes a permanent magnet synchronous motor driven by a current controlled voltage source. The battery pack, which consists of 25 cells, is 318-volt lead-acid battery with a capacity of 25 [Ah]. This model is directly adapted from ADVISOR software [48]. The remaining portion of the vehicle (vehicle body, spark ignition engine, manual

transmission, clutch and frictional brakes) directly comes from the model presented in previous chapters. Notice that, the model requires four inputs from the driver:

- throttle angle (alpha input in block diagrams),
- brake pedal angle (beta),
- clutch pedal angle (gamma),
- gear shift number (gear).

These inputs are to be provided by a driver model. However, in the course of simulations these inputs are manually adjusted (via one dimensional look-up tables) to give the desired vehicle speed at particular time instances in a standard driving cycle.

Even though these Simulink models discussed here offer realistic and detailed results, a simulation of a standard urban driving cycle (for instance ECE-15 Urban cycle explained in Appendix C) takes about 300-360 min. on an AMD 2500+ microprocessor based PC. Furthermore, the total number of cases to be studied through simulation is about 300 (10 different HEV configurations x 3 driving cycles x 10 different combinations of electrical components). Hence in order to complete the study, 36 days of continuous simulation time are needed. This is obviously not a feasible course of study owing to the fact that one has to spend at least twice more days to adjust the input parameters, to sort out (filter) the simulation data, and to figure out the critical results. Also, apart from these issues associated with the simulation time, another problem has been faced related with the applied nonlinear spark ignition engine model. Although it yields realistic results; at modes of engine braking and torque generation during cruising, the HEV model give unexpected results in some cases. This is due to the fact that the ICE model [23] and the supplied data are not exactly appropriate for this kind of research.

It is clear that simpler but more efficient HEV models are required to conduct the simulation in a reasonable amount of time. The next section concentrates on the development of a simplified HEV model.

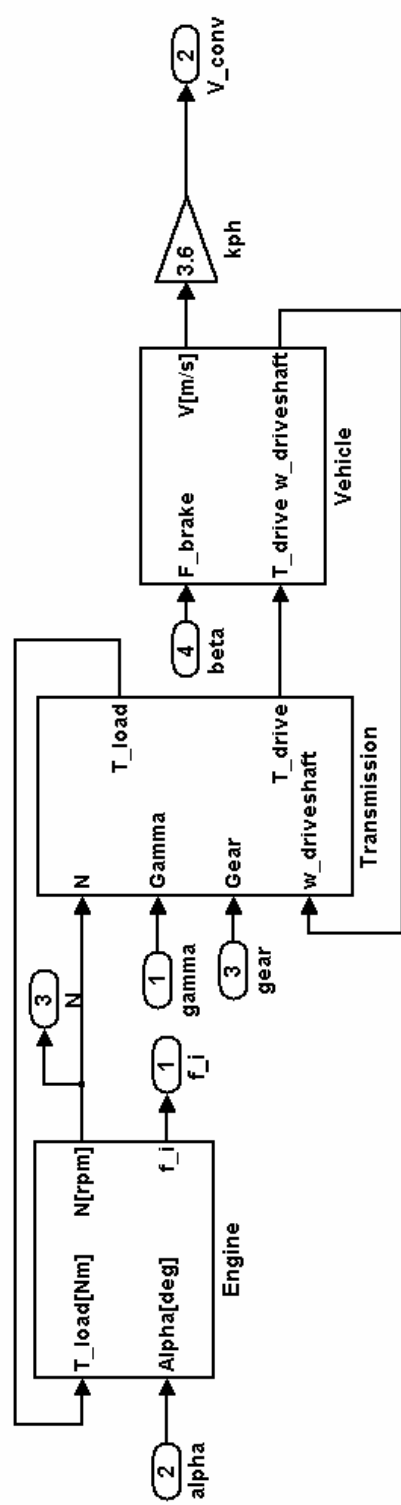


Fig 6.1 Simulink diagram of the conventional vehicle.

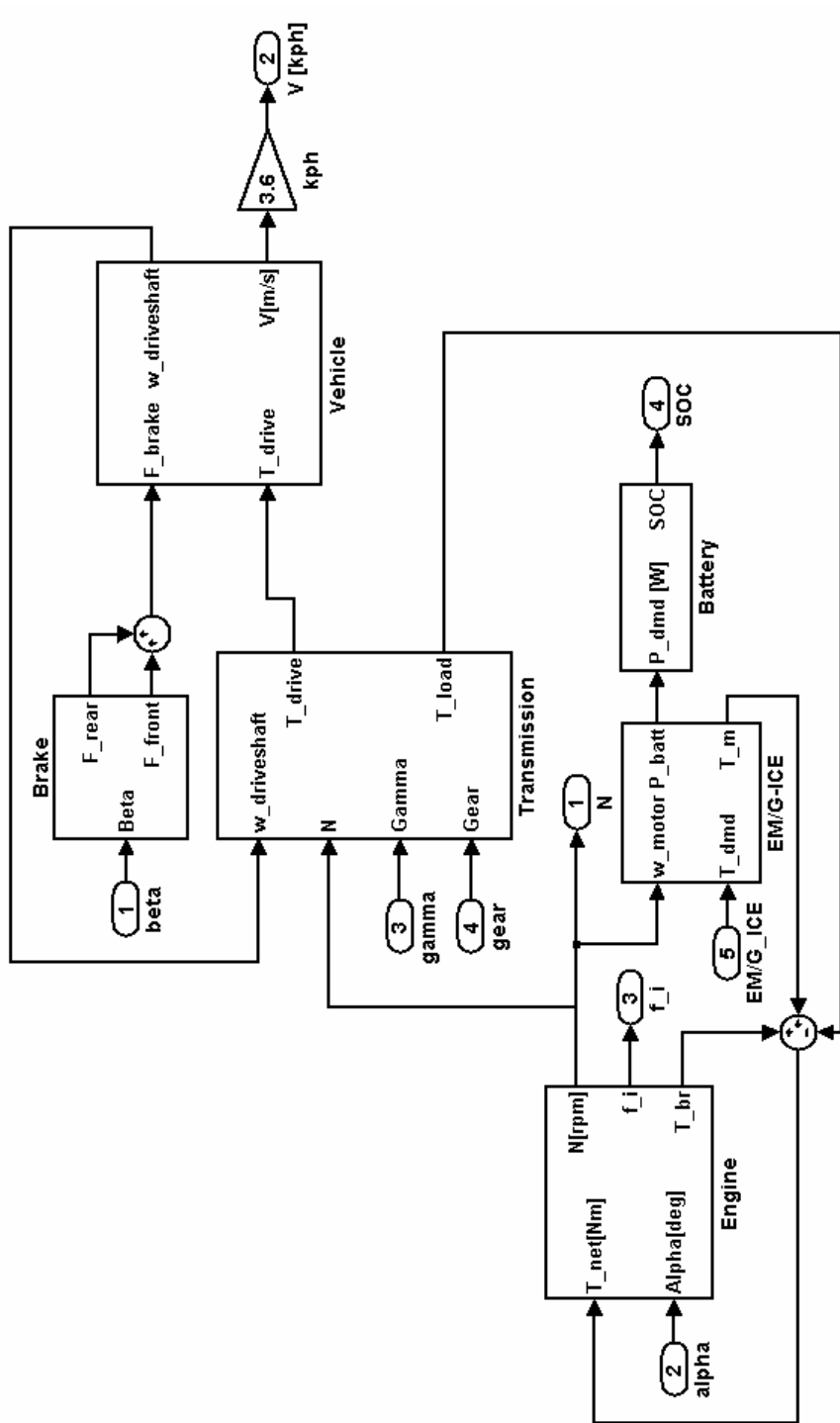


Fig 6.2 Simulink diagram of the HEV configuration P-1.

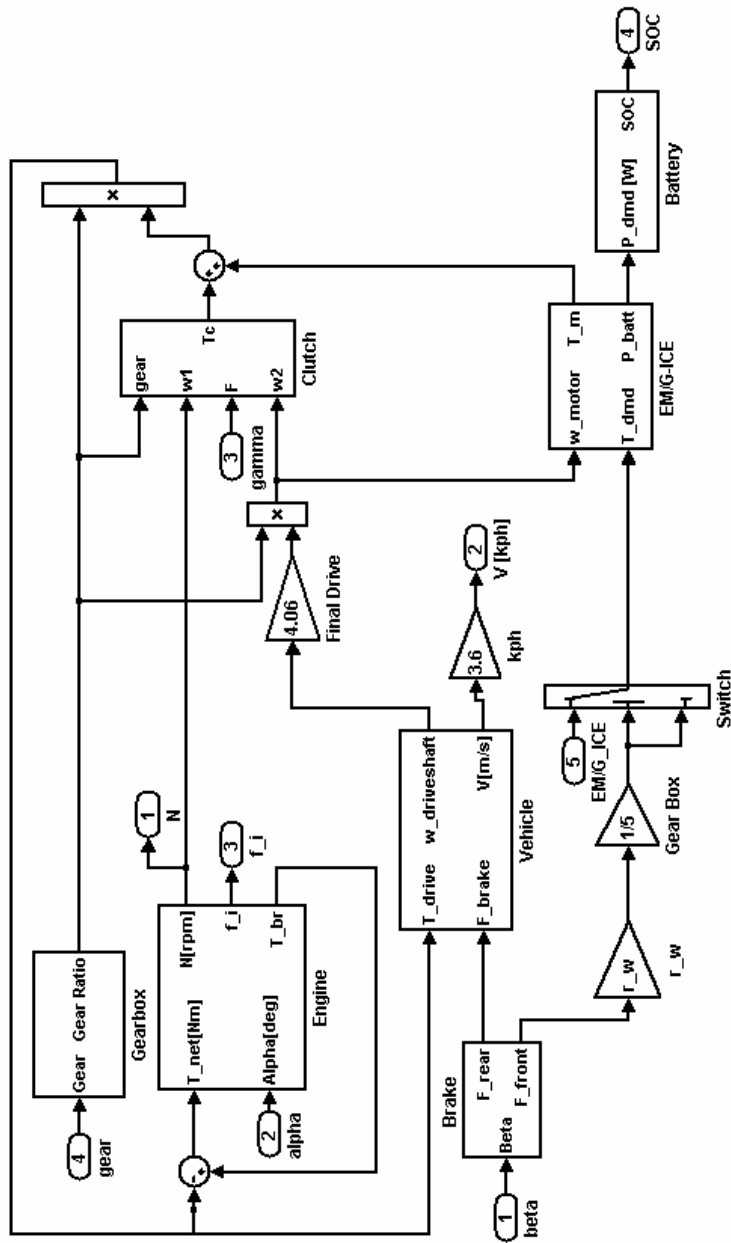


Fig 6.3 Simulink diagram of the HEV configuration P-2.

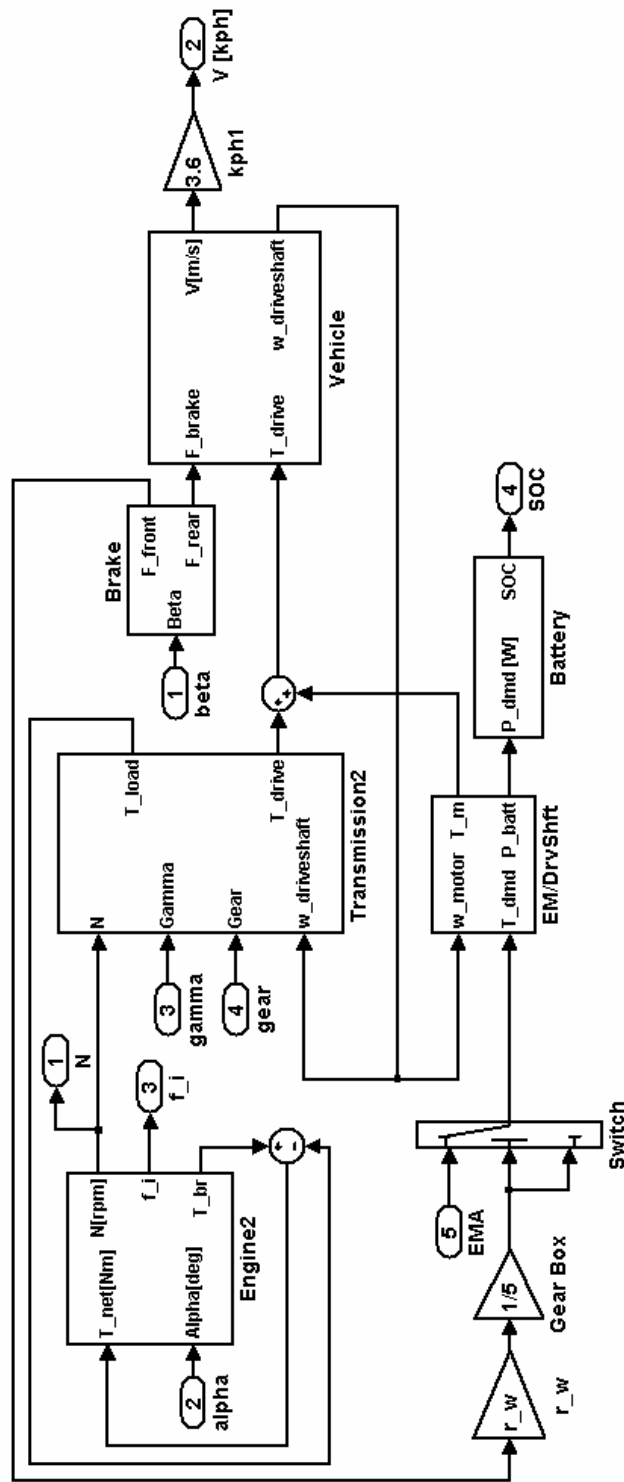


Fig 6.4 Simulink diagram of the HEV configuration P-3.

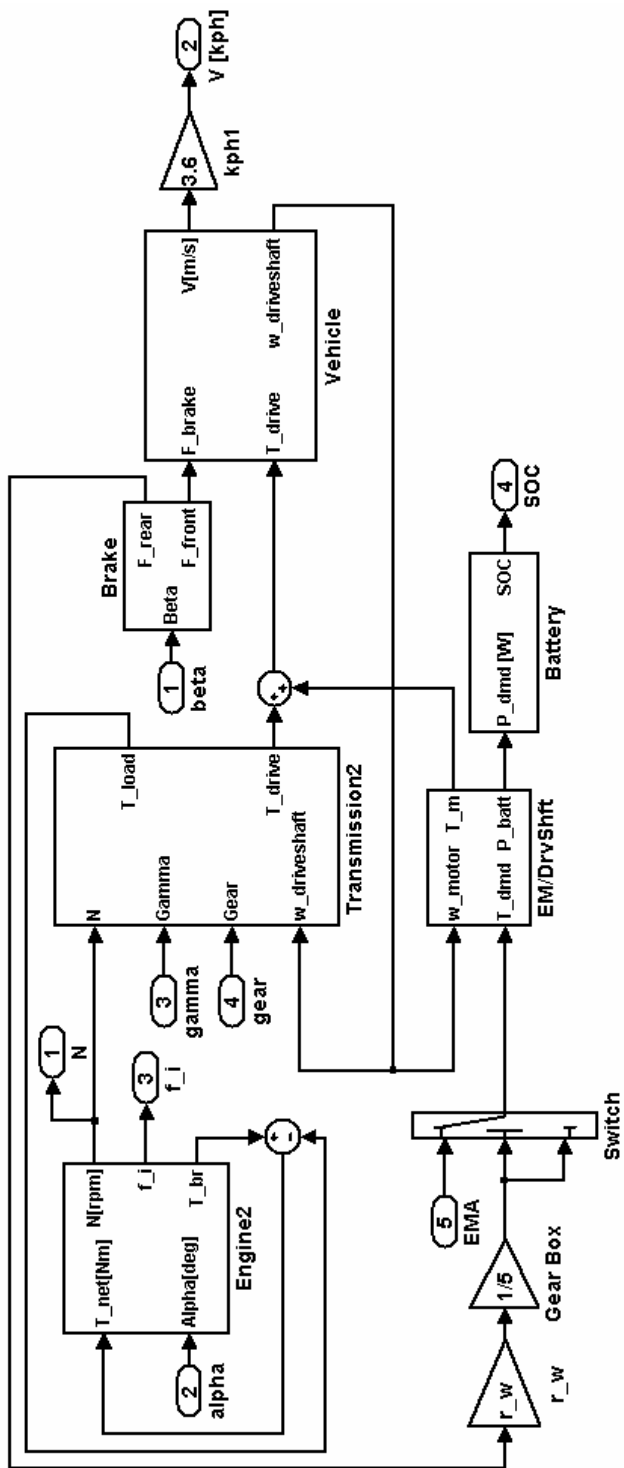


Fig 6.5 Simulink diagram of the HEV configuration P-4.

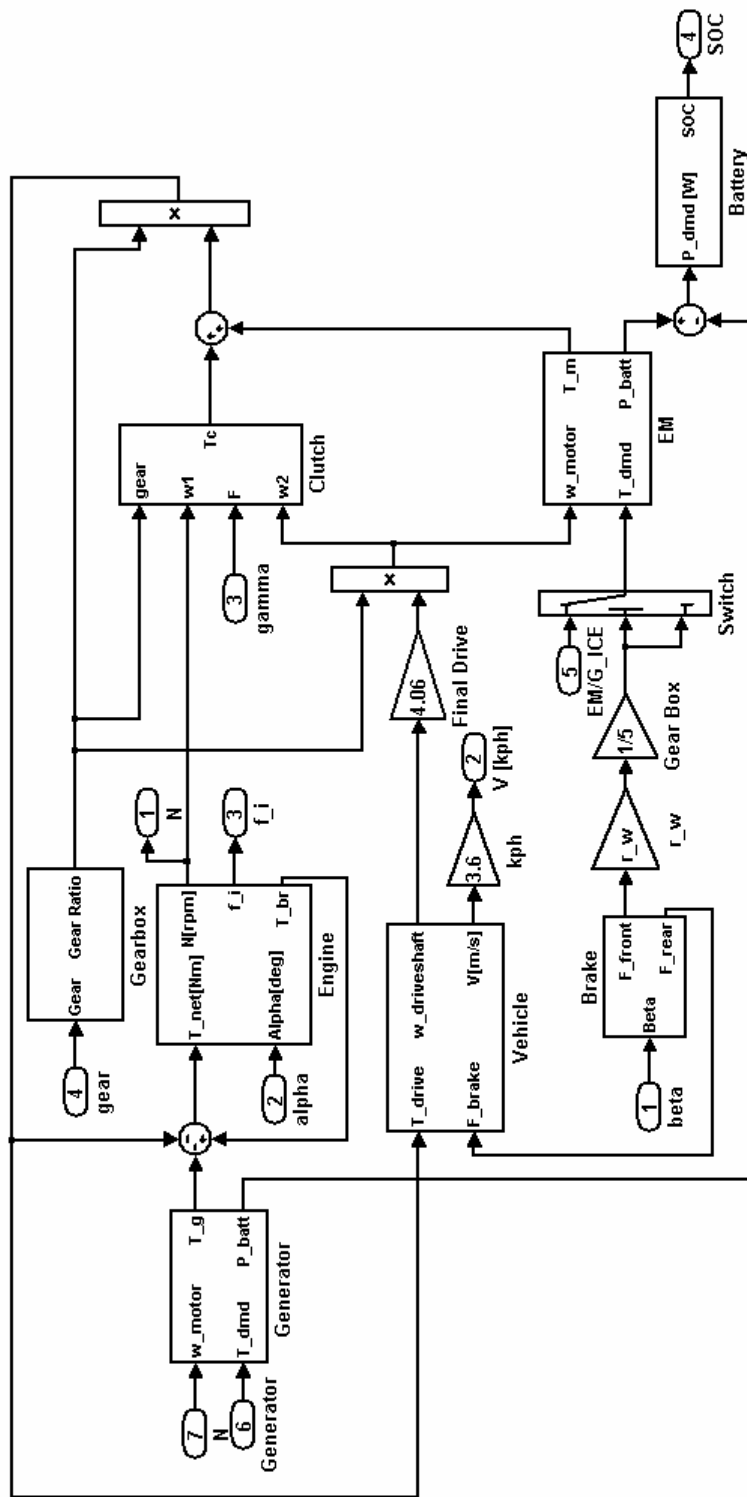


Fig 6.6 Simulink diagram of the HEV configuration SP-1.

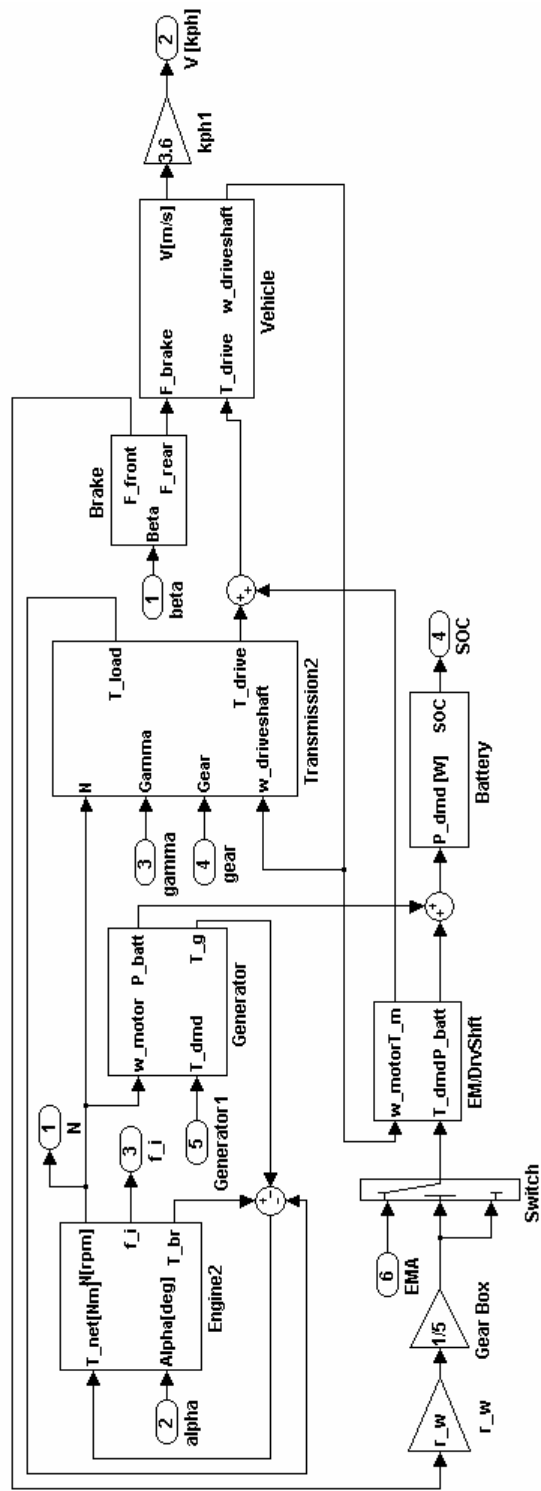


Fig 6.7 Simulink diagram of the HEV configuration SP-2.

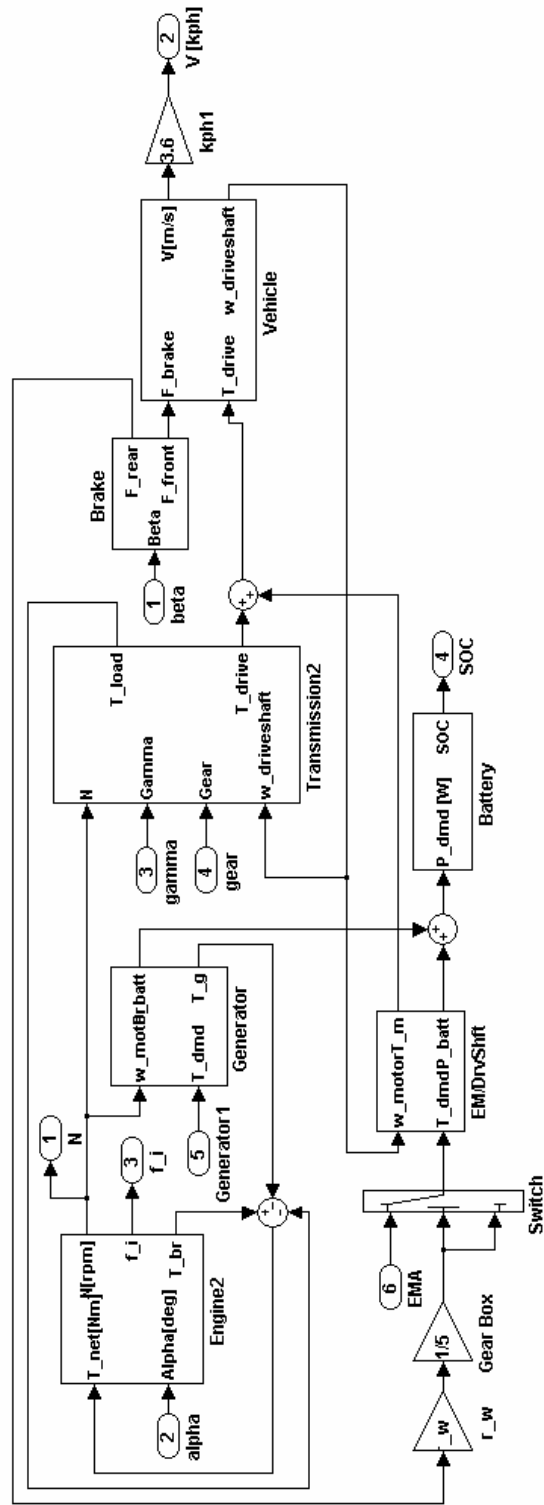


Fig 6.8 Simulink diagram of the HEV configuration SP-3.

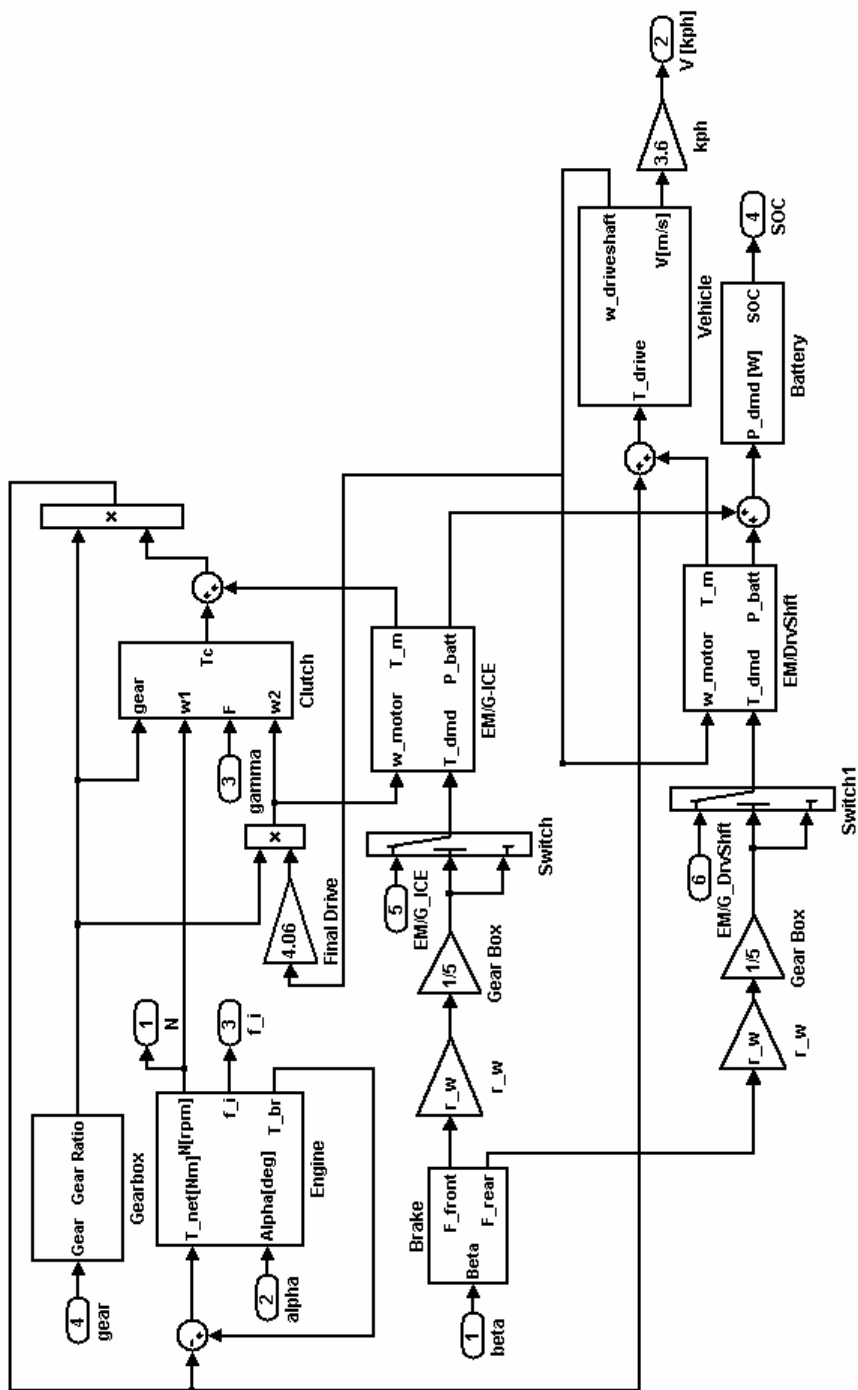


Fig 6.9 Simulink diagram of the HEV configuration C-1.

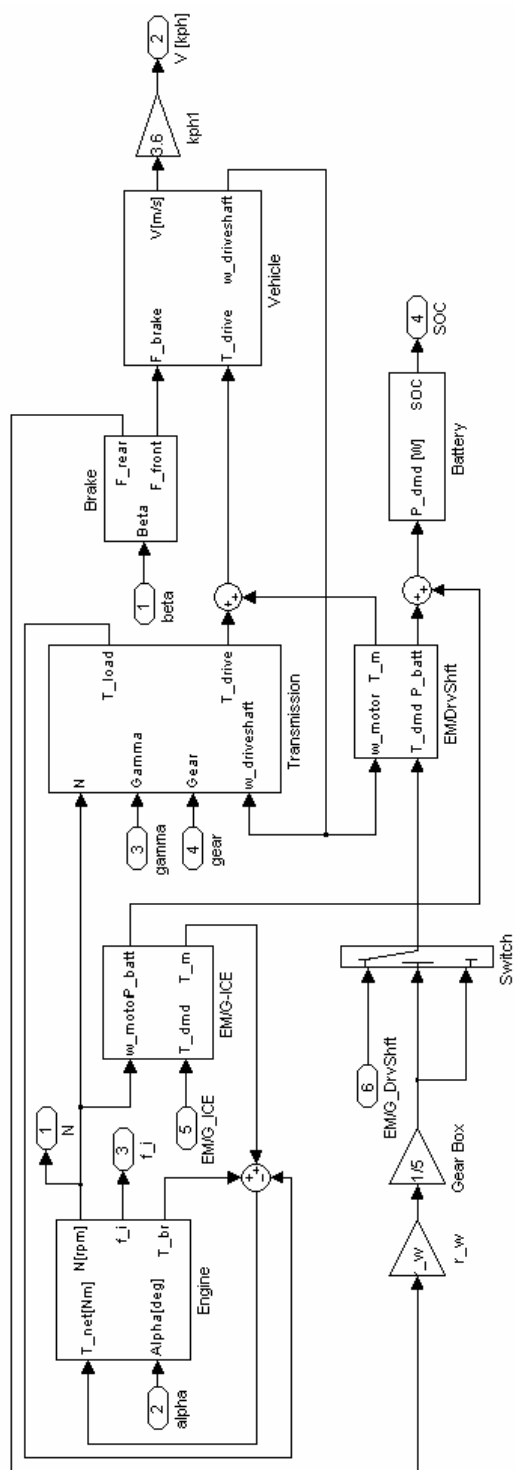


Fig 6.10 Simulink diagram of the HEV configuration C-2.

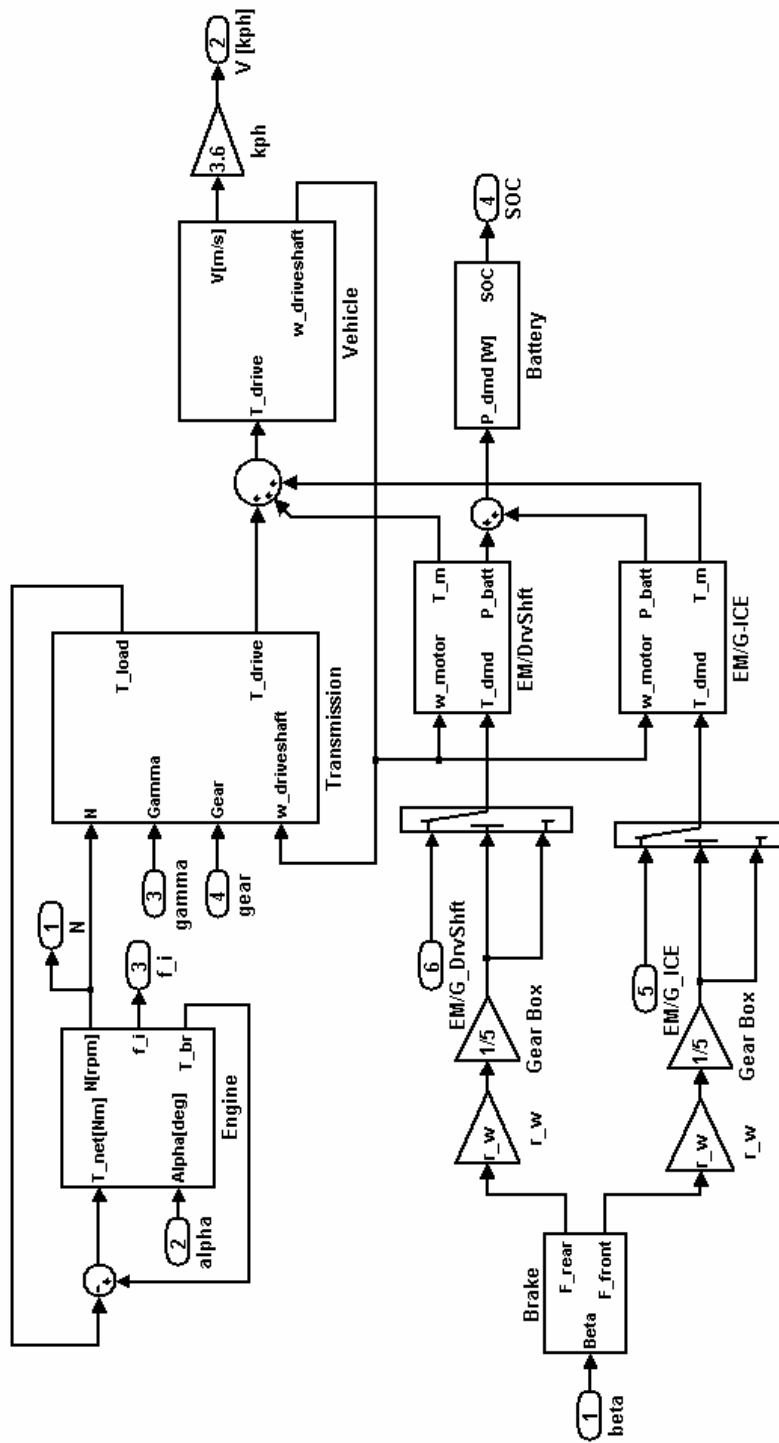


Fig 6.11 Simulink diagram of the HEV configuration C-3.

6.3 Simplified HEV Model

A simple model can be developed based on the power requirement of the target vehicle that is computed with the quasi-static power balance at a particular moment. Following the longitudinal vehicle model presented in Chapter 4, a plain model can be implemented as an efficient MATLAB code which in turn enables fast simulation on the available PC. Furthermore with the supplied diesel engine torque/speed vs. injected fuel data by Ford Otosan Co., which was mentioned in Chapter 4.2.2, is based on the fuel consumption of the diesel engine operating at the steady-state. Hence, it easily lends itself for a computational method which solely takes advantage of the quasi-static power balance of the target vehicle. The fuel map of 1.8 [liter] Ford Transit Connect (75[PS], 175[Nm]) diesel engine is utilized to accomplish the related simulations of the 10 different HEV configurations. The generalized HEV model is shown in Fig 6.12 which covers all of these designed HEV configurations.

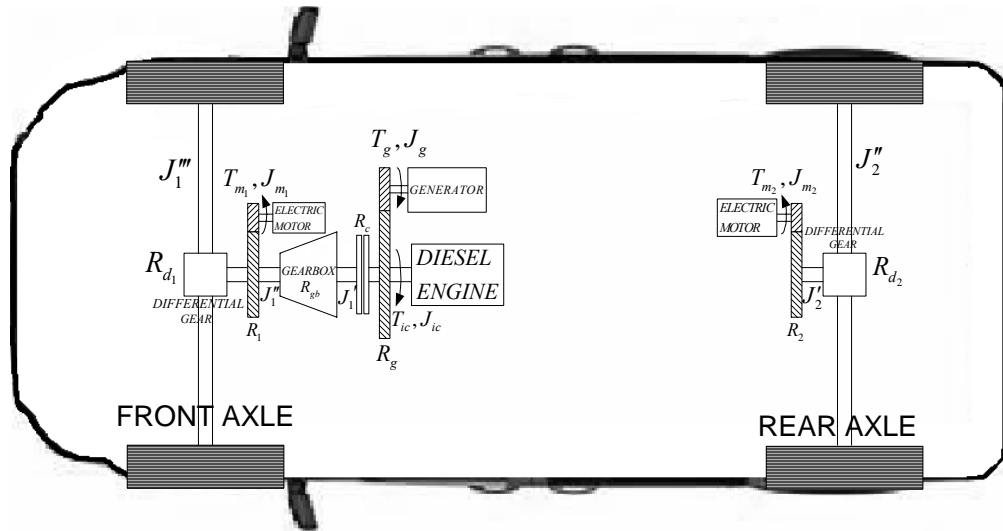


Fig 6.12 Generalized Vehicle Model.

The generalized vehicle model shown above can be modified to include all of the HEV models. In the developed generic MATLAB code, by omitting the related connections, desired HEV configuration could be assembled, which simplifies the simulations and decreases the preparation time for different kinds of HEV configurations. In Figs. 6.13-6.15, the front axle and rear axle of the generalized HEV model where the EM is behind gearbox is presented and the differential equations governing the dynamics of these axles are as follows:

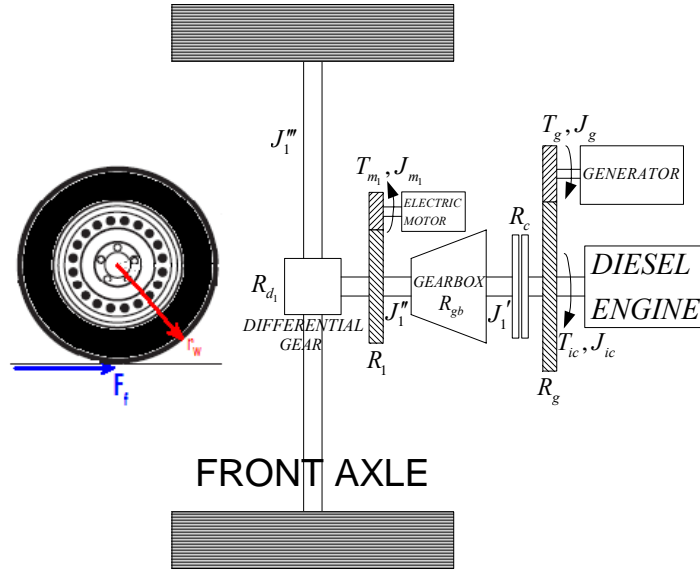


Fig. 6.13 Front axle of the generalized HEV (EM is behind the gearbox).

$$J_{e1} \frac{d\omega_1}{dt} + b_{e1} \omega_1 + T_{c1} \text{sgn}(\omega_1) = T_{m1} + \frac{R_c R_{gb}}{R_1} T_{ic} - \frac{R_c R_{gb}}{R_1 R_g} T_g - \frac{F_f r_w}{R_1 R_{d1}} \quad (6.1)$$

$$\omega_1 = \frac{v}{r_w} R_{d1} R_1 \quad (6.2)$$

The governing differential equation of the internal combustion engine side is:

$$\left(J_{ic} + \frac{J_g}{R_g^2} \right) \frac{d\omega_{ic}}{dt} + \left(b_{ic} + \frac{b_g}{R_g^2} \right) \omega_{ic} + \frac{T_g}{R_g} + \left(T_{ci} + \frac{b_{cg}}{R_g} \right) \text{sgn}(\omega_{ic}) = T_{ic} - R_c T_L \quad (6.3)$$

whereas the EM side has the following equation:

$$J_1 \frac{d\omega_1}{dt} + b_1 \omega_1 + T_{c_1} \text{sgn}(\omega_1) + \frac{F_f r_w}{R_1 R_{d_1}} = T_{m_1} + \frac{R_c R_{gb}}{R_1} T_L \quad (6.4)$$

where $J_{e_1} \triangleq J_{m_1} + \frac{J'_1 R_{gb}^2}{R_1^2} + \frac{J''_1}{R_1^2} + \frac{J'''_1}{R_1^2 R_{d_1}^2} + \frac{R_c R_{gb}^2}{R_1^2} J_{ic} + \frac{R_c R_{gb}^2}{R_1^2 R_g^2} J_g$ (6.5)

$$b_{e_1} \triangleq b_{m_1} + \frac{b'_1 R_{gb}^2}{R_1^2} + \frac{b''_1}{R_1^2} + \frac{b'''_1}{R_1^2 R_{d_1}^2} + \frac{R_c R_{gb}^2}{R_1^2} b_{ic} + \frac{R_c R_{gb}^2}{R_1^2 R_g^2} b_g \quad (6.6)$$

$$T_{c_1} \triangleq T_{cm_1} + \frac{T'_{c_1} R_{gb}}{R_1} + \frac{T''_{c_1}}{R_1} + \frac{T'''_{c_1}}{R_1 R_{d_1}} + \frac{R_c R_{gb}}{R_1} T_{ci} + \frac{R_c R_{gb}}{R_1 R_g} T_{cg} \quad (6.7)$$

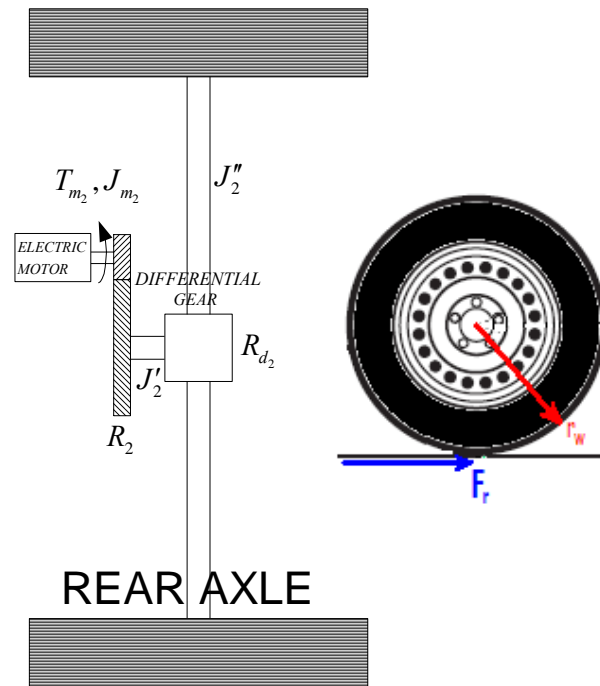


Fig. 6.14 Rear axle of the generalized HEV.

The rear axle has an EM coupled and the corresponding equations of motion are as follows:

$$J_{e_2} \frac{d\omega_2}{dt} + b_{e_2} \omega_2 + T_{c_2} \text{sgn}(\omega_2) + \frac{F_r r_w}{R_2 R_{d_2}} = T_{m_2} \quad (6.8)$$

$$\omega_2 = \frac{v}{r_w} R_{d_2} R_2 \quad (6.9)$$

where $J_{e_2} \triangleq J_{m_2} + \frac{J_2'}{R_2^2} + \frac{J_2''}{R_2^2 R_{d_2}^2}$ (6.10)

$$b_{e_2} \triangleq b_{m_2} + \frac{b_2'}{R_2^2} + \frac{b_2''}{R_2^2 R_{d_2}^2} \quad (6.11)$$

$$T_{c_2} \triangleq T_{cm_2} + \frac{T_{c_2}'}{R_2^2} + \frac{T_{c_2}''}{R_2^2 R_{d_2}^2} \quad (6.12)$$

$$\omega_2 = R_2 \omega_2' \quad (6.13)$$

$$\omega_2' = R_{d_2} \omega_2'' \quad (6.14)$$

Also the resistance forces acting on the vehicle are:

$$F_{resis} = F_r + F_f \\ = [(a + bv) Mg] + [\sin \theta Mg] + \left[\frac{1}{2} C_D A_D \rho v^2 \right] \quad (6.15)$$

When (6.1), (6.8) and (6.15) are combined, the driving torque needed by the vehicle in order to follow the power demanded by the driver could be computed as follows:

$$F_{drive} = M_{eq} \frac{dv}{dt} + C_{eq} v + (a + \sin \theta) \text{sgn}(v) Mg + \frac{1}{2} C_D A_D \rho v^2 + F_{brake} \\ = \frac{1}{r_w} [R_1 R_{d_1} T_{m_1} + R_2 R_{d_2} T_{m_2} + R_c R_{d_1} R_{gb} T_{ic} - \frac{R_c R_{gb} R_{d_1}}{R_g} T_g - R_2 R_{d_2} T_{c_2} \text{sgn}(v) \\ - R_1 R_{d_2} T_{c_1} \text{sgn}(v)] \quad (6.16)$$

where $M_{eq} = M + J_{e_1} \frac{R_1^2 R_{d_1}^2}{r_w^2} + J_{e_2} \frac{R_2^2 R_{d_2}^2}{r_w^2}$ (6.17)

$$C_{eq} = bMg + b_{e_1} \frac{R_1^2 R_{d_1}^2}{r_w^2} + b_{e_2} \frac{R_2^2 R_{d_2}^2}{r_w^2} \quad (6.18)$$

Note that the equations presented above can be used to represent all configurations except P-2 and C1. Unfortunately, the front axles of these configurations are inherently different than the previous ones owing to the fact that an EM is located at the engine side, in front of the clutch as illustrated in Fig 6.16.

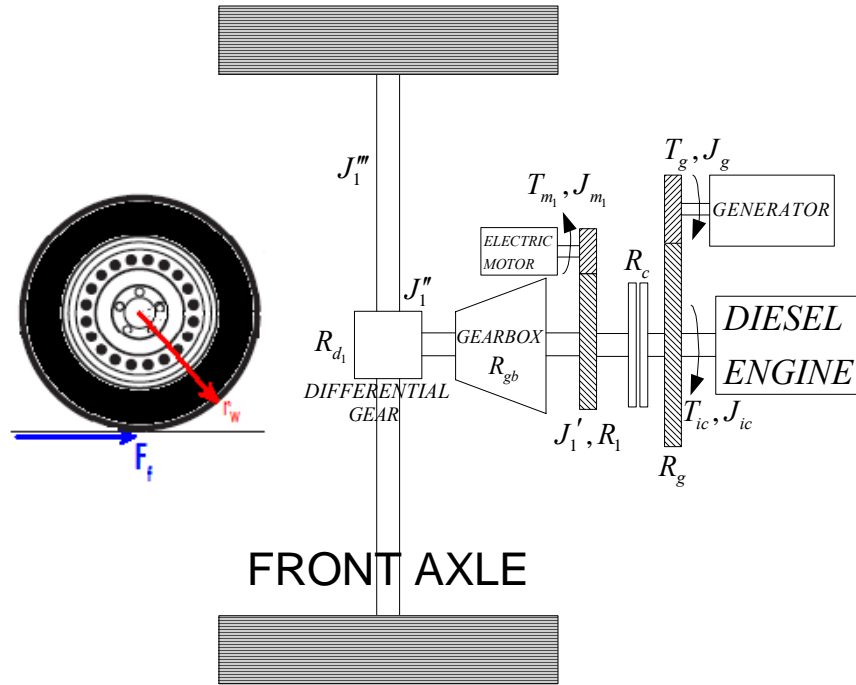


Fig. 6.15 Front axle of the generalized HEV (EM is between gearbox and clutch).

Hence, a new set of equations must be formed to accommodate this situation:

$$J_{e_1} \frac{d\omega_1}{dt} + b_{e_1} \omega_1 + T_{c_1} \text{sgn}(\omega_1) = T_{m_1} + R_c R_1 T_{ic} - \frac{R_c R_1}{R_g} T_g - \frac{F_f r_w R_1}{R_{d_1} R_{gb}} \quad (6.19)$$

$$\omega_1 = \frac{v}{r_w} \cdot \frac{R_{d_1} R_{gb}}{R_1} \quad (6.20)$$

The governing differential equation of the internal combustion engine side is:

$$\left(J_{ic} + \frac{J_g}{R_g^2} \right) \frac{d\omega_{ic}}{dt} + \left(b_{ic} + \frac{b_g}{R_g^2} \right) \omega_{ic} + \frac{T_g}{R_g} + \left(T_{ci} + \frac{b_{cg}}{R_g} \right) \text{sgn}(\omega_{ic}) = T_{ic} - R_c T_L \quad (6.21)$$

whereas the EM side has the following equation:

$$J_1 \frac{d\omega_1}{dt} + b_1 \omega_1 + T_{c_1} \text{sgn}(\omega_1) + \frac{F_f r_w R_1}{R_{d_1} R_{gb}} = T_{m_1} + R_c R_1 T_L \quad (6.22)$$

$$\omega_1 = \frac{\omega_{ic}}{R_1} \quad (6.23)$$

$$\text{where } J_{e_1} \triangleq J_{m_1} + J_1' R_1^2 + \frac{J_1'' R_1^2}{R_{gb}^2} + \frac{J_1''' R_1^2}{R_{d_1}^2 R_{gb}^2} + R_c R_1^2 J_{ic} + \frac{R_c R_1^2}{R_g^2} J_g \quad (6.24)$$

$$b_{e_1} \triangleq b_{m_1} + b_1' R_1^2 + \frac{b_1'' R_1^2}{R_{gb}^2} + \frac{b_1''' R_1^2}{R_{d_1}^2 R_{gb}^2} + R_c R_1^2 b_{ic} + \frac{R_c R_1^2}{R_g^2} b_g \quad (6.25)$$

$$T_{c_1} \triangleq T_{cm_1} + T_{c_1}' R_1 + \frac{T_{c_1}'' R_1}{R_{gb}} + \frac{T_{c_1}''' R_1}{R_{gb} R_{d_1}} + R_c R_1 T_{ic} + \frac{R_c R_1}{R_g} T_{cg} \quad (6.26)$$

When (6.1), (6.8) and (6.19) are combined, the driving torque needed by the vehicle in order to follow the power demanded by the driver could be computed as follows:

$$F_{drive} = M_{eq} \frac{dv}{dt} + C_{eq} v + (a + \sin \theta) \text{sgn}(v) Mg + \frac{1}{2} C_D A_D \rho v^2 + F_{brake} \quad (6.27)$$

$$\text{where } M_{eq} = M + J_{e_1} \frac{R_{d_1}^2 R_{gb}^2}{r_w^2 R_1^2} + J_{e_2} \frac{R_2^2 R_{d_2}^2}{r_w^2} \quad (6.28)$$

$$C_{eq} = bMg + b_{e_1} \frac{R_{d_1}^2 R_{gb}^2}{r_w^2 R_1^2} + b_{e_2} \frac{R_2^2 R_{d_2}^2}{r_w^2} \quad (6.29)$$

Notice that, in this simplified model, the clutch dynamics becomes irrelevant by taking $R_c = 1$ when it is engaged and thus it is not included in this quasi-static model. For a given vehicle speed (v) and acceleration/deceleration (dv/dt), the driving force (F_{drive}) can be easily calculated using (6.16) or (6.27) according to the target HEV configuration. Once the EM assistance torques (T_{m_1}, T_{m_2}) are specified, one could compute the corresponding torque to be supplied by the diesel engine (T_{ic}):

$$T_{ic} = \frac{1}{R_c R_{d_1} R_{gb}} \left[F_{drive} r_w - R_1 R_{d_1} T_{m_1} - R_2 R_{d_2} T_{m_2} + \frac{R_c R_{gb} R_{d_1}}{R_g} T_g \right] \quad (6.30)$$

Since the crank shaft speed (ω_{ic}) can be determined via corresponding kinematic relationship, the fuel consumption of the diesel engine may be assessed via the fuel map (Fig 4.8) which solely depends on T_{ic} and ω_{ic} .

$$\dot{m}_f = f(T_{ic}, \omega_{ic}) \quad (6.31)$$

Similarly, the demanded battery power can be calculated as a function of the specified EM torques and speeds:

$$P_{batt} = \frac{T_{m_1} \omega_{m_1}}{\eta_{e_1}} + \frac{T_{m_2} \omega_{m_2}}{\eta_{e_2}} - T_g \omega_g \eta_{eg} \quad (6.32)$$

where η_{e_1} , η_{e_2} and η_{eg} are the electrical efficiencies of the corresponding systems. Since the battery voltage assumed constant throughout the operation, the battery current becomes:

$$I_{batt} = \frac{P_{batt}}{V_{batt} \eta_{conv}} \quad (6.33)$$

where η_{conv} is the efficiency of the DC-DC power converter managing the battery current (charge) as well as the DC link voltage. Note that the shaft speeds of the electrical machines can be directly calculated by applying the relevant kinematic relationships presented in Equations (6.2), (6.9) and (6.20).

6.4 Simulation Study

As mentioned in the previous chapters, the drivetrain components are modeled in order to compose the targeted ten HEV configurations for evaluating their fuel consumption performance in some driving cycle simulations. The reader is encouraged to refer to Chapter 2 for the schematics of these configurations.

6.4.1 Simulation of HEV Configurations with Elaborate Physical models

Due to increased complexity of Simulink models and the corresponding time restrictions imposed by them, simulating all of the ten HEV configurations becomes an extremely time consuming and tedious job. Therefore, to overcome this limitation, one of HEV configuration (P-4), which seems to be the most promising design for Ford Otosan Co., is considered for the simulation in the urban city cruising.

Notice that, at the beginning of this study, a conventional Ford Tourneo Connect with spark-ignition engine is considered for HEV application. Therefore, a corresponding model (EMs, lead-acid battery pack, etc.) was developed for the purpose of modeling an entire family (configurations) of hybrid Ford Tourneo Connect vehicles. The vehicle to be simulated, which has the advantage of easy conversion from a conventional one, has the following properties:

- *Engine* :
 - 1.8 [l] Spark Ignition Engine
 - 85 [kW] at 5300 [rpm]
- *Vehicle* :
 - Load : 200 [kg]
 - Driver + 1 Passenger (2×70 kg)
- *Electric Motor*:
 - 12 [kW] with Gearbox (5:1)
 - Assembled to the rear wheel shaft
- *Battery Pack*:
 - Lead-Acid Battery
 - 25 A-h, 318-Volts

6.4.1.1 Simulation Study in ECE Cycle

To evaluate the performance of the HEV discussed in the previous section, a standard driving cycle, which constitutes acceleration, deceleration and steady-state driving conditions at various vehicle speeds, is considered. This cycle is the ECE-15 urban cycle is discussed fully in Appendix C. Hence, the fuel consumption along

with the corresponding charge state of the batteries is assessed to make a fair comparison among the performances of the hybrid vehicles and the conventional one.

In the simulation, there exist several alternatives to perform different driving conditions for a HEV. Hence depending on the charge state of the battery pack, seven different operating modes associated with HEV could be observed. Fig 6.16 illustrates these operating modes. These modes are as follows:

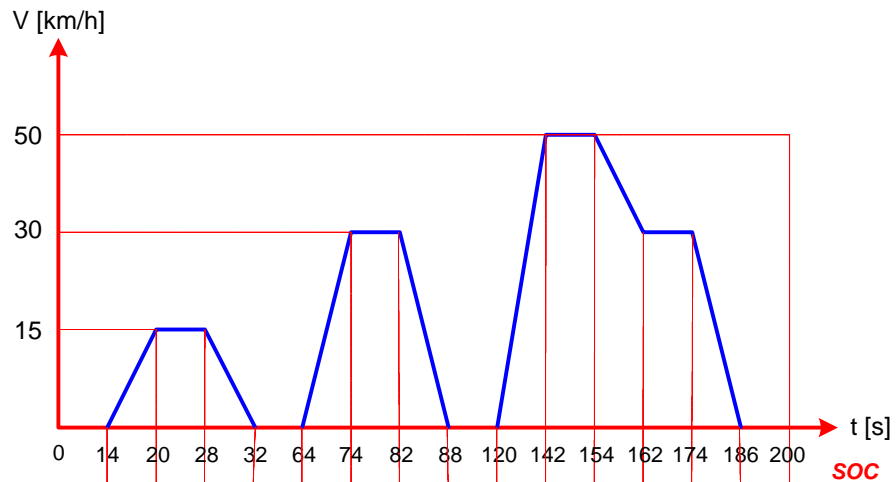
- **Motor assisted acceleration:** In this operating mode, an extra boost to the internal combustion engine is provided by the electric motor to accelerate the vehicle to the target speed. This operating mode is extremely important as the ICE is known to consume a relatively large amount of fuel at such transient regimes and thus it is not very efficient.
- **Motor only operation:** As mentioned in Chapter 3, the electric motors are capable of delivering 2-3 times of their rated torque at short intervals and thus this feature makes EMs very attractive for accelerating the vehicle to higher speeds. Note that EMs can operate at higher speeds and deliver sufficient torque at such speeds. Therefore they can be used to operate the vehicle in city where the average speed of the vehicle is relatively low (about 30 [km/h]) and interrupted driving is common.
- **ICE only operation:** In a HEV, main power source is the internal combustion engine. Because the energy stored in the battery cannot sustain the operation of the EM for long periods of time. Thus it is advantageous to use the ICE at the constant speeds (steady-state driving).
- **Regenerative braking:** Since EMs can be used as generators, some of the kinetic energy of the HEV can be recovered while the vehicle is decelerating. Unfortunately, the kinetic energy at high speeds is usually too large and hence the EM operating as generator cannot recover this energy in a short amount of time. Thus, the HEV should rely on mechanical brakes to stop the

vehicle in such cases. In Chapter 4, regenerative braking was discussed in detail.

- **ICE Idle / ICE Off:** During city cruising, it is a common occurrence that the vehicle stops and waits for short intervals of time (traffic jam, traffic light stop, etc.). In such situations, the engine is generally not turned off and consumes some amount of fuel in a conventional vehicle. On the other hand, in HEV, the engine could be turned off for long periods of time owing to the fact that the EM can be conveniently used to drive the vehicle in such interrupted driving regimes.
- **Battery charging during driving:** If the battery charge is relatively low, the EMs cannot be utilized. Hence, it could be solely used to recharge the battery itself. During driving cycle, EM acting as a generator draws power from the engine to restore the battery charge state to a tolerable level. Consequently, the fuel consumption of the ICE increases dramatically for the sake of recharging.

In the conducted simulation, these HEV operation modes are adapted to the ECE-15 cycle. As a result, nine different cases of power management schemes are encountered. In fact, each scheme represents an appropriate power management strategy determined by the current charge level of the battery. For instance, if the battery charge is too low (about 60-65%), it would be inadvisable to use the EM which will in turn push the charge level into a dangerous operating zone. Thus, one needs to recharge the battery by drawing power from the ICE throughout the driving cycle which corresponds to the power management case 9 and if the battery charge is very high (about 95 %), case 1 can be chosen. Consequently, the HEV controller can be extravagant in using the EM throughout the driving cycle, which will in turn reduce the fuel consumption of the vehicle. Fig 6.16 illustrates the operating modes inside the power management paradigms as applied to various intervals associated with the urban driving cycle. Note that in this table, the following abbreviations are employed to represent various operating modes:

1. *Electric Motor Only* (M)
2. *Internal Combustion Engine Only* (E)
3. *Dual Powered Driving* (A)
4. *Internal Combustion Engine OFF* (O)
5. *Regenerative Braking* (R)
6. *Internal Combustion Engine IDLE* (I)
7. *Battery Charging during Driving* (G)



	SOC															
Conventional	I	E	E	I	I	E	E	I	I	E	E	I	E	I	I	N/A
Case 1	O	M	M	R	O	M	M	R	O	A	E	R	M	R	O	Very High
Case 2	O	M	M	R	O	M	A	R	O	A	E	R	A	R	O	High
Case 3	I	M	M	R	I	M	A	R	I	A	A	R	A	R	I	High
Case 4	O	M	M	R	O	A	M	R	O	A	E	R	E	R	O	Medium-High
Case 5	I	M	M	R	I	A	M	R	I	A	E	R	E	R	I	Medium-High
Case 6	I	A	E	R	I	A	E	R	I	A	E	R	E	R	I	Medium
Case 7	O	A	G	R	O	A	G	R	O	A	G	R	G	R	O	Low-Medium
Case 8	I	G	G	R	I	G	G	R	I	E	G	R	G	R	I	Very Low
Case 9	I	E	E	R	I	E	E	R	I	E	E	R	E	R	I	Low

Fig. 6.16 Nine Different Operating Modes.

6.4.1.2 Simulation Results

To make a fair comparison, a conventional vehicle is first simulated within the context of the ECE-15 cycle. The simulation parameters used in the study are as follows:

- Runge-Kutta 5 (Dormand-Prince) is utilized as the integration algorithm
- During simulation, fixed time step is used, which has the value $T = 0.001[s]$.
Maximum simulation time performed is $T_{\max} = 300 [s]$.

Similarly, the HEV discussed in Art. 6.4.1.1, is simulated for these operating modes. The simulation results associated with these modes are tabulated in Tables 6.1-6.4.

Figs 6.17-6.21 show the dynamic behaviors of both HEV and conventional one at various instances at the ECE cycle. It is obvious from Fig 6.17 that motor assist makes a significant difference in the fuel consumption of the ICE owing to the fact that ICE behaves very poorly at transient regimes. Notice that to make a fair comparison between them, the vehicle and the engine speeds have to be meticulously matched and the driver should not experience any change in the dynamic behaviors of both vehicles. During the motor assisted driving modes, the power supplied by the electric motor is illustrated in the Fig 6.20 while the corresponding SOC is shown in Fig 6.21. It is critical to note that the rated nominal power of the EM is 12 [kW] in this case. The maximum power supplied by the motor only reached half of the rated one.

Table 6.1. Injected Fuel Rate [g/s].

time [s]	0-14	14-20	20-28	28-32	32-64	64-74	74-82	82-88	88-120	120-142	142-154	154-162	162-174	174-186	186-200
Speed [kph]	0	7.5	15	7.5	0	15	30	15	0	25	50	40	30	15	0
Duration [s]	14	6	8	4	32	10	8	6	32	22	12	8	12	12	14
Case 0	0.16	0.662	0.35	0.16	0.16	0.816	0.5	0.16	0.16	0.947	0.54	0.16	0.33	0.16	0.16
Case 1	0	0	0	0.16	0	0	0	0.16	0	0.392	0.54	0.16	0	0.16	0
Case 2	0	0	0	0.16	0	0	0.28	0.16	0	0.392	0.54	0.16	0.169	0.16	0
Case 3	0.16	0	0	0.16	0.16	0	0.28	0.16	0.16	0.392	0.169	0.16	0.169	0.16	0.16
Case 4	0	0	0	0.16	0	0.409	0	0.16	0	0.392	0.54	0.16	0.33	0.16	0
Case 5	0.16	0	0	0.16	0.16	0.409	0	0.16	0.16	0.392	0.54	0.16	0.33	0.16	0.16
Case 6	0.16	0.551	0.35	0.16	0.16	0.409	0.5	0.16	0.16	0.392	0.54	0.16	0.33	0.16	0.16
Case 7	0	0.551	0.59	0.16	0	0.409	1.15	0.16	0	0.392	1.33	0.16	0.475	0.16	0
Case 8	0.16	0.759	0.59	0.16	0.16	0.816	1.15	0.16	0.16	0.947	1.33	0.16	0.475	0.16	0.16
Case 9	0.16	0.662	0.35	0.16	0.16	0.816	0.5	0.16	0.16	0.947	0.54	0.16	0.33	0.16	0.16

Table 6.2. Fuel Consumption [l/100km].

time [s]	0-14	14-20	20-28	28-32	32-64	64-74	74-82	82-88	88-120	120-142	142-154	154-162	162-174	174-186	186-200
Speed [kph]	0	7.5	15	7.5	0	15	30	15	0	25	50	40	30	15	0
Duration [s]	14	6	8	4	32	10	8	6	32	22	12	8	12	12	14
Case 0	N/A	37.829	10.11	9.143	N/A	23.31	7.114	4.571	N/A	16.23	4.63	1.714	4.72	4.58	N/A
Case 1	N/A	0	0	9.143	N/A	0	0	4.571	N/A	6.72	4.63	1.714	0	4.58	N/A
Case 2	N/A	0	0	9.143	N/A	0	3.986	4.571	N/A	6.72	4.63	1.714	2.42	4.58	N/A
Case 3	N/A	0	0	9.143	N/A	0	3.986	4.571	N/A	6.72	1.45	1.714	2.42	4.58	N/A
Case 4	N/A	0	0	9.143	N/A	11.69	0	4.571	N/A	6.72	4.63	1.714	4.72	4.58	N/A
Case 5	N/A	0	0	9.143	N/A	11.69	0	4.571	N/A	6.72	4.63	1.714	4.72	4.58	N/A
Case 6	N/A	31.486	10.11	9.143	N/A	11.69	7.114	4.571	N/A	6.72	4.63	1.714	4.72	4.58	N/A
Case 7	N/A	31.486	16.71	9.143	N/A	11.69	16.43	4.571	N/A	6.72	11.4	1.714	6.79	4.58	N/A
Case 8	N/A	43.343	16.71	9.143	N/A	23.31	16.43	4.571	N/A	16.23	11.4	1.714	6.79	4.58	N/A
Case 9	N/A	37.829	10.11	9.143	N/A	23.31	7.114	4.571	N/A	16.23	4.63	1.714	4.72	4.58	N/A

Table 6.3. State-of-Charge Change [%].

time [s]	0-14	14-20	20-28	28-32	32-64	64-74	74-82	82-88	88-120	120-142	142-154	154-162	162-174	174-186	186-200
Speed [kph]	0	7.5	15	7.5	0	15	30	15	0	25	50	40	30	15	0
Duration [s]	14	6	8	4	32	10	8	6	32	22	12	8	12	12	14
Case 0	N/A														
Case 1	0	-0.08	-0.01	0.03	0	-0.18	-0.03	0.06	0	-0.27	0	0.04	-0.03	0.02	0
Case 2	0	-0.08	-0.01	0.03	0	-0.18	-0.02	0.06	0	-0.27	0	0.04	-0.05	0.02	0
Case 3	0	-0.08	-0.01	0.03	0	-0.18	-0.02	0.06	0	-0.27	-0.01	0.04	-0.05	0.02	0
Case 4	0	-0.08	-0.01	0.03	0	-0.08	-0.03	0.06	0	-0.27	0	0.04	0	0.02	0
Case 5	0	-0.08	-0.01	0.03	0	-0.08	-0.03	0.06	0	-0.27	0	0.04	0	0.02	0
Case 6	0	-0.01	0	0.03	0	-0.08	0	0.06	0	-0.27	0	0.04	0	0.02	0
Case 7	0	-0.01	0.02	0.03	0	-0.08	0.03	0.06	0	-0.27	0.12	0.04	0.03	0.02	0
Case 8	0	0.01	0.02	0.03	0	0.02	0.03	0.06	0	0	0.12	0.04	0.03	0.02	0
Case 9	0	0	0	0.03	0	0	0	0.06	0	0	0	0.04	0	0.02	0

Table 6.4. Critical results obtained in the simulation.

	Charge Level	Fuel Consumption [l/100km]	ΔSOC [%]	ΔSOC in 3 hours [%]	Time to discharge (charge) [hours]
Conventional	NA	11.13		N/A	
Case 1	Very High	3.18	-0.45	-24.3	4.94
Case 2	High	3.86	-0.46	-24.84	4.83
Case 3	High	5.5	-0.47	-25.38	4.73
Case 4	Medium → High	4.47	-0.32	-17.28	6.94
Case 5	Medium → High	6.82	-0.32	-17.28	6.94
Case 6	Medium	8.43	-0.21	-11.34	10.58
Case 7	Low → Medium	9.0	-0.01	-0.54	222.2
Case 8	Very Low	14.14	0.38	20.52	(5.85)
Case 9	Low	11.13	0.15	8.1	(14.82)

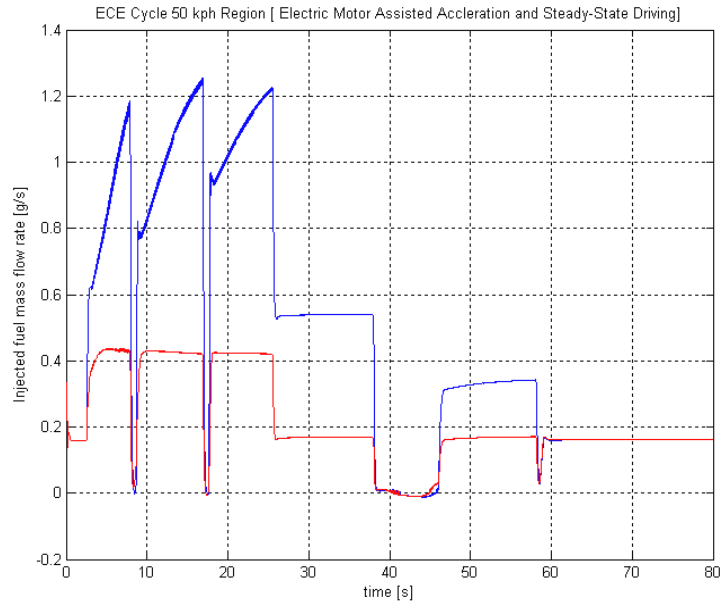


Fig. 6.17 Injected Fuel Rate of EM assisted urban cruising cycle.

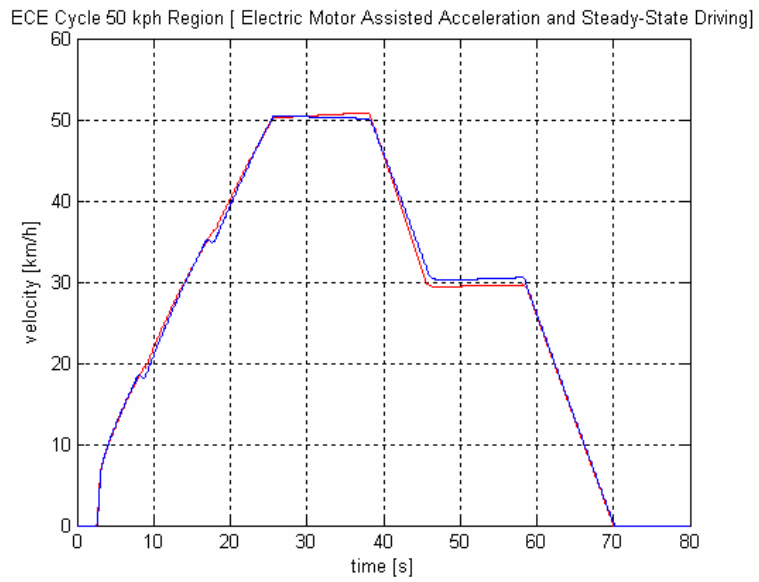


Fig. 6.18 Velocity Profile of EM assisted urban cruising cycle.

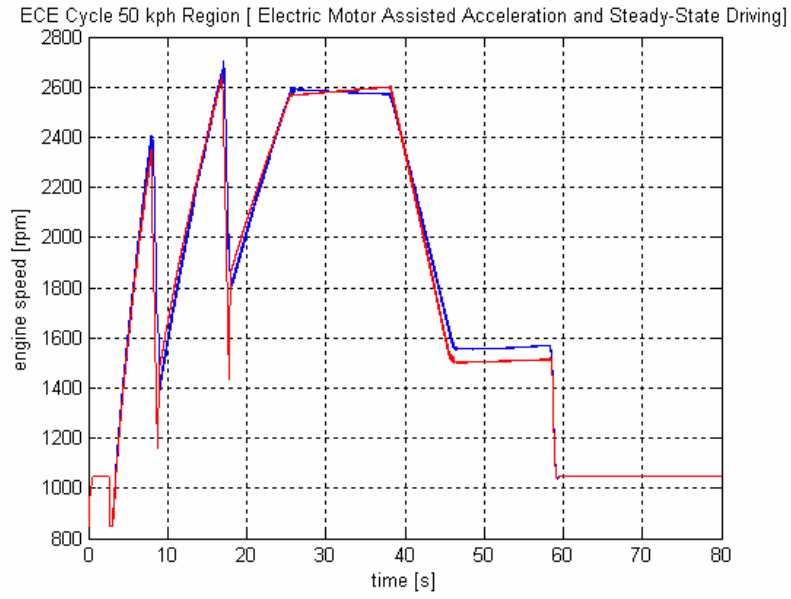


Fig. 6.19 Engine Speed Variation in EM assisted urban cycle.

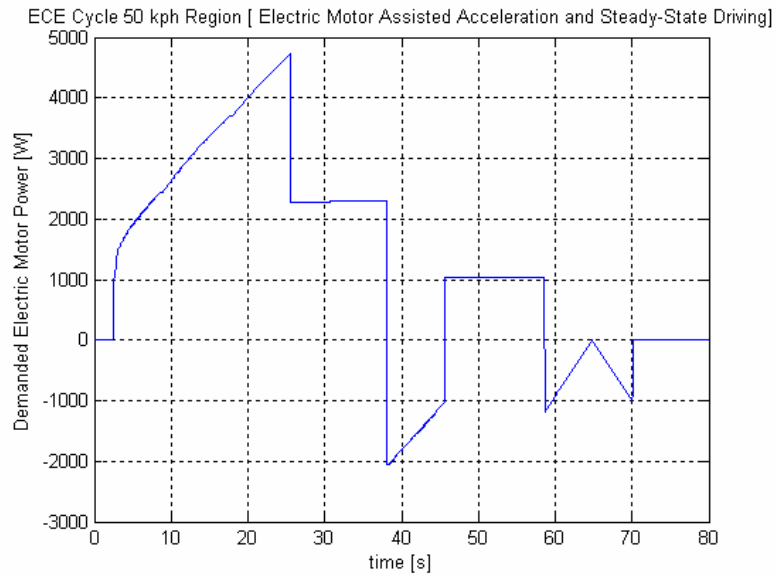


Fig. 6.20 Demanded Power of EM in urban cruising cycle.

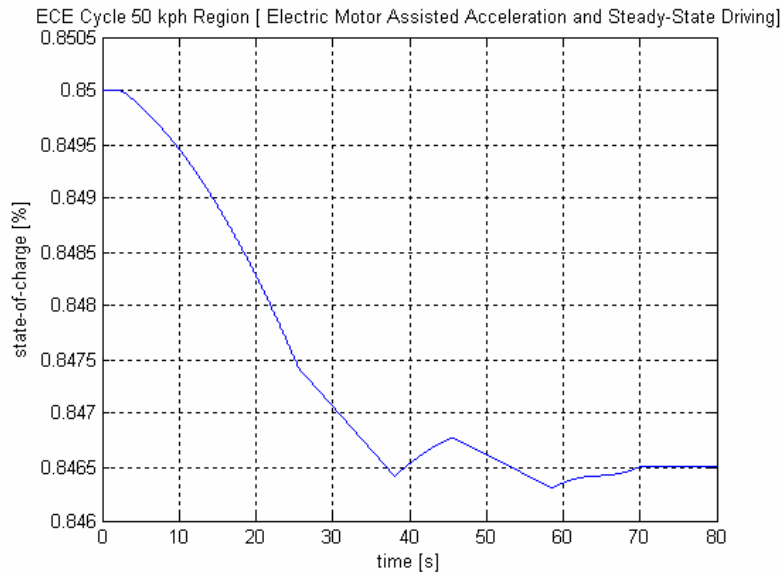


Fig. 6.21 SOC of the Battery in urban cruising cycle.

From the simulation data, it was observed that depending on the operating mode of the HEV, the fuel consumption of the simulated vehicle has varied within a large range. In the simulation, the battery SOC was also monitored. Not surprisingly, for EM heavy cases, the battery charge was to be depleted within five hours of city cruising. Hence various power management strategies had to be employed side by side for maximum fuel efficiency.

After simulation of P-4, other configurations were taken into consideration. C-3 was first to be considered, however simulation of the 50 [km/h] region of ECE Cycle took about 6 hours to be completed after arranging the proper driver commands. Therefore, a simple but effective HEV model was needed to accomplish around 300 simulations in order to evaluate the proposed HEV designs. Next section presents the simulation of them with the simplified HEV model.

6.4.2 Simulation of HEV Configurations with Simplified Model

As mentioned earlier, a simulation through complex physical model is proven to be quite ineffective due to large amount of time required to complete even a short simulation. Therefore, simplified models discussed in Art. 6.3 are considered.

In the comparative simulation studies, the dynamic performances of ten different HEV configurations have been taken into account and are tested in detail by evaluating their performance (fuel economy and battery SOC). The common properties of the simulated vehicles are as follows:

- *Engine* :
 - 1800 [cc] Diesel Engine
 - 75 [PS]
- *Vehicle* :
 - Gross Vehicle Mass : 1450 [kg]
 - Load : 200[kg]
 - Driver + 1 Passenger (2 x 70 kg)
 - CD : 0.373
- *Electric Motor*:
 - 8-12-16 [kW]
 - Rated Speed : 100 [rad/s]
- *Battery Pack*:
 - 42 V – 1300 Watt-h
 - Mass : 200 [kg]

Two distinct cases are studied: city and highway. In city cruising, standard ECE-15 Urban Cycle, which is elaborated in the Appendix C, is considered. Similarly, to test the highway performance of the simulated vehicle, a custom highway driving cycle, which is also discussed in Appendix C, is formed. As can be seen from Fig C.2 that

this cycle exhibits aggressive driving features owing to the fact that acceleration and deceleration can be as high as $1 \text{ [m/s}^2\text{]}$. In the simulation cases two aspects of HEVs are investigated:

- **Electric Motor Assistance (EMA)**: During acceleration, EM(s) provide(s) an extra power boost to the vehicle. Similarly EMs are utilized to pump up the kinetic energy to the battery while deceleration.
- **Battery Charging**: At the steady-state, the EMs/generators are employed as generators so as to replenish the battery charge. At the same time, regenerative braking is in place as well.

It should be noted that, in EMA cases, vehicles with electric motors of various power ratings are considered which are shown in Table 6.5:

Table 6.5 Power ratings of EMs

Rated Torque [Nm]	80	120	160
Rated Speed [rad/s]	100	100	100
Nominal Power [kW]	8	12	16

While EMA mode; a fraction (0%, 25%, 50%, 75%, 100%) of the demanded power in order to drive the vehicle is supplied from the both EMs. Note that, in HEV configurations with a generator, the corresponding rating of the machine is just like the ones given in the Table 6.5.

For the self-containment of this work, all simulation data obtained are given in the Appendix A. As can be seen from the tabulated data, higher the EM assistance, lower the fuel consumption. This is due to the fact that at transient state, the diesel engine is quite inefficient. Unfortunately, higher motor assistance also leads to fast depletion of battery charge. Thus, one needs to consider the conservation of the battery charge in the long run. The price to be paid here is the increased fuel consumption. Moreover, the fractions shown in the accompanying tables correspond to the

percentage (20%, 60%, and 100%) of the nominal power being drawn by the generator from the diesel engine in the generation mode during cruising at constant speed.

Tables 6.6-6.7 summarize the critical simulation results for the above mentioned driving cycles. Since the fuel efficiency of the hybrid electric vehicle tends to improve as the power rating of its EMs goes up, only the simulation results associated with HEV designs containing 16 [kW] electric motors are presented in these tables. Here, the mean fuel consumption, which is measured in [l/100km], refers to the calculated value at the end of the simulation cycles. Similarly, the SOC, which is the integral of the battery current, represents the deviation of the final battery charge state from the initial one. The positive values in the SOC change column indicate the battery is charged due to either regenerative braking or generation during cruising through the electrical machines. Also another important notice for the simulation is that the ICE is stopped during the idling periods, which increased fuel efficiency of the HEV configurations.

Table 6.6 Critical results related with urban cruising.

Config.	Mean Fuel Consumption [l/100 km]	Δ SOC [%]	Mean Fuel Consumption [l/100 km]	Δ SOC [%]
P-1	3.1244	-0.073036	11.913	0.057636
P-2	3.1278	-0.086595	11.905	0.10038
P-2	3.529	-0.05452	12.006	0.11285
P-4	3.529	-0.055965	12.006	0.1114
SP-1	3.2132	-0.086051	12.096	0.066916
SP-2	3.5897	-0.053971	12.149	0.079383
SP-3	3.6853	-0.056112	12.363	0.077242
C-1	2.7973	-0.14164	17.578	0.21213
C-2	2.6954	-0.12915	17.413	0.16889
C-3	2.7319	-0.10959	17.469	0.22467

Table 6.7 Critical results related with highway cruising.

Config.	Mean Fuel Consumption [l/100 km]	Δ SOC [%]	Mean Fuel Consumption [l/100 km]	Δ SOC [%]
P-1	7.8486	-0.36187	11.521	0.73192
P-2	7.8741	-0.020225	11.297	0.31228
P-2	7.917	-0.013946	11.531	0.31247
P-4	7.917	-0.017937	11.531	0.30848
SP-1	8.0399	-0.018774	11.562	0.24432
SP-2	8.0985	-0.012526	11.561	0.24448
SP-3	8.3555	-0.017417	11.3	0.23959
C-1	7.0299	-0.036152	13.437	0.62198
C-2	6.9858	-0.093408	13.399	0.4627
C-3	7.0354	-0.029705	13.437	0.62242

In order to find out the best design suitable for the hybrid Ford electric vehicle, the tables presented in the Appendix A are found to be ineffective, and maybe a bit confusing. Therefore two evaluation charts, which include other design aspects of the vehicle, are formed. The merit of a particulate HEV design is evaluated in various categories by assigning appropriate points outlining the desirability of that design in that particular category. That is,

- *Regeneration capability of the HEV configuration (abbreviated as **Rgn.Cap.**):*
 - 1: Limited recharging capability through front **OR** rear axle (least desirable)
 - 2: Full recharging capability through front **OR** rear axle
 - 3: Limited recharging capability through front **AND** rear axle
 - 4: Full recharging capability through front **AND** rear axle (highly desirable)

- *Charging the battery when the engine is at idle (abbreviated as **Chrg.(Idle)**):*
 - 1: Possible
 - 0: Not possible
- *The ease of adaptation of a particular HEV configuration to the conventional Ford Tourneo Connect vehicle (abbreviated as **Adapt.**):* In order to assess adaptation capability of a specific HEV design following formula is employed:

$$Adaptation\ Point = 5 - N_{EM} - N_{GB} - P \quad (6.34)$$

Note that 5 leads to excellent adaptability while 0 refers to poor adaptation.

In this formula:

N_{EM} : the number of the electric machinery.

N_{GB} : the number of the gearboxes used.

P : the penalty point for a design requiring dramatic changes under the hood.

1: Drastic change is needed

0: Simple or no change is needed

Apart from these categories, the simulation results are used to grade the performance of HEV in city and highway cruising. Both categories concentrate on fuel efficiency as well as battery utilization in these driving regimes. A merit (cost) function is designed to evaluate these attributes.

$$J = w_1 \cdot \left(\frac{FC_{max} - FC}{FC_{max} - FC_{min}} \right) + w_2 \cdot \left(1 - \frac{SOC_{max} - SOC}{SOC_{max} - SOC_{min}} \right) \quad (6.35)$$

where

w_1 (0...10) and w_2 (10...0) are the weights of the function ($w_1+w_2=10$).

FC : Fuel consumption of a particular HEV configuration in [l/100km].

FC_{min} : The best fuel consumption among all HEV configurations.

FC_{max} : The worst fuel consumption among all HEV configurations.

SOC : State of charge value of a particular HEV configuration in [%].

SOC_{min} : The best charge conservation among all HEV configurations.

SOC_{max} : The worst charge conservation among all HEV configurations.

The same merit function is used to assess the fuel economy as well as charge conservation of a specific HEV design. First of all, the maximum and minimum values for both SOC and fuel consumption are found among all simulation data for 10 HEV designs. FC_{min} , FC_{max} , SOC_{min} , and SOC_{max} are simply replaced by these values. If urban (fuel) or highway (fuel) cost value of a particular HEV configuration is of interest, then, the best fuel consumption value of that HEV design at the related driving cycle is taken as FC value in (6.35). It should be noticed that, the SOC value of the corresponding fuel consumption is placed as SOC value in (6.35). If the merit function value for the charge conservation of a specific HEV design is to be calculated for urban or highway cycle, the best SOC percentage value of that HEV design at the related driving cycle is used as SOC value in (6.35). The FC value of the corresponding to the best charge conservation value is substituted into (6.35).

In Table 6.8, fuel consumption and charge conservation is equally weighted ($w_1 = w_2 = 5$), which means that both of these attributes have equal importance during driving or battery charging. In the second evaluation table (Table 6.9), the merit function values are calculated as:

- $w_1=7$ and $w_2=3$ when fuel economy is of concern;
- $w_1=3$ and $w_2=7$ when charge conservation is of concern.

This means that during normal cruising, fuel economy of the HEV is more important than the charge drawn by the EMs, whereas throughout battery charging phase, the effective charge increase has more significance than the fuel consumed during that period.

Table 6.8 Hybrid Ford Connect Evaluation Chart ($w_1 = w_2 = 0.5$ in (6.35))

Config.	Rgn. Cap.	Chrg. (Idle)	Adapt.	Urban (fuel)	Urban (SOC)	Highway (fuel)	Highway (SOC)	Points
P-1	1	0	2	6.75	4.99	1.85	9.48	26.07
P-2	1	1	2	5.96	6.28	6.65	5.74	28.63
P-3	2	0	3	5.76	6.56	6.58	5.19	29.09
SP-1	1	1	0	5.56	5.11	6.06	4.43	23.16
SP-2	2	1	1	5.48	5.44	5.94	4.43	25.29
SP-3	3	1	1	4.88	5.18	4.93	4.99	24.98
C-1	3	0	1	4.49	4.62	9.5	3.88	26.49
C-2	3	1	1	5.71	3.48	8.84	2.35	25.38
C-3	4	0	2	6.64	5.10	9.57	3.89	31.2
P-4	2	0	4	5.68	6.52	6.52	5.15	29.87
TOTAL	4	1	5	10	10	10	10	50

Table 6.9 Hybrid Ford Connect Evaluation Chart ($w_1=0.7, w_2=0.3$ in (6.35))

Config.	Rgn. Cap.	Chrg. (Idle)	Adapt.	Urban (fuel)	Urban (SOC)	Highway (fuel)	Highway (SOC)	Points
P-1	1	0	2	6.31	3	2.59	9.69	24.59
P-2	1	1	2	5.83	4.79	5.39	4.03	24.04
P-3	2	0	3	4.09	5.26	5.23	3.71	23.29
SP-1	1	1	0	5.24	3.29	4.56	2.7	17.79
SP-2	2	1	1	3.68	3.78	4.31	2.7	18.47
SP-3	3	1	1	2.93	3.58	2.96	3	17.47
C-1	3	0	1	6.28	6.47	9.57	5.44	31.76
C-2	3	1	1	7.43	4.75	9.31	3.26	29.75
C-3	4	0	2	7.84	7.06	9.6	5.44	35.94
P-4	2	0	4	4.04	5.2	5.19	3.65	24.08
TOTAL	4	1	5	10	10	10	10	50

Based on the merit function values, C-3 and P-4 configurations turn out to be the best design alternatives. The next chapter concentrates on the driving performance of these vehicles under the action of smart controller topologies.

6.5 Closure

In this chapter, a detailed simulation study was conducted to assess the performance of ten HEV configurations using two standard driving cycles. First, the simulation of a HEV utilizing detailed nonlinear models (e.g. a sophisticated spark ignition engine) was performed. The results indicated that depending on the electric motor assistance, the fuel consumption of a HEV can be dramatically reduced in city cruising. Unfortunately, the simulation studies employing such complex models were found to be quite inefficient in terms of computation time involved. Hence, through the use of simple but effective HEV models, a comparative simulation study was performed so as to highlight the performance differences among ten HEV designs. Two evaluation charts based on the merit of these designs were created. Prospective HEV design for Ford turns out to be complex and parallel type of HEV configurations.

CHAPTER 7

SMART CONTROLLER DESIGN FOR HYBRID ELECTRIC VEHICLES

7.1 Introduction

Smart controllers are the brains of the HEVs which make them be superior to the conventional ones and the electric vehicles. This chapter mainly discusses the control system architecture developed for the HEVs mentioned in the previous chapter and will be used in the evaluation of the proposed HEV configurations for the target vehicle, Ford Tourneo Connect. With proper design of powertrain components and well-selected power management strategies, HEVs have the potential to reach higher fuel efficiency and reduced gas emissions if compared to conventional vehicles.

In this study, a conceptual intelligent power management system for HEVs, which is based on the driving conditions (or modes), is proposed. The suggested expert system deals with the external information about the driving conditions and driver's driving habits as well as the states of the internal combustion engine and the battery state of charge. It then decides on the power among different power supplies using prescribed algorithms. Details on the algorithms and power management strategies follow.

7.2 HEV Smart Controller Topology

HEVs are composed of many complex sub-systems that have their own characteristics, performance issues and efficiency criteria. For instance, internal combustion engine has optimal an operating region at which its fuel efficiency is highest and whereas, braking system must operate according to the ideal

proportioning characteristics in order to achieve the highest possible energy dissipation at a particular instant. The transmission system, electrical machines and batteries are also the integral elements of a typical HEV. In most cases, each element has their independent low-level controllers to enhance their own performances. On the other hand, these subsystems must be coordinated properly in order to achieve overall objectives such as fuel efficiency, battery charge balance, reduction in harmful gas emissions, driving stability and satisfaction of the driver. Therefore, a high-level controller, which harmoniously coordinates the collective action of these individual subsystems, is to be developed in this work to reach the above-mentioned goals.

7.2.1 High-level Controller Design for HEVs

The need for a high-level control system arises from the fact that a generic HEV with increased complexity requires coordination among its sub-systems as stated in [12]. A smart power management topology is necessary to get maximum fuel efficiency out of the HEV system. In Fig 7.1, this high-level power management system is illustrated. The proposed controller, which is named as “HEV Commander”, in fact orchestrates the communication between the individual low-level control systems (I/O communications) and coordinates the actions of all sub-systems to satisfy the demanded performance. Hence, the system, in turn, regulates the power flow between the ICE and the EM according to the selected power management strategy.

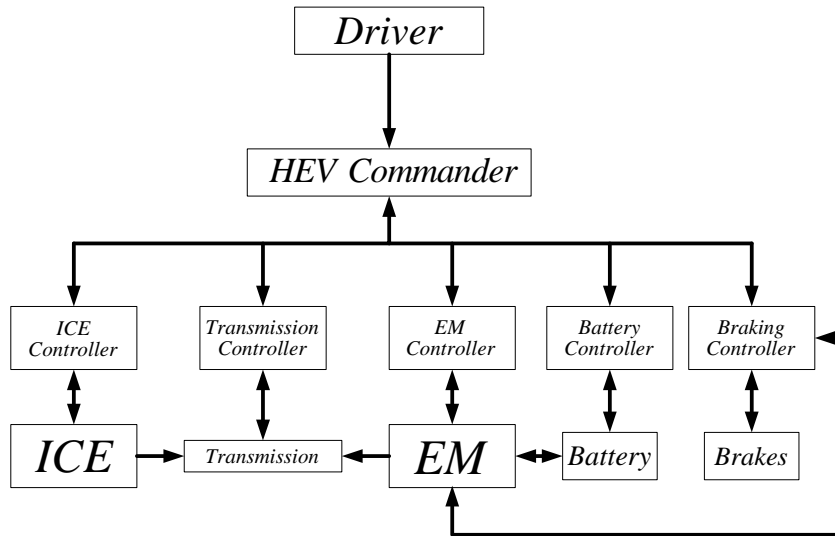


Fig. 7.1 Control system architecture for HEVs [12].

The block diagram of the proposed control system is illustrated in Fig. 7.2. Here, a command generator, which mainly employs throttle- (α) and brake pedal (β) angles, creates the desired driving torque command (T_{dr}^*). Note that several power control parameters along with the vehicle states (including gradient angle and vehicle speed), are fed into the HEV commander. Employing T_{dr}^* , the commander generates appropriate reference signals to the each low-level control system. That is, dictated by the current power management strategy at that particular instant, it issues appropriate throttle commands to the ICE controller while producing the electromagnetic torque commands to the EM drives while generating pneumatic brake commands if deemed necessary.

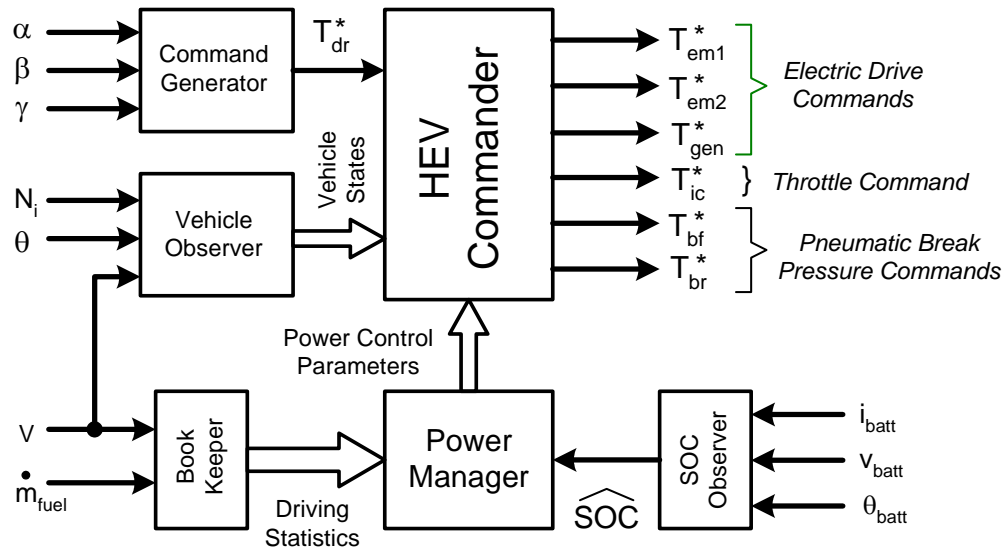


Fig 7.2 Smart power management topology.

At each sampling instant, HEV commander sends commands to each sub-system control module while receiving the status signals from each sub-system. The low-level control systems follow the commands of the HEV commander unless the local constraints are violated.

It is critical to note that the HEV commander needs a power management strategy at a particular instant. This strategy will dictate the commander how to utilize available power sources of the vehicle. Unfortunately, determining an appropriate power management strategy depends not only on the current driving regime but also important HEV states such as SOC, average value of the fuel consumption, etc. Therefore, a smart controller labeled as “Power Manager” is designed to determine the power management strategy to be followed by the HEV commander. Next section elaborates the mentioned expert system.

7.2.2 Power Manager

As mentioned previously, the HEV commander requires various power control parameters such as EM assistance percentage, generation percentage, etc so as to generate commands. Therefore these parameters are passed onto the commander by an expert system called “power manager.” This is inherently an intelligent power controller as it has the capability to predict the current driving regime of the vehicle (and/or driver’s driving habits) and to adopt the power management strategy accordingly. This is accomplished by keeping various driving statistics of the vehicle and employing SOC estimate of the battery.

It is obvious that the driving characteristics of the driver and the driving conditions have significant impact on the fuel consumption of the vehicle and the power distribution and battery SOC level must be adopted along with these variable conditions. As can be seen from Fig. 7.2, the power manager “decides” on the power management strategy with the help of the information on driving statistics and the SOC level estimate of the SOC observer. The driving statistics are generated by another system called the “Book Keeper”. This system essentially keeps track of the fuel consumption of the vehicle while recording the velocity of the vehicle.

The power control parameters include several relevant states. The **EM assistance** (EMA) and power generation percentage parameters are the most important ones to be utilized by the HEV manager which is the executive and tracker of these decisions. Notice that the sampling frequencies of the HEV commander and the Power Manager do differ from each other. The HEV manager should check the subsystem controllers as very frequent as possible in order to operate them properly based on the demanded performance. However, power manager samples the driving characteristics of the vehicle in appropriate time intervals which are long enough to figure out the mode of the cruising.

The power manager essentially uses the driving statistics for the purpose of predicting five different driving modes of the vehicle. These modes include the following:

1. *Interrupted driving*: In this driving mode the vehicle stops at extended periods of time. This is the case representing loading and unloading of its cargo.
2. *Suburban driving*: In this mode the vehicle apparently cruises at relatively high speeds (average speed is higher than 35 [km/h]). Even though the vehicle stops occasionally, the frequency of these stops is less than that of the urban driving conditions.
3. *Urban cruising*: This mode represents all the conditions commonly encountered in city driving (frequent stops, extended waiting periods, low average speed, etc.).
4. *Highway cruising*: In this mode, the vehicle travels at constant high speeds. No stops are usually expected during this cruising mode. Hence, the fuel economy is generally very satisfactory.
5. *Mixed cruising*: At this mode, the vehicle is mostly operated at the highway; however entrance to the city is eminent from time to time.

To determine the appropriate driving mode, driving statistics of the vehicle are needed. Hence the “bookkeeper” keeps track of the following states of the vehicle:

- Average speed
- Average acceleration and its frequency
- Average deceleration and its frequency
- Frequency of full stops
- Average idle time
- Average fuel consumption / km per liter
- Frequency of gear changes
- Distribution of gears

The power manager also requires the SOC estimate of the battery, so that appropriate EMA as well as the charging rates are issued. Fig 7.3 shows the algorithm of this system.

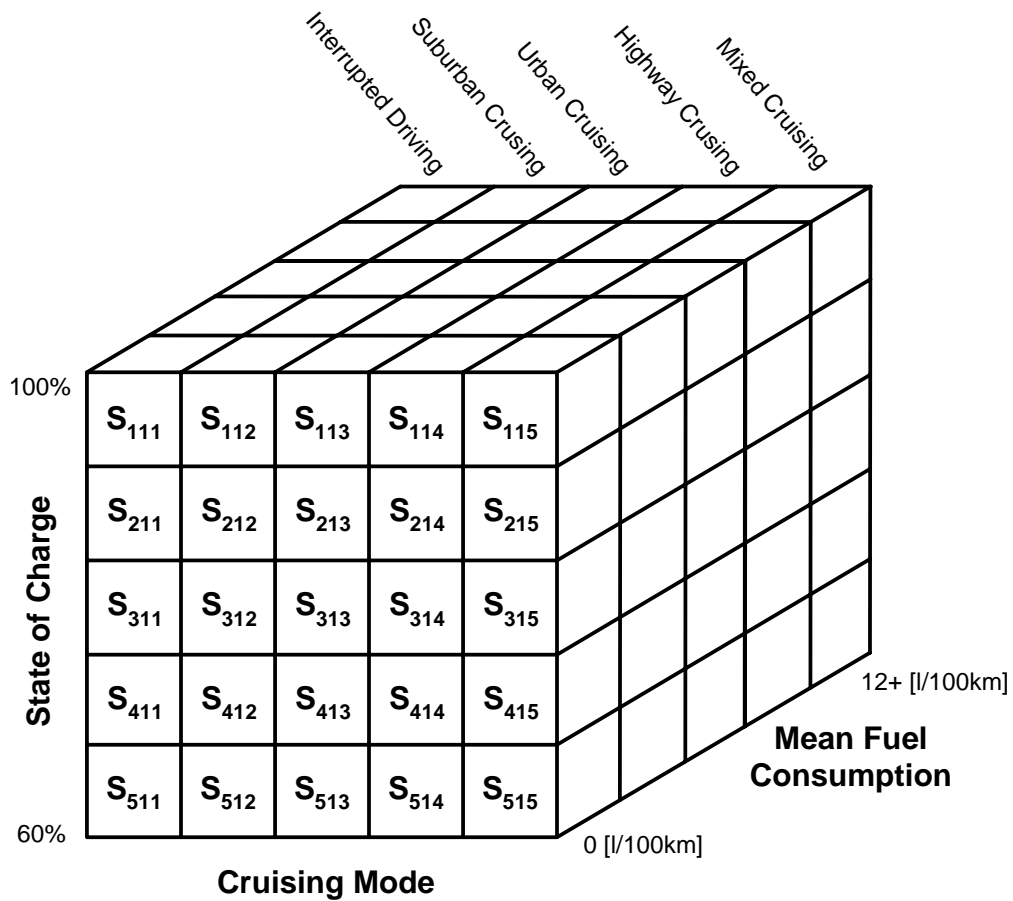


Fig 7.3 Power Manager Algorithm.

As can be seen from the figure, depending on the SOC as well as the driving mode, an appropriate power management strategy (S_{ijk}) is selected. S_{ijk} is a vector of EMA and generation rate commands depending on the mean fuel consumption of the vehicle in the sampling period. For instance, if the SOC rate and the mean fuel consumption of the vehicle are relatively low, the power manager picks up a strategy where EMA is relatively low while charging through the generator is mostly utilized.

Each strategy is associated with a number of control parameters to be passed to HEV commander. These control parameters are as follows:

- *Internal combustion engine state*: This parameter could be ON, OFF or OFF when idle. When power is needed from ICE, this parameter is turned to ON, while in only EM cruising it is OFF. For some HEV configurations, it is possible to turn the ICE OFF during idling which enhances the fuel economy of the vehicle.
- *EM1/EM2 state*: This state has the possible values of ON, OFF, motor only, and generator only which depend on the HEV configuration, i.e. in some of the designs HEV has two propulsive EMs. If power manager decides on EMA cruising, this state is sent to HEV manager as ON, or vice a versa OFF for ICE only driving if SOC level is low. Also, depended upon the HEV design, only EMs could propel the vehicle solely with “motor only” state. When needed, EMs could only be operated as generators for charging the battery.
- *Generator/Alternator state*: If there is a generator/alternator in the configuration, power manager could turn this state ON or OFF according to the charge level of the battery.
- *Regenerative braking mode*: This state could be ON or OFF. Although regenerative braking is a very superior aspect of HEVs, if the SOC of the battery is at its highest level, in order to prevent the battery from overcharging, this mode is turned OFF.
- *EM assistance mode*: This is one of the crucial parameter that the power manager decides on. EMA could be turned ON for the whole cruising like in an electric vehicle or with “ON while acceleration” mode, EM would support the ICE for utilization of the driver demand. It could also be turned OFF due to lack of SOC in the battery.
- *Battery charging mode*: This feature could be “always ON” or OFF is the SOC level is at the predefined limits. In the “always ON” state, the battery is always charged by the ICE through the EM or generator. In addition, “ON at idle”, “ON at ICE OFF” and “ON at constant speed” states could also be utilized according to the HEV configuration. If a generator or EM is

available between the clutch and ICE, batter charging is possible at the idling period or at the stops.

- *Battery charging source*: This state could be “NONE”, “generator/alternator only”, “motors only” and “ALL” depending on the HEV configuration and the driving mode.
- *EM assistance rate*: Power manager decides on the EMA rate which changes between 0 to 100 percent according to the selected strategy.
- *Power generation rate*: Power generation rate also changes between 0 to 100 percent according to the selected strategy.

In order to check all of the power managing capability of the proposed controller, five different driving cycles should be applied in the simulation study. Each of them must be consistent with the mode they are designed for. Also some transient parts should be made for observation of the change of the mode in the power manager. However, three of the five modes could be visualized in this study. ECE-15 Urban cycle, a highway cycle with high acceleration and deceleration demands and finally EUDC cycle are taken into consideration during the simulation of the selected HEV configurations. For each cruising mode, smart power management algorithms were designed. According to the SOC and mean fuel consumption value of the vehicle in the sampling period, the EMA and the generation rates are supplied to the HEV manager in order to execute and track these commands. The performance of the proposed smart controller will be discussed in the next chapter with the aid of the simulations.

7.3 HEV Simulation with Smart Control Algorithms

In the light of the results presented in Chapter 6, two best performing (C-3 and P-4) HEV configurations with highest EM power rating (16 [kW]) are to be simulated with smart controllers presented Art. 7.2. Three driving cycles, which are elaborated in Appendix C, are taken into consideration in the simulation: urban (ECE), highway, and mixed (EUDC) cycles. Note that, while simulating the smart controllers,

bookkeeper algorithm along with the observers is not realized for the sake of simplicity. Consequently, it is assumed that a particular driving cycle is selected properly and the corresponding power management parameters are sent to the HEV commander.

In order to compare the simulation results, the conventional vehicle is first investigated. The results are presented in Figs 7.4-7.21.

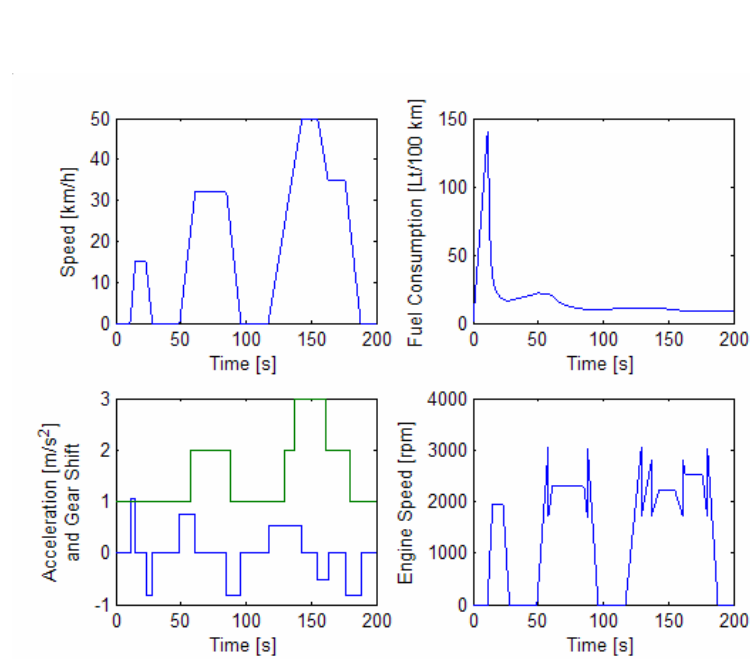


Fig. 7.4 Driving performance of conventional vehicle for urban cruising.

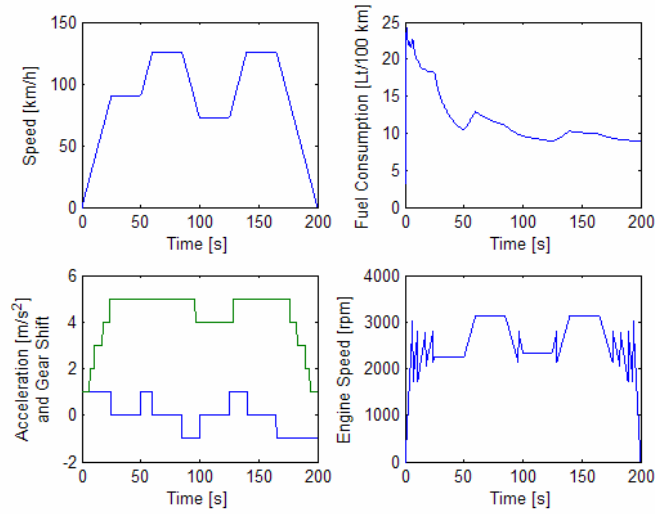
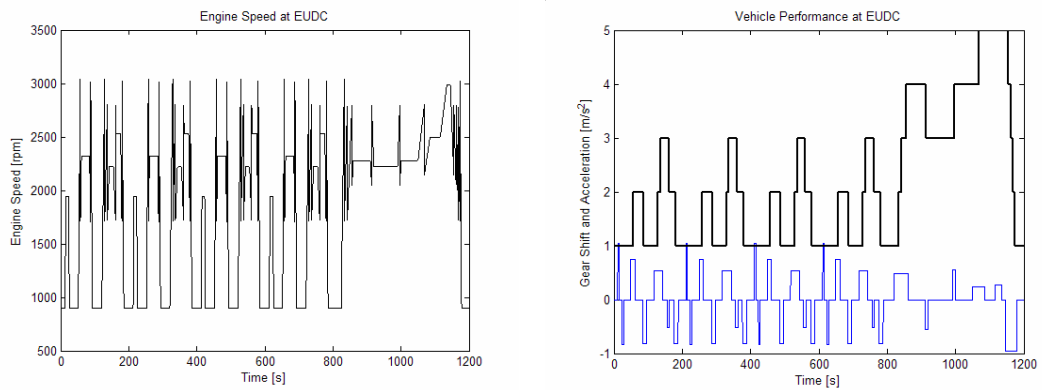
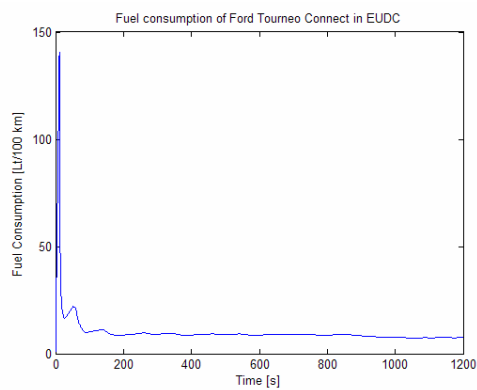


Fig. 7.5 Driving performance of conventional vehicle for highway cruising.



(a) Engine Speed

(b) Gearshift and acceleration



(c) Fuel Consumption

Fig. 7.6 Characteristics of conventional vehicle in EUDC.

As can be seen, the fuel consumption of the vehicle is poor during acceleration and idling. Hence, there exists a large margin of improvement in that area. Notice that, mean fuel consumption of the conventional vehicle is as follows:

- 8.72 [l/100km] for ECE-15 cycle,
- 9.02 [l/100km] for highway cycle and
- 7.48 [l/100km] for EUDC respectively.

As can be seen from Fig 7.7, the gear shifts usually take place between 2000 and 2500 [rpm] in order to have the best fuel efficiency of the vehicle according to the presented map in Chapter 4. However, more dynamic gear changes at relatively high engine speeds (representing aggressive driver behavior) could be also simulated by changing the gear shift algorithm. Besides, it is critical to notice that the mean fuel consumption of the conventional vehicle at the highway cycle (9.02 [l/100km]) is higher than that of the urban cycle (8.72 [l/100km]). This result seems to be contradictory to common sense as it is a well known fact that the fuel consumption of a conventional vehicle decreases significantly when the vehicle is operated at a constant speed on the highway. However, it should be noted that the highway cycle chosen here is a non-standard one and that it signifies an aggressive driving regime where the acceleration is roughly 1 [m/s²]. Considering that the mass of the vehicle is approximately 2000 [kg]; the resulting fuel consumption increases significantly at such driving patterns due to large inertial effects on the vehicle. Another important point to be noticed is that the fuel consumption at the mixed driving cycle (EUDC) is considerably lower if compared to that of the urban cycle (ECE). At the first glance, this result appears to make no sense at all as EUDC constitutes partly the ECE cycle itself. Hence, one expects a notable increase in the fuel consumption. However, this is not the case in the simulation study conducted. In fact, if one takes a close look at the fuel consumption at the urban and the highway parts associated with the EUDC, the resulting figures are read as 8.78 [l/100km] and 6.72 [l/100km] respectively. Consequently, the mean fuel consumption of the conventional vehicle averages out to the reported value. This is due to the fact that the highway portion of the EUDC is not as demanding as the highway cycle utilized in this study.

First of all, three power manager algorithms are devised for the individual driving cycles. Tables 7.1-7.3 show the power control parameters associated with the algorithms. In these tables, average fuel consumption as well as the SOC of the battery are the principle inputs. Therefore, depending on these two important inputs, the relevant percentages of EMA along with power generation rate are determined. In the tables, *EMA* refers to EM assistance in percent of the demanded power at that instance while *GEN* denotes power generation in percent of the rated power of the EMs. The HEV commander essentially utilizes these two important parameters. Note that, the parameters represent the common sense of a human being. Thus the logic (the fuzzy logic) essentially captures how an expert system would make a decision under the given circumstances.

It is important to notice that, the sampling rate of two inputs (average fuel consumption and SOC) plays a key role in the dynamics of the smart controller topology. Hence, in order to visualize the performance of the vehicle depending on the sampling frequency of the power manager, simulations are carried out for different sampling times in mixed cycles. For urban and highway cycles, the sampling is carried out in every hour (which corresponds to 18 cycles); however, for EUDC, the sampling time is selected as 4 hours (12 cycles) to evaluate the frequency depending performance of the power manager.

Table 7.1 Power Manager Algorithm for ECE.

$\begin{matrix} l/100km \\ SOC \end{matrix}$	0 → 3	3 → 6	6 → 12	≥ 12
60% → 70%	<i>EMA</i> = 0% <i>GEN</i> = 75%	<i>EMA</i> = 0% <i>GEN</i> = 50%	<i>EMA</i> = 0% <i>GEN</i> = 50%	<i>EMA</i> = 0% <i>GEN</i> = 50%
70% → 80%	<i>EMA</i> = 25% <i>GEN</i> = 50%	<i>EMA</i> = 25% <i>GEN</i> = 50%	<i>EMA</i> = 50% <i>GEN</i> = 25%	<i>EMA</i> = 100% <i>GEN</i> = 25%
80% → 90%	<i>EMA</i> = 50% <i>GEN</i> = 25%	<i>EMA</i> = 50% <i>GEN</i> = 25%	<i>EMA</i> = 100% <i>GEN</i> = 25%	<i>EMA</i> = 100% <i>GEN</i> = 0%
90% → 100%	<i>EMA</i> = 100% <i>GEN</i> = 0%	<i>EMA</i> = 100% <i>GEN</i> = 0%	<i>EMA</i> = 100% <i>GEN</i> = 0%	<i>EMA</i> = 100% <i>GEN</i> = 0%

Table 7.2 Power Manager Algorithm for Highway cycle.

$I/100km$ SOC	3 → 5	5 → 6	6 → 8	≥ 8
60% → 70%	$EMA = 0\%$ $GEN = 75\%$	$EMA = 0\%$ $GEN = 50\%$	$EMA = 0\%$ $GEN = 50\%$	$EMA = 0\%$ $GEN = 100\%$
70% → 80%	$EMA = 100\%$ $GEN = 50\%$	$EMA = 100\%$ $GEN = 25\%$	$EMA = 50\%$ $GEN = 50\%$	$EMA = 100\%$ $GEN = 50\%$
80% → 90%	$EMA = 100\%$ $GEN = 0\%$	$EMA = 100\%$ $GEN = 0\%$	$EMA = 50\%$ $GEN = 0\%$	$EMA = 50\%$ $GEN = 0\%$
90% → 100%	$EMA = 100\%$ $GEN = 0\%$	$EMA = 100\%$ $GEN = 0\%$	$EMA = 100\%$ $GEN = 0\%$	$EMA = 100\%$ $GEN = 0\%$

Table 7.3 Power Manager Algorithm for EUDC.

$I/100km$ SOC	3 → 5	5 → 6	6 → 8	≥ 8
60% → 70%	$EMA = 0\%$ $GEN = 100\%$	$EMA = 0\%$ $GEN = 100\%$	$EMA = 0\%$ $GEN = 100\%$	$EMA = 0\%$ $GEN = 100\%$
70% → 80%	$EMA = 0\%$ $GEN = 50\%$	$EMA = 0\%$ $GEN = 50\%$	$EMA = 0\%$ $GEN = 50\%$	$EMA = 0\%$ $GEN = 50\%$
80% → 90%	$EMA = 100\%$ $GEN = 0\%$	$EMA = 100\%$ $GEN = 0\%$	$EMA = 50\%$ $GEN = 0\%$	$EMA = 50\%$ $GEN = 0\%$
90% → 100%	$EMA = 100\%$ $GEN = 0\%$	$EMA = 100\%$ $GEN = 0\%$	$EMA = 100\%$ $GEN = 0\%$	$EMA = 100\%$ $GEN = 0\%$

At first, configurations C-3 and P-4 are simulated with these algorithms for ECE, highway cycles and EUDC. Similarly, the configuration P-4 is tested in the same cycles using the same smart controllers to make a comparison between the performances of both vehicles. Related results are presented in Fig 7.7-7.14.

In these simulations, the urban and highway driving cycles are repeated numerous times to yield an effective driving period of 8 hours. Similarly, following the same thought process, the driving period is extended to three months for EUDC. Notice that, initially, SOC of the battery is 100%. As the driving process proceeds, that physical quantity drops down to an equilibrium value depending on the power manager algorithm being used. For the same driving regime, that equilibrium value stays the same. It is obvious that if the driving mode changes, the power manager

will adapt a new power management strategy accordingly. Thus, the SOC will converge to a new equilibrium point. This equilibrium point is significantly higher than 60% of the total capacity of the battery. It is crucial to notice that the true fuel consumption of the vehicle cannot be estimated unless the SOC reaches to an equilibrium point. In fact, the vehicle consumes the electrical energy stored initially at this battery. Hence it looks as if the fuel consumption is way too low owing to the fact that smart controller is using this extra energy available in the battery for EMA.

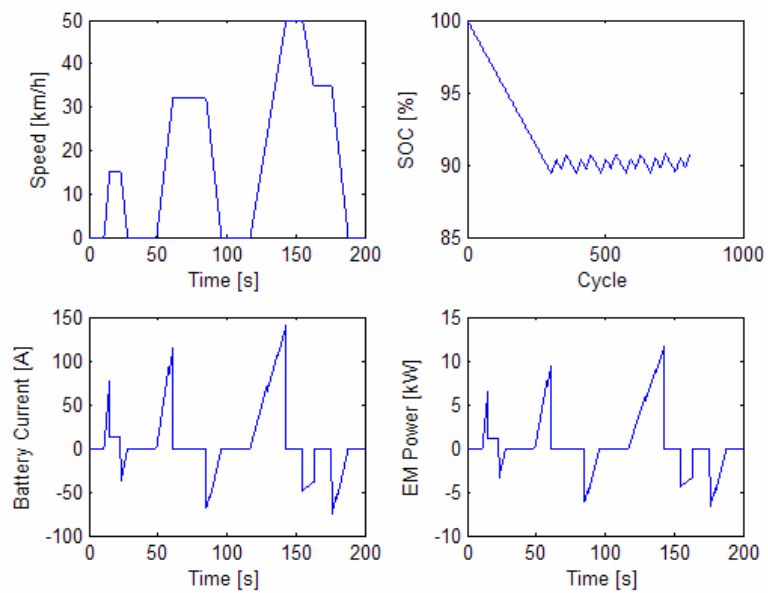


Fig. 7.7 Driving performance of configuration C-3 for urban cruising.

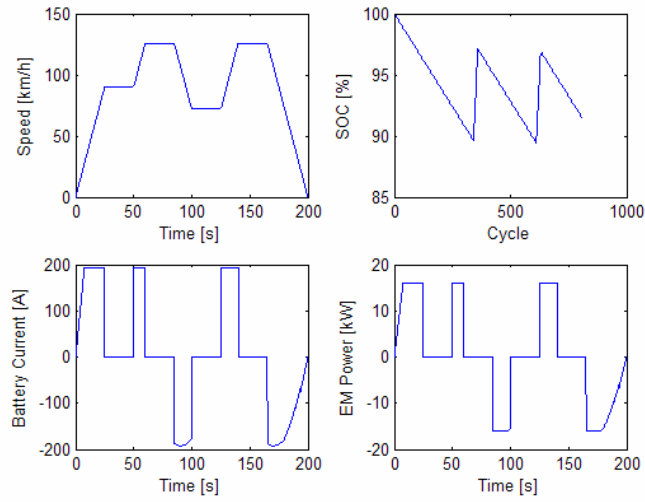
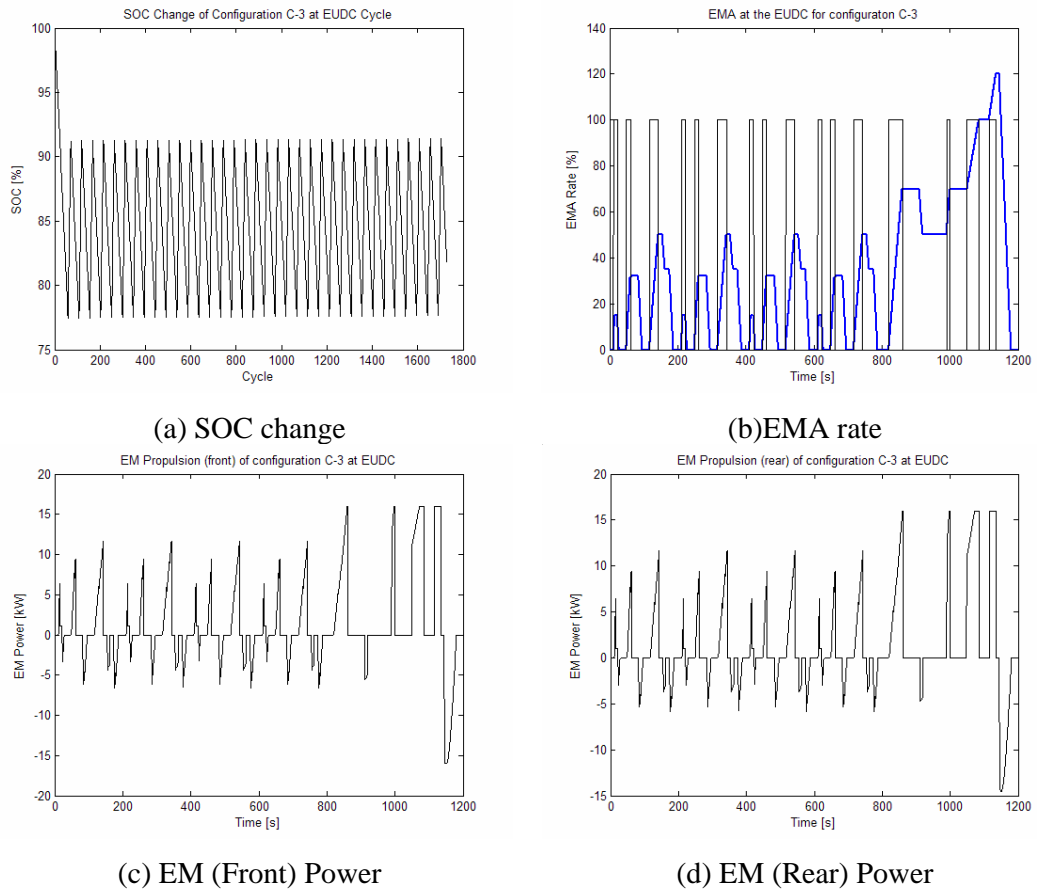


Fig. 7.8 Driving performance of configuration C-3 for highway cruising.



(a) SOC change

(b) EMA rate

(c) EM (Front) Power

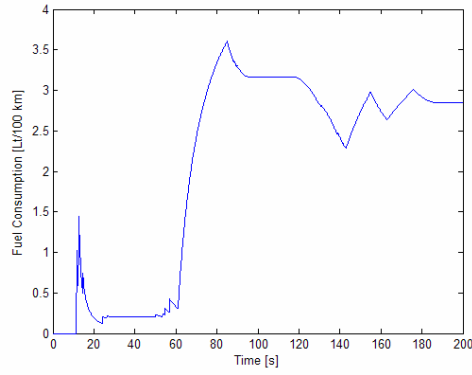
(d) EM (Rear) Power

Fig. 7.9 Characteristics of configuration C-3 at EUDC.

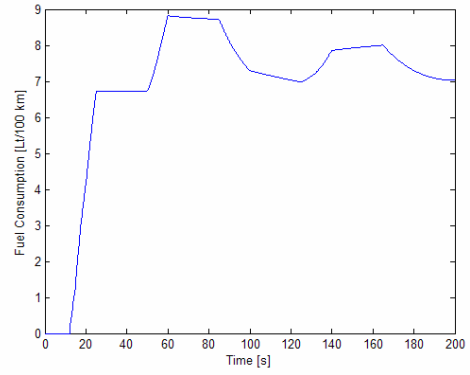
When Fig 7.7 is examined closely, the fluctuations associated with SOC (Fig 7.7b) in urban driving cycle are relatively small at the equilibrium point. It is interesting to note that an EM power output for assistance is pretty low in ECE cycle: about 2/3 of the rated power of EM. This obviously due to the fact that, in urban driving, the cruising speed as well as the acceleration rate is moderately low.

Fig 7.8, for SOC the fluctuations are rather significant when smart control algorithm presented in Table 7.2. It clearly demonstrates the importance of the choice for power management parameters. Fig 7.8 also indicates that, in highway driving where high acceleration is observed, the EM power is insufficient for full assistance. Therefore, the corresponding battery currents drawn from the battery by motor drivers are, not surprisingly, high (about 200 A).

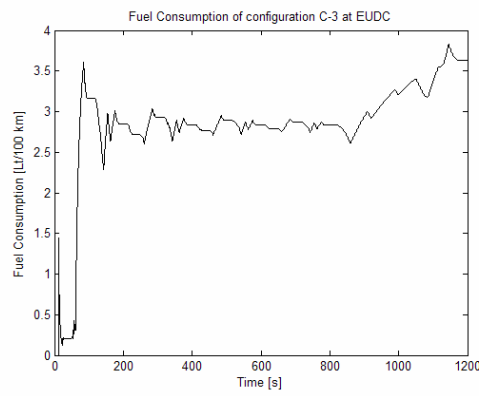
Fig 7.9 shows that, the oscillations in the SOC are in the saw tooth form. These triangular waveforms are formed by switching back and forth among various strategies shown in Table 7.3. Thus, the control algorithm simply boils down to hysteresis control. The extreme points in the figure are associated with the power management strategies where either too much power is drawn from the battery via EMs or relatively large power is generated through the EMs at the expense of high fuel consumption. Also, as a result of utilizing different sampling rates, the frequency and the amplitude of the oscillations are different from the urban and highway cycle results. Their amplitudes have increased whereas the frequency of oscillations decreased. Notice that, in Fig 7.9, the power associated with the rear and front EMs are also illustrated. Since the center of gravity of Ford Tourneo Connect is towards the front side of the vehicle, the regenerative power of the front EM is slightly higher than that of the rear EM. In another words the braking torque needed at the front side is much higher.



(a) Urban (ECE)



(b) Highway



(c) Mixed (EUDC)

Fig. 7.10 Fuel consumption of HEV configuration C-3.

Fig 7.10 exhibits the fuel consumptions of HEV configuration C-3. The comparison of the fuel consumption values for each driving cycle is further discussed.

The performance of configuration P-4 for all cycles is presented in Figs 7.11-7.13. Different from the configuration C-3, P-4 has no EM at the front axle.

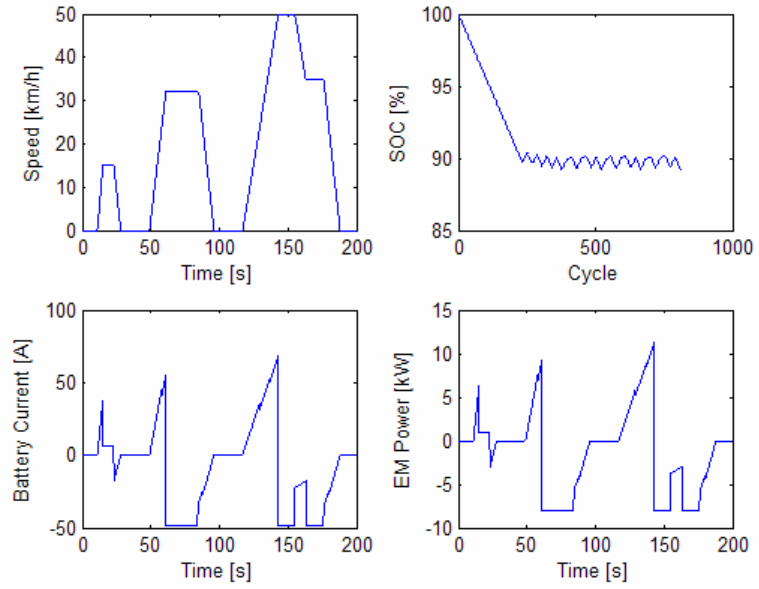


Fig. 7.11 Driving performance of configuration P-4 for urban cruising.

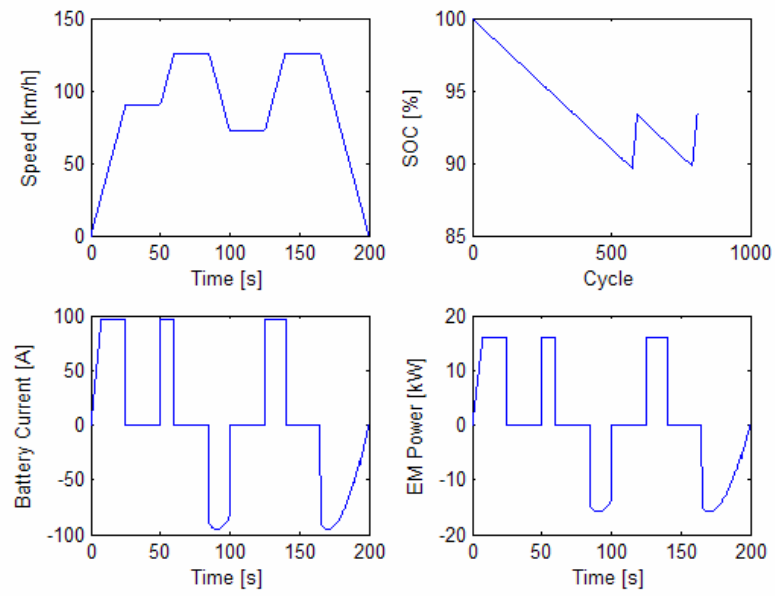


Fig. 7.12 Driving performance of configuration P-4 for highway cruising.

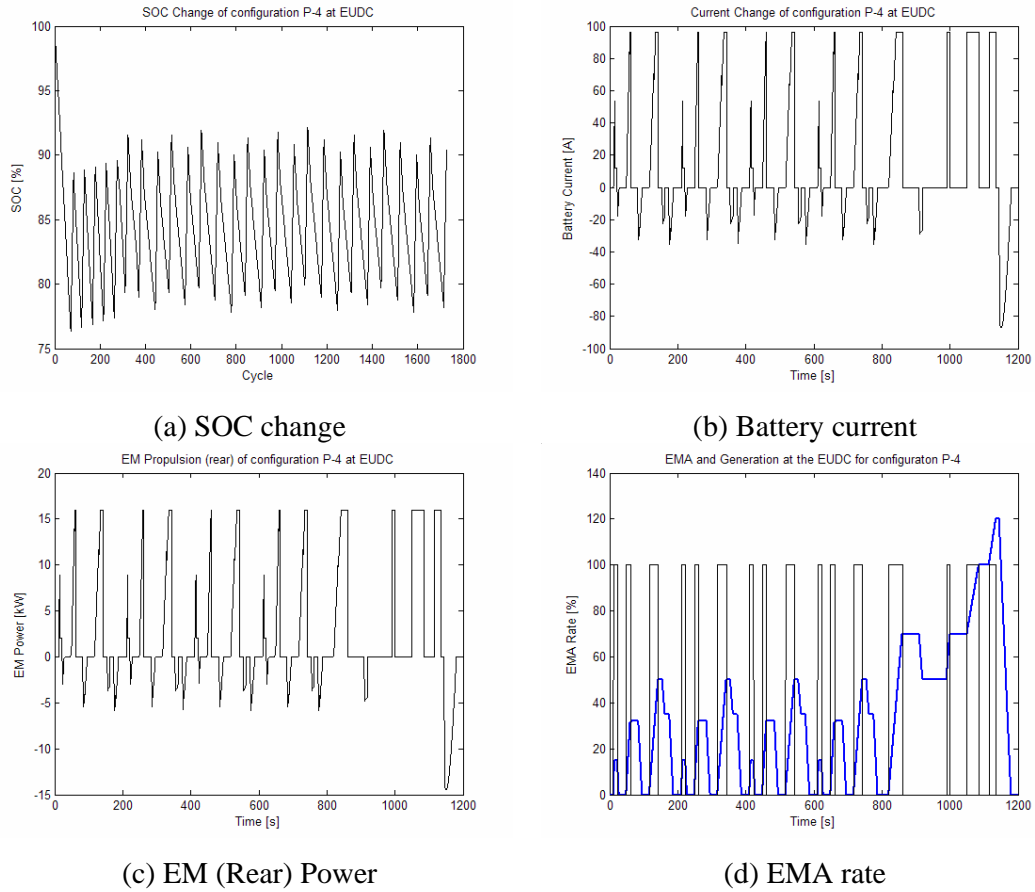


Fig. 7.13 Fuel consumption of HEV configuration P-4.

Similar observations can be asserted for this topology as well. The characteristics of each curve is comparable to that of configuration C-3 except that the fuel consumption of this topology is higher as it constitutes a single EM at the rear axle. Therefore, the regeneration capability is only limited to this motor. Half of the kinetic energy is wasted via conventional frictional brakes.

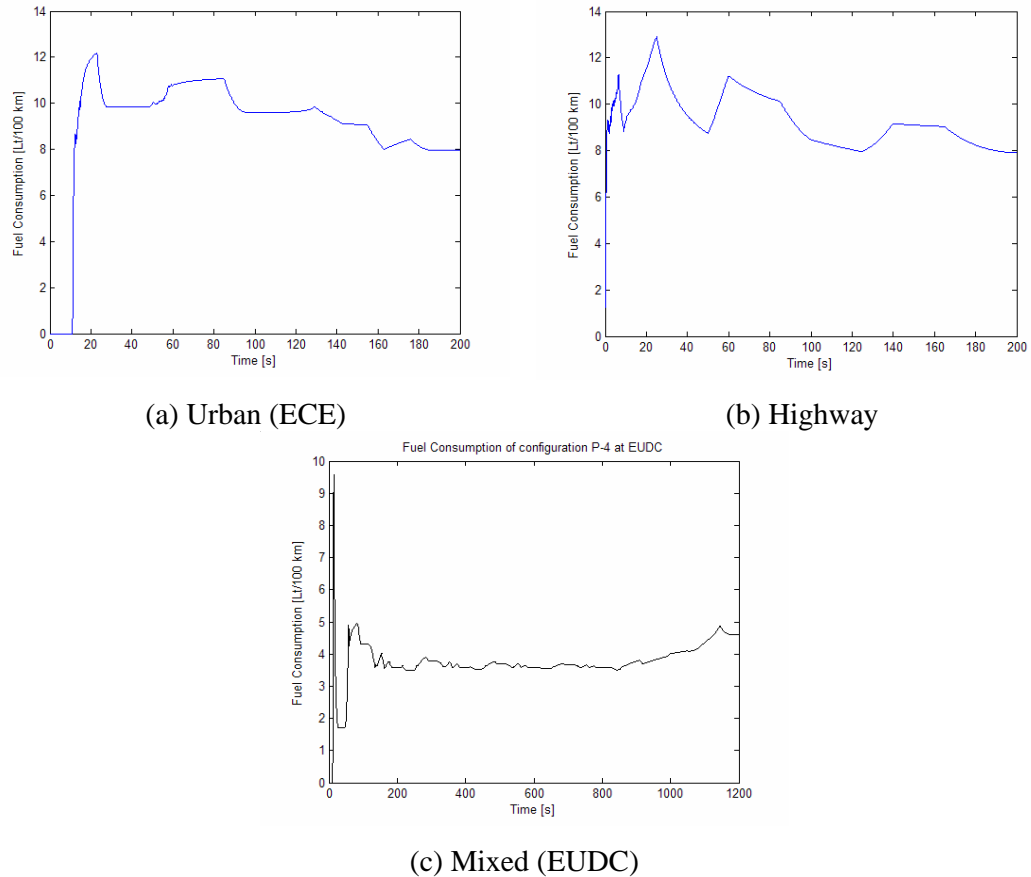


Fig. 7.14 Fuel consumption of HEV configuration P-4.

Based on simulation results presented in Fig 7.4-7.14, Table 7.4 which tabulates the critical results such as mean fuel consumption of various HEV configurations is created. As seen from the Table 7.4, configuration C-3 has better fuel efficiency if compared to that of P-4 due to its extra EM at the front axle, which improves the vehicles' power regeneration ability through regenerative braking. Furthermore, the motor assistance power is essentially doubled which relieves the load of the diesel engine in the transient regimes.

Table 7.4 Average Fuel Consumption for the simulated cases.

Driving Cycle	Ford Connect	Configuration C-3		Configuration P-4	
	Mean Fuel Consumption [l/100 km]	Mean Fuel Consumption [l/100 km]	Fuel Efficiency [%]	Mean Fuel Consumption [l/100 km]	Fuel Efficiency [%]
Urban (ECE)	8.72	5.17	41	5.87	32.7
Highway	9.02	7.36	18.4	8.13	9.7
Mixed (EUDC)	7.48	5.48	27	6.25	17

Please note that both HEVs have superior fuel consumption attributes if compared to the conventional vehicle in the urban cycle where the average speed of the vehicle is about 17 [km/h]. Commercial vehicles like Ford Tourneo Connect are mostly used in urban transportation and the effect of hybridization usually leads to 40% improvement in fuel efficiency which is obviously very attractive for the customer.

Finally, in order to observe the switching among various power management strategies a frequency chart is created in Tables 7.5-7.6 for two HEV configurations in EUDC driving regime. It is interesting to note that some regions of power management domain are never utilized. This means that average fuel consumption and SOC values of that region are never reached. Hence, one needs to modify accordingly in order to utilize these recessive regions.

Table 7.5 Frequency of Utilization in Power Manager Algorithm for C-3 at EUDC.

$\begin{matrix} l/100km \\ SOC \end{matrix}$	3 → 5	5 → 6	6 → 8	≥ 8
60% → 70%	0	0	0	0
70% → 80%	30	285	0	0
80% → 90%	90	1121	0	0
90% → 100%	24	178	0	0

Table 7.6 Frequency of Utilization in Power Manager Algorithm for P-4 at EUDC.

$\begin{matrix} l/100km \\ SOC \end{matrix}$	3 → 5	5 → 6	6 → 8	≥ 8
60% → 70%	0	0	0	0
70% → 80%	14	58	150	0
80% → 90%	38	204	1143	0
90% → 100%	20	13	88	0

7.4 Closure

This chapter introduced smart controller topologies as well as corresponding algorithms suitable for HEV applications. These control algorithms were utilized in a simulation study to see the performance improvement for two prospective HEV designs (C-3 & P-4).

Detailed simulation results including vehicle speed, EM power, currents, SOC and average fuel consumption were all presented to make a comparative analysis between these two designs. Based on these results, C-3 seemed to be a very suitable candidate owing to the fact that the fuel efficiency of this design is 20-40% better than that of the conventional vehicle. The study also showed that selection of power management strategies play a key role in the fuel consumption dynamics as well as the state of charge of the battery. Three different power management algorithms were presented for various driving cycles. These algorithms could be modified to accommodate other driving regimes as well. Hence, smart controller topologies, which resemble fuzzy logic controllers, were proven to have a significant potential in improving the fuel economy of any HEV designs.

CHAPTER 8

CONCLUSION and FUTURE WORK

8.1 Conclusion

This thesis, which is sponsored by Ford Otosan Co., aimed at studying feasibility of a commercial hybrid electric vehicle and targets to evaluate the performances of different types of HEV designs that could be easily adapted to the current Ford Tourneo Connect via a detailed simulation study. In addition, this thesis proposes a smart power management strategy which could be applied to any kind of hybrid electric vehicle (HEV) configuration. The suggested expert system deals with the external information about the driving conditions and modes of the driver as well as the internal circumstances of the internal combustion engine efficiency and the state of charge of the battery. Additionally, it decides on the power flow among two different supplies based on the predefined algorithms. The work also shows the power flow of HEV configurations with the developed smart power management system and therefore, the effectiveness of power management strategies has been evaluated in detail.

The work first develops relevant system models for the vehicle including powertrain, braking system, electrical machines and battery. According to the presented HEV configurations in the scientific literature, ten different HEV configurations, which could be applied to the Ford Tourneo Connect, were designed and the system models were assembled for detailed assessment of the fuel consumption of them in various driving cycles via Matlab/Simulink software package. Also, a gasoline engined Ford Tourneo Connect was modeled for the comparison of the fuel efficiency performances of them. However, even though these Simulink models offered

realistic and detailed results, the simulation run time was not appropriate for a feasibility study aiming to make around 300 different simulations and the spark ignition engine model was giving unexpected results in some of the configurations during power generation mode by electric motor. Hence, simpler but more efficient HEV model was developed, which was devised as a MATLAB code (m-script) which in turn enabled fast simulation, with the supplied diesel engine torque vs. injected fuel rate map by Ford Otosan Co. This model was based on the power requirement of the target vehicle computed with the quasi-static power balance at that moment.

The targeted ten HEV configurations were simulated in both urban and highway cycles for various electric motor power ratings. Raw data of the results were not found to be adequate for the assessment of the configuration solely, hence an evaluation chart (including cost, design, manufacturing and adaptation aspects) was prepared in order to select the best performing (technically and economically feasible) HEV configurations among ten HEV designs. Based on the results, C-3 and P-4 were chosen to be very suitable candidates for the hybridization of the Ford Tourneo Connect.

In the further stages of the study, the selected configurations are tested in three different driving cycles with the developed power management controller. The proposed controller has different power flow strategies depending on the cruising type. In order to monitor these various strategies, an urban cycle, a highway cycle and a mixed cycle were taken into consideration in the fuel efficiency assessment of the two configurations. According to the detailed simulation results including vehicle speed, EM power, currents, SOC and average fuel consumption, both HEVs have superior fuel consumption attributes if compared to the conventional vehicle in the urban cycle where the average speed of the vehicle is about 17 [km/h]. Also C-3 seemed to be a very suitable design for commercial vehicles like Ford Tourneo Connect which are mostly used in urban transportation and the effect of hybridization usually leads to 40% improvement in fuel efficiency which is

obviously very attractive for the customer. Besides, based on the fuel efficiency results with the applied power management strategies, C-3 is superior to P-4 due to its increased ability of generating power from braking and relieve the load on diesel engine during acceleration or at transient regimes.

The study also showed that selection of power management strategies play a key role in the fuel consumption dynamics as well as the state of charge of the battery. Three different power management algorithms were presented for various driving cycles. These algorithms could be modified to accommodate other driving regimes as well. Hence, smart controller topologies, which resemble fuzzy logic controllers, were proven to have a significant potential in improving the fuel economy of any HEV designs.

8.2 Future work

The work conducted in this thesis is mostly completed. It turns out that instead of using detailed Simulink models, developing simple yet efficient mathematical models for HEV components happens to be more effective in terms of computational cost associated with the simulation study. Therefore, it is advisable to develop appropriate state-space models for the entire HEV design and devise corresponding fixed time step integration routines. Even though such an approach initially requires significant development efforts, it pays off in terms of dramatic reduction in the simulation time. Furthermore, smart controller designs discussed in this thesis are rather limited. One can explore various controller topologies like neural networks, genetic algorithms and fuzzy logic algorithms, etc.

REFERENCES

- [1] Gillespie, T.D., "Fundamentals of Vehicle Dynamics", Society of Automotive Engineers, Inc., 1992.

- [2] Powell, B.K.; Bailey, K.E.; Cikanek, S.R., "Dynamic Modeling and control of Hybrid Electric Vehicle Powertrain Systems", IEEE Control Systems Magazine, October, pp. 17-33, 1998.

- [3] Güvey, S., "Dynamic Simulation and Performance Optimization of a car with Continuously Variable Transmission", MSc Thesis, Middle East Technical University, Ankara, September 2003.

- [4] Husain, I., "Electric and Hybrid Vehicles: Design Fundamentals", CRC Press, 2003.

- [5] K.T. Chau, Y.S. Wong, "Energy Conversion and Management", 43, pp. 1953-1968, 2002.

- [6] Honda world wide site, Press release,
<http://world.honda.com/news/2001/4011213.html>, Last Checked: 19.09.2005,
Published: 13.12.2001.

- [7] Office of Energy Efficiency of Canada, "Vehicle and Fuel availability",
<http://oee.nrcan.gc.ca/transportation/fuels/electric/electric-availability.cfm>,
Last Checked: 19.09.2005, Last Modified: 03.05.2005.

- [8] Autospeed Magazine, "Revisited: the GM Concept Cars", http://autospeed.drive.com.au/cms/A_1970/article.html, Last Checked: 19.09.2005, Published: 22.11.2003.
- [9] Lin, C.C.; Filipi, Z.; Wang, Y.; Louca, L.; Peng, H.; Assanis, D.; Stein, J., "Integrated, Feed-forward Hybrid Electric Vehicle Simulation in SIMULINK and its Use for Power Management Studies", SAE Technical Paper No. 2001-01-1334, 2001.
- [10] Glenn, B.; Washington, G.; Rizzoni, G., "Operation and Control Strategies for Hybrid Electric Automobiles", SAE Technical Paper No. 2000-01-1537, 2000.
- [11] Wipke K.; Cuddy M.; Buch S., "ADVISOR 2.1: a user-friendly advanced powertrain simulation using a combined backward/forward approach", IEEE Transaction on Vehicular Technology, Vol.48, No: 6, pp.1751-1761, 1999.
- [12] Lin, C.C.; Peng, H.; Grizzle J.W.; Liu, J.; Busdiecker, M., "Control System Development for an Advanced-Technology Medium-Duty Hybrid Electric Truck", SAE Technical Paper No. 2003-01-3369, 2003.
- [13] Johnson, V.H.; Wipke, K.B.; Rausen, D.J., "HEV Control Strategy for Real-time Optimization of Fuel Economy and Emissions", SAE Technical Paper No. 2000-01-1543, 2000.
- [14] Bauman, Bernd M.; Washington, G; Glenn, Bradley C.; Rizzoni, G., "Mechatronic design and control of hybrid electric vehicles", IEEE/ASME Transactions on Mechatronics, v5 n1 2000. p 58-72, 2000.

- [15] Rajagopalan A.; Washington, G; Rizzoni, G.; Guezennec Y., “Development of fuzzy logic and neural network control and advanced emissions modeling for parallel hybrid vehicles”, The National Renewable Energy Laboratory (NREL) Report, <http://www.nrel.gov/docs/fy04osti/32919.pdf>, Published:15.12.2003, Last Checked: 19.09.2005.
- [16] Stroh, D.J.; Franchek, M.A.; Kerns, J.M, “Eliminating Maps from Engine Fuelling Control Algorithms”, SAE Technical Paper No. 2000-01-0259, 2001.
- [17] Powell, B.K. and Cook J.A., “Modeling of an Internal Combustion Engine for Control Analysis”, IEEE Control Systems Magazine, August, pp. 20-26, 1988.
- [18] Isermann, R.; Sinsel, S.; Schaffnit, J., “Modeling and Real-time Simulation of Diesel Engines for Control Design”, SAE Technical Paper No. 980796, 1998.
- [19] Benninger, N.F. and Plapp, G.; “Requirements and Performance of Engine Management Systems under Transient Conditions”, SAE Technical Paper No. 910083, 1991.
- [20] Moskwa, J.J. and Hedrick, J.K.; “Modeling and Validation of Automotive Engines for Control Algorithm Development”, Trans. ASME, J. Dynamical Systems, Measurement, and Control, Vol.114, pp. 278-285.
- [21] Hendricks E. and Sorenson, S.C.; “Mean Value Modeling of Spark Ignition Engines”, SAE Technical Paper No. 900616, 1990.
- [22] Hendricks, E.; Chevalier, A.; Jensen, M.; Sorenson S.C.; Trumph D.; Asik, J., “Modeling of the Intake Manifold Filling Dynamics”, SAE Technical Paper No. 960037, 1996.

- [23] Yoon, P. and Sunwoo, M.; “A nonlinear dynamic modeling of SI engines for controller design”, *Int. J. of Vehicle Design*, Vol. 26, Nos. 2/3, pp. 277-297, 2001.
- [24] Stefanopoulou, A.G.; Cook, J.A.; Grizzle, J.W.; Freudenberg J.S., “Joint Air-Fuel Ratio and Torque Regulation Using Secondary Cylinder Air Flow Actuators”, *Trans. ASME, J. Dynamical Systems, Measurement, and Control*, Vol.121, pp. 638-646, 1999.
- [25] Lu, Z.; Thompson, G.J.; Mucino, V.H; Smith, J.E., “Simulation of a Continuously Variable Power Split Transmission”, *SAE Technical Paper No. 1999-01-0062*, 1999.
- [26] Yasuoka, M.; Uchida, M.; Katakura, S.; Yoshino, T., “An integrated Control Algorithm for an SI Engine and a CVT”, *SAE Technical Paper No. 1999-01-0752*, 1999.
- [27] Osamura, K; Itoyama, H.; Iwano, H., “Improvement of drive torque response by applying an integrated control algorithm for a diesel engine and CVT”, *JSAE Review* 22, pp. 293-298, 2001.
- [28] Kim, C.K.; NamGoong E.; Lee, S.; Kim, T.; Kim, H., “Fuel Economy Optimization for Parallel Hybrid Vehicles with CVT”, *SAE Technical Paper No. 1999-01-1148*, 1999.
- [29] Hattori, N.; Aoyama, S.; Kitada, S.; Matsuo, I, “Functional Design of a Motor Integrated CVT for a Parallel HEV”, *SAE Technical Paper No. 1999-01-0753*, 1999.

- [30] Matsuo, I.; Nakazawa, S.; Maeda H.; Inada, E., “Development of a High-Performance Hybrid Propulsion System Incorporating a CVT”, SAE Technical Paper No. 2000-01-0992, 2000.
- [31] Oba, H.; Yamanaka, A.; Katsuta, H.; Kamichi, K., “Development of a Hybrid Powertrain System Using CVT in a Minivan”, SAE Technical Paper No. 2002-01-0991, 2002.
- [32] Saalani, M.K. and Heydinger, G.J., “Powertrain and Brake Modeling of the 1994 Ford Taurus for the National Advanced Driving Simulator”, SAE Technical Paper No. 981190, 1998.
- [33] Schultz, A.G.; Tsai, L.W.; Higuchi, N.; Tong, I.C., “Development of a Novel Parallel Hybrid Transmission”, SAE Technical Paper No. 2001-01-0875, 2001.
- [34] Davis, G.W., “The Development of an Electro-hydraulically Controlled, Five Speed Transmission for a Hybrid Electric Vehicle”, SAE Technical Paper No. 980830, 1998.
- [35] Gao, Y. and Ehsani, M., “Electronic Braking System of EV and HEV--- Integration of Regenerative Braking, Automatic Braking Force Control and ABS”, SAE Technical Paper No. 2001-01-2478, 2001.
- [36] Nakamura, E.; Soga, M.; Sakai, A.; Otomo, A.; Kobayashi, T., “Development of Electronically Controlled Brake System for Hybrid Vehicle”, SAE Technical Paper No. 2002-01-0300, 2002.
- [37] Panagiotidis, M.; Delagrammatikas, G.; Assanis, D., “Development and Use of a Regenerative Braking Model for a Parallel Hybrid Electric Vehicle”, SAE Technical Paper No. 2000-01-0995, 2000.

- [38] Gao, Y.; Chen, L.; Ehsani, M., “Investigation of the Effectiveness of Regenerative Braking for EV and HEV”, SAE Technical Paper No. 1999-01-2910, 1999.
- [39] Walker, A.M.; Lampert, M.U.; Wilkins S., “On Friction Demand with Regenerative Braking”, SAE Technical Paper No. 2002-01-2581, 2002.
- [40] Ünlüsoy, Y.S., “Performance of Motor Vehicles”, Lecture Notes on Automotive engineering I, Middle East Technical University, Ankara, 1999.
- [41] Ünlüsoy, Y.S. and Akkök, M., “Motorlu Taşıtlarda Kavrama Dinamiğinin İncelenmesi”, Makina Tasarımı ve İmalat Dergisi, Cilt 4, Sayı 1, Mayıs 2001, pp. 47-55.
- [42] Shaver, R., “Manual transmission clutch systems”, Warrendale PA, Society of Automotive Engineers, 1997.
- [43] Moore, S.W.; Rahman, K.M.; Ehsani, M., “Effect on Vehicle Performance of Extending the Constant Power Region of Electric Drive Motors”, SAE 1999-01-1152, 1999.
- [44] Rahman, Z.; Ehsani, M.; Butler, K.L., “An Investigation of Electric Motor drive Characteristics for EV and HEV Propulsion Systems”, SAE 2000-01-3062, 2000.
- [45] Fellner, C. and Newman J., “High-power batteries for use in Hybrid Vehicles”, Journal of Power Sources, 85, pp. 229-236, 2000.
- [46] Chau, K.T.; Wong, Y.S.; Chan, C.C., “An Overview of the Energy Sources for Electric Vehicles”, Energy Conversion & Management, 40, pp. 1021-1039, 1999.

- [47] Gutman, G., "Hybrid Electric Vehicles and Electrochemical Storage Systems-A technology Push-Pull Couple", *Journal of Power Sources*, 84, pp. 275-279, 1999.
- [48] Markel, T.; Brooker, A.; Hendricks, T.; Johnson, V.; Kelly, K.; Kramer, B.; O'Keefe, M.; Sprik, S.; Wipke, K., "ADVISOR: a systems analysis tool for advanced vehicle modelling", *Journal of Power Sources*, 110, pp. 255-266, 2002.
- [49] Bitsche, O. and Gutman G., "Systems for Hybrid Cars", *Journal of Power Sources*, 127, pp. 8-15, 2004.
- [50] Chan, C.C. and Chau, K.T., "Modern Electric Vehicle Technology", Oxford University Press, 2001.
- [51] Unnewehr, L.E. and Nasar, S.A., "Electric Vehicle Technology", John Wiley & Sons Inc., 1982.
- [52] DieselNet, http://www.dieselnet.com/standards/cycles/ece_eudc.html, Last Checked: 19.09.2005

APPENDIX A

SIMULATION RESULTS

This section introduces all simulation data executed in Chapter 6 with the simplified HEV model. The positive values in the SOC change column indicate the battery is charged due to either regenerative braking or generation during cruising through the electrical machines.

Table A.1 Urban cruising with EMA for configuration P-1.

EM Power [kW]	%EMA	[Lt/100 km]	Δ SOC (%)
8	0	6.4643	-0.0088395
	25	6.0857	-0.01614
	50	5.6564	-0.02344
	75	5.2382	-0.030388
	100	4.719	-0.036518
12	0	6.4484	-0.013259
	25	5.7884	-0.024211
	50	5.2013	-0.03516
	75	4.4622	-0.045581
	100	3.9169	-0.054777
16	0	6.3426	-0.017679
	25	5.5347	-0.032281
	50	4.5207	-0.04688
	75	3.7545	-0.060775
	100	3.1244	-0.073036

Table A.2 Generator mode operation of configuration P-1 for urban cruising.

EM Power [kW]	%GEN	[Lt/100 km]	Δ SOC (%)
8	20	6.9765	-0.001308
	60	8.7142	0.013755
	100	9.0967	0.028818
12	20	7.0288	-0.001962
	60	8.9851	0.020632
	100	10.777	0.043227
16	20	6.9913	-0.002616
	60	9.5006	0.02751
	100	11.913	0.057636

Table A.3 Highway cruising with EMA for configuration P-1.

EM Power [kW]	%EMA	[Lt/100 km]	Δ SOC (%)
8	0	9.0457	0
	25	8.9975	-0.045837
	50	8.7971	-0.091669
	75	8.5328	-0.13695
	100	8.4068	-0.18093
12	0	9.0457	0
	25	8.9487	-0.068755
	50	8.5322	-0.1375
	75	8.3664	-0.20543
	100	8.2089	-0.2714
16	0	9.0457	0
	25	8.7971	-0.091673
	50	8.402	-0.18334
	75	8.205	-0.2739
	100	7.8486	-0.36187

Table A.4 Generator mode operation of configuration P-1 for highway cruising.

EM [kW]	%GEN	[Lt/100 km]	Δ SOC (%)
8	20	9.1205	0.073192
	60	10.085	0.21958
	100	10.237	0.36596
12	20	9.7064	0.10979
	60	10.199	0.32937
	100	10.641	0.54894
16	20	9.7366	0.14638
	60	10.312	0.43915
	100	11.521	0.73192

Configuration P-2 has an EM between the clutch and the gearbox. An EM in front of the clutch supplies an advantage of regenerative braking ability and the disadvantage of loss of battery charging ability at the vehicle idling or when the vehicle is stopped. As seen from the Fig 6.15, EM is placed at the position of EM₁, hence R₁ value is taken as 1 while R₂ and R_g is taken as 0. The related results for configuration P-2 is shown in Tables A.5-A.8.

Table A.5 Urban cruising with EMA for configuration P-2.

EM Power [kW]	%EMA	[Lt/100 km]	Δ SOC (%)
8	0	6.4394	0.0034031
	25	5.4188	-0.016817
	50	4.5418	-0.035251
	75	4.5346	-0.035422
	100	4.5346	-0.035422
12	0	6.4025	-0.0027701
	25	5.0069	-0.033101
	50	3.7994	-0.060751
	75	3.7892	-0.061009
	100	3.7892	-0.061009
16	0	6.389	-0.0089433
	25	4.4915	-0.049384
	50	3.1346	-0.086251
	75	3.1278	-0.086595
	100	3.1278	-0.086595

Table A.6 Generator mode operation of configuration P-2 for urban cruising.

EM [kW]	%GEN	[Lt/100 km]	Δ SOC (%)
8	20	7.0828	0.025268
	60	9.3472	0.058066
	100	9.3472	0.058066
12	20	8.6101	0.030028
	60	10.679	0.079225
	100	10.679	0.079225
16	20	8.7906	0.034787
	60	11.905	0.10038
	100	11.905	0.10038

Table A.7 Highway cruising with EMA for configuration P-2.

EM Power [kW]	%EMA	[Lt/100 km]	Δ SOC (%)
8	0	8.9014	0.050931
	25	8.7572	0.023414
	50	8.3496	-0.0035479
	75	8.3506	-0.0037615
	100	8.3506	-0.0037615
12	0	8.9014	0.072048
	25	8.6199	0.030773
	50	8.1229	-0.0096701
	75	8.1248	-0.0099906
	100	8.1248	-0.0099906
16	0	8.9014	0.089161
	25	8.3496	0.034126
	50	7.8864	-0.019797
	75	7.8741	-0.020225
	100	7.8741	-0.020225

Table A.8 Generator mode operation of configuration P-2 for highway cruising.

EM [kW]	%GEN	[Lt/100 km]	Δ SOC (%)
8	20	9.8225	0.095554
	60	10.058	0.16249
	100	10.058	0.16249
12	20	9.901	0.13898
	60	11.11	0.23938
	100	11.11	0.23938
16	20	9.9795	0.17841
	60	11.297	0.31228
	100	11.297	0.31228

In the configuration P-3, EM is behind the gearbox and coupled to the driveshaft of front axle. Again, the positioning of an EM on the driveshaft gives the advantage of regenerative braking ability and the disadvantage of loss of battery charging ability during idling of the vehicle or when the vehicle is stopped. R_1 value is taken as 1 while R_2 and R_g is taken as 0 which are seen in Fig.6.13. In Tables A.9-A.12, related results for configuration P-2 are presented.

Table A.9 Urban cruising with EMA for configuration P-3.

EM Power [kW]	%EMA	[Lt/100 km]	Δ SOC (%)
8	0	6.5344	0.0097464
	25	5.6547	-0.0079831
	50	5.0118	-0.019157
	75	5.0074	-0.019273
	100	5.0074	-0.019273
12	0	6.4377	0.0066331
	25	5.2231	-0.019961
	50	4.5604	-0.036721
	75	4.5546	-0.036897
	100	4.5546	-0.036897
16	0	6.4342	0.0035198
	25	4.654	-0.031939
	50	3.5409	-0.054286
	75	3.529	-0.05452
	100	3.529	-0.05452

Table A.10 Generator mode operation of configuration P-3 for urban cruising.

EM [kW]	%GEN	[Lt/100 km]	Δ SOC (%)
8	20	7.1836	0.031612
	60	9.1672	0.064409
	100	9.1672	0.064409
12	20	8.688	0.039431
	60	10.768	0.088628
	100	10.768	0.088628
16	20	8.8758	0.04725
	60	12.006	0.11285
	100	12.006	0.11285

Table A.11 Highway cruising with EMA for configuration P-3.

EM Power [kW]	%EMA	[Lt/100 km]	Δ SOC (%)
8	0	9.0578	0.050985
	25	8.8408	0.024231
	50	8.4525	-0.00048893
	75	8.4498	-0.00066445
	100	8.4498	-0.00066445
12	0	9.0578	0.07215
	25	8.5542	0.032019
	50	8.2476	-0.0050608
	75	8.2446	-0.0053241
	100	8.2446	-0.0053241
16	0	9.0578	0.089354
	25	8.4167	0.035845
	50	7.9199	-0.013595
	75	7.917	-0.013946
	100	7.917	-0.013946

Table A.12 Generator mode operation of configuration P-3 for highway cruising.

EM [kW]	%GEN	[Lt/100 km]	Δ SOC (%)
8	1	9.7459	0.095608
	3	10.248	0.16254
	5	10.248	0.16254
12	1	10.096	0.13908
	3	10.654	0.23949
	5	10.654	0.23949
16	1	10.172	0.1786
	3	11.531	0.31247
	5	11.531	0.31247

Configuration SP-1 has an EM between clutch and the gearbox while a generator is coupled to the ICE. A generator coupled to the ICE has an advantage of charging battery when the vehicle is either idle or parked (ignition off) and SP-1 has also the ability of regenerative braking which increases the fuel efficiency of SP-1. As seen from Fig 6.15, R_1 is taken as 1; R_2 is taken as zero while R_g is taken as 2. The related results for configuration SP-1 is presented in Tables A.13-A.16.

Table A.13 Urban cruising with EMA for configuration SP-1.

EM Power [kW]	%EMA	[Lt/100 km]	Δ SOC (%)
8	0	6.5459	0.0039472
	25	5.5296	-0.016273
	50	4.659	-0.034707
	75	4.6491	-0.034878
	100	4.6491	-0.034878
12	0	6.5081	-0.002226
	25	5.13	-0.032557
	50	3.9362	-0.060207
	75	3.9222	-0.060464
	100	3.9222	-0.060464
16	0	6.4914	-0.0083993
	25	4.6045	-0.04884
	50	3.2141	-0.085707
	75	3.2132	-0.086051
	100	3.2132	-0.086051

Table A.14 Generator mode operation of configuration SP-1 for urban cruising.

EM [kW]	%GEN	[Lt/100 km]	Δ SOC (%)
8	20	7.0609	0.011479
	60	8.8098	0.026542
	100	9.514	0.041605
12	20	7.0914	0.0090712
	60	9.0589	0.031666
	100	10.862	0.05426
16	20	7.1429	0.0066637
	60	9.667	0.03679
	100	12.096	0.066916

Table A.15 Highway cruising with EMA for configuration SP-1.

EM Power [kW]	%EMA	[Lt/100 km]	Δ SOC (%)
8	0	9.0917	0.051126
	25	8.9578	0.023609
	50	8.4956	-0.0033526
	75	8.4905	-0.0035663
	100	8.4905	-0.0035663
12	0	9.0917	0.07257
	25	8.7559	0.031295
	50	8.3069	-0.0091482
	75	8.3032	-0.0094687
	100	8.3032	-0.0094687
16	0	9.0917	0.090611
	25	8.4956	0.035577
	50	8.0443	-0.018347
	75	8.0399	-0.018774
	100	8.0399	-0.018774

Table A.16 Generator mode operation of configuration SP-1 for highway cruising.

EM [kW]	%GEN	[Lt/100 km]	Δ SOC (%)
8	20	9.7166	0.066497
	60	10.13	0.097237
	100	10.281	0.12798
EM [kW]	%GEN	[Lt/100 km]	Δ SOC (%)
12	20	9.7468	0.095626
	60	10.243	0.14174
	100	10.689	0.18785
16	20	9.9541	0.12135
	60	10.357	0.18283
	100	11.562	0.24432

Configuration SP-2 has an EM behind the gearbox and in addition, a generator is coupled to the ICE. A generator coupled to the ICE creates the opportunity of battery charging during idling or stopped and SP-2 has also the ability of regenerative braking. Note that, in the model (Fig 6.13) R_1 is taken as 1; R_2 is taken as zero while R_g is taken as 2. The related results for configuration SP-2 is shown in Tables A.17-A.20.

Table A.17 Urban cruising with EMA for configuration SP-2.

EM Power [kW]	%EMA	[Lt/100 km]	Δ SOC (%)
8	0	6.6572	0.010295
	25	5.7211	-0.0074344
	50	5.0854	-0.018608
	75	5.0782	-0.018725
	100	5.0782	-0.018725
12	0	6.5595	0.0071818
	25	5.3428	-0.019412
	50	4.6459	-0.036173
	75	4.64	-0.036348
	100	4.64	-0.036348
16	0	6.5561	0.0040685
	25	4.7442	-0.03139
	50	3.6045	-0.053738
	75	3.5897	-0.053971
	100	3.5897	-0.053971

Table A.18 Generator mode operation of configuration SP-2 for urban cruising.

EM [kW]	%GEN	[Lt/100 km]	Δ SOC (%)
8	20	7.1717	0.017827
	60	8.9159	0.03289
	100	9.6195	0.047952
EM [kW]	%GEN	[Lt/100 km]	Δ SOC (%)
12	20	7.1423	0.018479
	60	9.1051	0.041073
	100	10.904	0.063668
16	20	7.2071	0.019131
	60	9.7259	0.049257
	100	12.149	0.079383

Table A.19 Highway cruising with EMA for configuration SP-2.

EM Power [kW]	%EMA	[Lt/100 km]	Δ SOC (%)
8	0	9.0921	0.051178
	25	8.9814	0.024424
	50	8.5575	-0.00029613
	75	8.5534	-0.00047166
	100	8.5534	-0.00047166
12	0	9.0921	0.072668
	25	8.7996	0.032536
	50	8.3398	-0.0045435
	75	8.3427	-0.0048068
	100	8.3427	-0.0048068
16	0	9.0921	0.090773
	25	8.5238	0.037264
	50	8.1036	-0.012175
	75	8.0985	-0.012526
	100	8.0985	-0.012526

Table A.20 Generator mode operation of configuration SP-2 for highway cruising.

EM [kW]	%GEN	[Lt/100 km]	Δ SOC (%)
8	20	9.7159	0.066548
	60	10.13	0.097289
	100	10.281	0.12803
12	20	9.746	0.095723
	60	10.243	0.14183
	100	11.382	0.18795
16	20	10.054	0.12151
	60	10.357	0.183
	100	11.561	0.24448

Configuration SP-3 has an EM at the rear axle and a generator is coupled to the ICE. A generator coupled to the ICE gives an advantage of ability of battery charging when the vehicle is stopped and at idle. SP-1 has also the ability of regenerative braking. It is important to notice that, R_1 is taken as zero; R_2 is taken as 1 while R_g is taken as 2 which could be seen from Fig.6.13. Tables A.21-A.24 present the related simulation results of configuration SP-3.

Table A.21 Urban cruising with EMA for configuration SP-3.

EM Power [kW]	%EMA	[Lt/100 km]	Δ SOC (%)
8	0	6.8506	0.0081539
	25	5.8673	-0.0095756
	50	5.1972	-0.020749
	75	5.1958	-0.020866
	100	5.1958	-0.020866
12	0	6.7437	0.0050406
	25	5.3099	-0.021554
	50	4.7474	-0.038314
	75	4.7413	-0.038489
	100	4.7413	-0.038489
16	0	6.7404	0.0019273
	25	4.8146	-0.033532
	50	3.7009	-0.055879
	75	3.6853	-0.056112
	100	3.6853	-0.056112

Table A.22 Generator mode operation of configuration SP-3 for urban cruising.

EM [kW]	%GEN	[Lt/100 km]	Δ SOC (%)
8	20	7.4023	0.015685
	60	9.3058	0.030748
	100	9.6693	0.045811
12	20	7.3588	0.016338
	60	9.4715	0.038932
	100	10.408	0.061527
16	20	7.419	0.01699
	60	10.106	0.047116
	100	12.363	0.077242

Table A.23 Highway cruising with EMA for configuration SP-3.

EM Power [kW]	%EMA	[Lt/100 km]	Δ SOC (%)
8	0	9.3742	0.050553
	25	9.2132	0.023798
	50	8.8209	-0.00092151
	75	8.8189	-0.001097
	100	8.8189	-0.001097
12	0	9.3742	0.071122
	25	9.0712	0.03099
	50	8.5546	-0.0060891
	75	8.5512	-0.0063524
	100	8.5512	-0.0063524
16	0	9.3742	0.085883
	25	8.7786	0.032374
	50	8.3558	-0.017066
	75	8.3555	-0.017417
	100	8.3555	-0.017417

Table A.24 Generator mode operation of configuration SP-3 for highway cruising.

EM [kW]	%GEN	[Lt/100 km]	Δ SOC (%)
8	20	9.4406	0.065923
	60	9.7738	0.096664
	100	10.716	0.1274
12	20	9.4737	0.094178
	60	10.683	0.14029
	100	10.879	0.1864
16	20	9.5069	0.11662
	60	10.781	0.1781
	100	11.3	0.23959

Configuration C-1 has EM_1 between clutch and the gearbox while the EM_2 is coupled to rear axle. The positioning of an extra EM at the rear axle has an advantage of increased ability of regenerative braking which enhances the fuel efficiency of C-1 drastically as two axles of regenerative braking is possible. As seen from Fig 6.15, R_1 is taken as 1; R_2 is taken as 1 while R_g is taken as zero. The related results for configuration SP-1 is presented in Tables A.25-A.28.

Table A.25 Urban cruising with EMA for configuration C-1.

EM Power [kW]	%EMA	[Lt/100 km]	Δ SOC (%)
8	0	6.6137	0.011987
	25	5.5795	-0.0080015
	50	4.7271	-0.025963
	75	4.057	-0.041824
	100	3.3939	-0.05557
12	0	6.6	0.0027301
	25	5.2133	-0.027252
	50	4.0124	-0.054195
	75	3.1185	-0.077987
	100	2.7973	-0.098605
16	0	6.6	-0.0065267
	25	4.7001	-0.046503
	50	3.3196	-0.082426
	75	2.7973	-0.11415
	100	2.7973	-0.14164

Table A.26 Generator mode operation of configuration C-1 for urban cruising.

EM [kW]	%GEN	[Lt/100 km]	Δ SOC (%)
8	20	7.2658	0.033852
	60	9.7905	0.077583
	100	12.22	0.12131
12	20	8.8644	0.035528
	60	11.688	0.10112
	100	14.879	0.16672
16	20	9.0557	0.037204
	60	12.778	0.12466
	100	17.578	0.21213

Table A.27 Highway cruising with EMA for configuration C-1.

EM Power [kW]	%EMA	[Lt/100 km]	Δ SOC (%)
8	0	9.1102	0.10164
	25	8.9834	0.074194
	50	8.5429	0.047373
	75	8.3401	0.021204
	100	8.0992	-0.004309
12	0	9.1263	0.14358
	25	8.8272	0.1024
	50	8.3494	0.06217
	75	7.9069	0.022916
	100	7.524	-0.015353
16	0	9.1315	0.17575
	25	8.561	0.12085
	50	8.1075	0.067211
	75	7.5291	0.014873
	100	7.0299	-0.036152

Table A.28 Generator mode operation of configuration C-1 for highway cruising.

EM [kW]	%GEN	[Lt/100 km]	Δ SOC (%)
8	20	10.072	0.14627
	60	10.374	0.23551
	100	11.578	0.32476
12	20	10.163	0.21051
	60	11.522	0.34438
	100	12.993	0.47825
16	20	10.244	0.265
	60	11.889	0.44349
	100	13.437	0.62198

The configuration C-2 has an EM₁ coupled to ICE while an EM₂ coupled to rear axle. An extra EM at the rear axle gives an advantage of increased ability of regenerative braking which enhances the fuel efficiency of C-1 drastically as two axles of regenerative braking is possible and another EM coupled to the ICE provides an ability of battery charging during idling of the vehicle or when the vehicle is stopped. As seen from Fig 6.13, R₁ is taken as zero; R₂ is taken as 1 while R_g is taken as 2. Tables A.29-A.32 present the results for configuration C-2.

Table A.29 Urban cruising with EMA for configuration C-2.

EM Power [kW]	%EMA	[Lt/100 km]	ΔSOC (%)
8	0	6.5685	-0.0006856
	25	5.3881	-0.025716
	50	4.3348	-0.044189
	75	3.7297	-0.051253
	100	3.3255	-0.057384
12	0	6.4635	-0.0082186
	25	4.4277	-0.045764
	50	3.0018	-0.073474
	75	2.8017	-0.08407
	100	2.6954	-0.093266
16	0	6.4635	-0.015752
	25	3.8668	-0.065812
	50	2.6954	-0.10276
	75	2.6954	-0.11689
	100	2.6954	-0.12915

Table A.30 Generator mode operation of configuration C-2 for urban cruising.

EM [kW]	%GEN	[Lt/100 km]	ΔSOC (%)
8	20	8.8272	0.028711
	60	11.378	0.076572
	100	12.161	0.091635
12	20	9.0091	0.035876
	60	12.628	0.10767
	100	14.722	0.13026
16	20	9.6333	0.043042
	60	15.094	0.13876
	100	17.413	0.16889

Table A.31 Highway cruising with EMA for configuration C-2.

EM Power [kW]	%EMA	[Lt/100 km]	Δ SOC (%)
8	0	9.0921	0.050553
	25	8.8054	0.014173
	50	8.3418	-0.020172
	75	8.2138	-0.029857
	100	8.0852	-0.039093
12	0	9.0921	0.071122
	25	8.4525	0.016552
	50	7.8914	-0.034965
	75	7.6663	-0.049492
	100	7.4952	-0.063346
16	0	9.0921	0.085883
	25	8.3165	0.013122
	50	7.4948	-0.055567
	75	7.2465	-0.074936
	100	6.9858	-0.093408

Table A.32 Generator mode operation of configuration C-2 for highway cruising.

EM [kW]	%GEN	[Lt/100 km]	Δ SOC (%)
8	20	10.13	0.11055
	60	11.418	0.20822
	100	11.561	0.23896
12	20	10.243	0.16111
	60	11.849	0.30762
	100	12.961	0.35374
16	20	10.357	0.20587
	60	13.023	0.40122
	100	13.399	0.4627

Configuration C-3 has EM₁ coupled to the front axle and the EM₂ is coupled to rear axle. The positioning of an extra EM at the rear axle supplies an advantage of increased ability of regenerative braking which enhances the fuel efficiency of C-3 drastically as two axles of regenerative braking is possible. Note that, in Fig 6.13, R₁ is taken as 1; R₂ is taken as 1 while R_g is taken as zero. The related results for configuration C-3 is presented in Tables A.33-A.36.

Table A.33 Urban cruising with EMA for configuration C-3.

EM Power [kW]	%EMA	[Lt/100 km]	ΔSOC (%)
8	0	6.6084	0.018474
	25	5.5935	-0.00084877
	50	4.7852	-0.016985
	75	4.1863	-0.029821
	100	3.6406	-0.039332
12	0	6.516	0.012247
	25	5.1258	-0.016737
	50	3.9126	-0.040941
	75	3.0412	-0.060196
	100	2.7319	-0.074462
16	0	6.516	0.0060206
	25	4.6103	-0.032624
	50	3.2335	-0.064897
	75	2.7319	-0.09057
	100	2.7319	-0.10959

Table A.34 Generator mode operation of configuration C-3 for urban cruising.

EM [kW]	%GEN	[Lt/100 km]	ΔSOC (%)
8	20	7.2601	0.040339
	60	9.7794	0.084069
	100	12.203	0.1278
12	20	8.7752	0.045045
	60	11.593	0.11064
	100	14.777	0.17624
16	20	8.9664	0.049751
	60	12.682	0.13721
	100	17.469	0.22467

Table A.35 Highway cruising with EMA for configuration C-3.

EM Power [kW]	%EMA	[Lt/100 km]	Δ SOC (%)
8	0	9.1241	0.10175
	25	8.9984	0.074503
	50	8.5722	0.048243
	75	8.366	0.023008
	100	8.1365	-0.0011961
12	0	9.133	0.14378
	25	8.8604	0.10291
	50	8.3565	0.063517
	75	7.9244	0.025663
	100	7.5344	-0.010642
16	0	9.134	0.17619
	25	8.573	0.12169
	50	8.1127	0.069174
	75	7.5354	0.018703
	100	7.0354	-0.029705

Table A.36 Generator mode operation of configuration C-3 for highway cruising.

EM [kW]	%GEN	[Lt/100 km]	Δ SOC (%)
8	20	10.085	0.14638
	60	10.388	0.23562
	100	11.59	0.32487
12	20	10.169	0.21071
	60	11.528	0.34458
	100	12.996	0.47845
16	20	10.246	0.26544
	60	11.89	0.44393
	100	13.437	0.62242

Finally, the configuration P-4 has an EM coupled to the rear axle. The positioning of an EM at the rear axle gives an advantage of ability of regenerative braking which allows the energy conversion during braking and decreases the fuel efficiency of P-4. Notice that, R_1 and R_g in Fig 6.13 are taken as zero while R_2 is taken as 1 as an EM is coupled to the rear axle. The related results for configuration P-4 is presented in Tables A.37-A.40.

Table A.37 Urban cruising with EMA for configuration P-4.

EM Power [kW]	%EMA	[Lt/100 km]	Δ SOC (%)
8	0	6.5344	0.0083015
	25	5.6547	-0.0094279
	50	5.0118	-0.020601
	75	5.0074	-0.020718
	100	5.0074	-0.020718
12	0	6.4377	0.0051882
	25	5.2231	-0.021406
	50	4.5604	-0.038166
	75	4.5546	-0.038341
	100	4.5546	-0.038341
16	0	6.4342	0.002075
	25	4.654	-0.033384
	50	3.5409	-0.055731
	75	3.529	-0.055965
	100	3.529	-0.055965

Table A.38 Generator mode operation of configuration P-4 for urban cruising.

EM [kW]	%GEN	[Lt/100 km]	Δ SOC (%)
8	20	7.1836	0.030167
	60	9.1672	0.062965
	100	9.1672	0.062965
12	20	8.688	0.037986
	60	10.768	0.087183
	100	10.768	0.087183
16	20	8.8758	0.045805
	60	12.006	0.1114
	100	12.006	0.1114

Table A.39 Highway cruising with EMA for configuration P-4.

EM Power [kW]	%EMA	[Lt/100 km]	Δ SOC (%)
8	0	9.0578	0.050597
	25	8.8408	0.023843
	50	8.4525	-0.00087718
	75	8.4498	-0.0010527
	100	8.4498	-0.0010527
12	0	9.0578	0.07118
	25	8.5542	0.031049
	50	8.2476	-0.0060309
	75	8.2446	-0.0062942
	100	8.2446	-0.0062942
16	0	9.0578	0.085362
	25	8.4167	0.031853
	50	7.9199	-0.017586
	75	7.917	-0.017937
	100	7.917	-0.017937

Table A.40 Generator mode operation of configuration P-4 for highway cruising.

EM [kW]	%GEN	[Lt/100 km]	Δ SOC (%)
8	20	9.7459	0.09522
	60	10.248	0.16215
	100	10.248	0.16215
12	20	10.096	0.13811
	60	10.654	0.23852
	100	10.654	0.23852
16	20	10.172	0.17461
	60	11.531	0.30848
	100	11.531	0.30848

APPENDIX B

ELECTRICAL SYSTEMS MODELING FOR HYBRID ELECTRIC VEHICLES

B.1 Electric Machines in HEVs

As briefly outlined in the Chapters 2&3, the electric machines play a critical role in the dynamic performance of a HEV. The main functions performed by an electric machine in a typical HEV configuration can be stated as follows:

1. The overall power conversion efficiency of a generic electric machine (70 % to 90 %) is much higher if compared to that of an internal combustion (e.g. diesel or spark ignition) engine, which ranges in between 10-30 %. Furthermore, an electric machine operated as a motor can provide full torque at low speeds while its instantaneous power rating can be two or three times the nominal (rated) one. As a key propulsion system element, an electric motor conveniently assists the engine during acceleration- and start-up regime of the vehicle. In such cases, the internal combustion engine (ICE) is known to consume notable amount of extra fuel. Hence, the electric motor, which is said to be more responsive in terms of torque production, not only reduces the fuel consumption but also provides a smoother transition at such operating regimes.
2. During braking, the kinetic energy of a conventional vehicle is ordinarily wasted over the brakes in terms of heat generated. Thus, the fuel efficiency of such vehicles become, not surprisingly, poor in the city cruising where the vehicles have to decelerate to full stop and then to accelerate to resume their course many times. When used in generator (a.k.a. regenerative braking) mode, the electric machine in a HEV can help recover most of that energy by generating electric energy and then pumping it to the battery pack of the vehicle. Consequently, the

overall fuel efficiency of the HEV in the city would be dramatically improved. In city where the average speed of the vehicle is usually less than 30 km/h; the HEV may actually switch off the inefficient ICE and could effectively rely on the electric motor as the prime-mover. Hence, the emission of (environmentally) harmful gasses (CO_x , SO_x , NO_x) could be totally eliminated in that case. Furthermore, the acoustic noise emission of the vehicle could be reduced drastically.

3. Whether it is a diesel or spark-ignition engine, an ICE, by design, operates at the peak fuel efficiency along a certain trajectory in its operating space (torque vs. speed). If coupled to the engine, the electric machine could be used to operate the engine at its peak efficiency by boosting or sinking (some portion of) the engine power when needed during the operation. Consequently, the fuel efficiency of the HEV can be increased dramatically by 20-50%.
4. Due to the redundancy in the architecture of a HEV, the electrical machinery could improve the reliability of the vehicle. In case the vehicle is out-of-fuel or the engine malfunctions, the electric machine can be safely used to drive the vehicle to the nearest service station.

At the expense of added complexity and cost; the electric machines make significant contributions to the performance of the HEV that manifest themselves in terms of improved mileage (fuel efficiency), lowered harmful gas emissions, lower noise, and enhanced reliability. The desired properties of an electric motor within the context of HEV can be summarized as follows:

- Ruggedness and low maintenance
- High torque-to-inertia ratio
- High power-to-weight ratio
- High efficiency
- High maximum torque generation capability at extended periods
- High speed operation
- Extended constant power region
- Low acoustic noise emission

- Low electromagnetic interference (EMI)
- Low cost
- Ease of control and flexibility

Unfortunately, none of the contemporary electrical machinery does possess these listed features all together. Hence, a compromise should be made to select a machinery to satisfy only the most essential properties of a HEV application. Not surprisingly, a wide variety of electric motors/generators are employed in HEV technology including

- Conventional (brush type) DC motors
 - Separately excited DC motor
 - Series DC motors (a.k.a. universal motors)
 - DC shunt motors
 - Compound motors (differential and integral)
- Permanent magnet synchronous motors
 - Trapezoidal winding (a.k.a. brushless DC motor)
 - Sinusoidal winding (a.k.a. AC-servomotor)
- Induction (asynchronous) motors
- Switched reluctance motors.

Mathematical models for common motors follow:

B.1.1 Conventional DC Motors

Before 1980s, conventional DC motors were usually the first choice due to their low cost and simplicity associated with their control. However, the size and maintenance requirements of DC motors make them obsolete in almost all major applications such as automotive, aviation/aerospace, industrial automation, robotics, consumer goods etc.

Even though the recent advancements in power electronics and electronically commutated (synchronous, induction, and switched reluctance) machines has limited the use of DC machines to mostly low-end motion control applications, DC motors still form the basis of most electrical machinery (including the AC machines). In fact, with some relevant assumptions on the control strategies, the models for some modern electrical machine systems (e.g. permanent magnet synchronous motor, induction motor) boil down to that of a conventional DC motor itself. Thus, the model of conventional DC motor with a separate field winding will be briefly summarized in the text.

The conventional DC machines have two sets of windings: the field windings, which produce a stationary magnetic field, are housed inside the stator of the machine. On the other hand, the armature windings are located on the rotor and get to rotate inside this magnetic field created by the field windings. Note that the magneto-motive-force (MMF) of each excited winding interacts with each other to produce the torque. The orthogonality of these MMFs, which is essential to generate the highest electromagnetic torque possible while avoiding the magnetic coupling between two windings, is maintained via a set of mechanical apparatus called commutators and armature brushes.

When the armature and field windings are supplied from independently controlled DC sources, it is referred to as the *separately excited DC* machine. Fig. B.1 illustrates the equivalent circuit of such a machine. The corresponding model of the machine becomes

$$V_a = R_a i_a + L_a \frac{di}{dt} + e_a \quad (\text{B.1})$$

$$V_f = R_f i_f + L_f \frac{di_f}{dt} \quad (\text{B.2})$$

where $V_a \equiv$ Armature (terminal) voltage [V];

$V_f \equiv$ Field voltage [V];

$R_a, R_f \equiv$ Resistances of armature- and field windings respectively [Ω];

$L_a, L_f \equiv$ Inductances of armature- and field windings respectively [H];

$i_a, i_f \equiv$ motor current and field current [A];

$e_a \equiv$ back electro-motive-force (emf) [V].

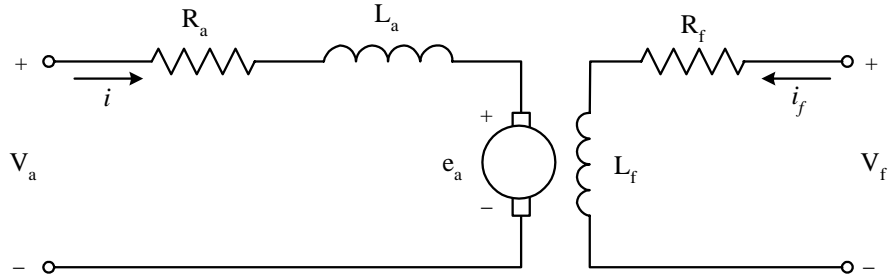


Fig. B.1 Equivalent circuit of a separately excited DC motor.

The mechanical coupling equations can be expressed as

$$e_a = K \phi \omega \quad (\text{B.3})$$

$$T_m = K \phi i_a \quad (\text{B.4})$$

Here, ω and T_m are the angular speed of the motor [rad/s] and the electromagnetic torque [Nm] generated by the motor respectively. Note that K is a machine constant that depends on the machine design, number of conductors in the windings, and properties of the core material. Notice that the field flux ϕ is a nonlinear function of the field current i_f .

To improve the torque generation capability of the machine, the field windings are replaced by permanent magnets. In that case, the magnets produce a field with uniform magnetic flux density. Hence, i_f and ϕ are treated as constant in the formulation above. Consequently, the coupling expressions (B.3) and (B.4) become

$$e_a = K_e \omega \quad (\text{B.5})$$

$$T_m = K_t i_a \quad (\text{B.6})$$

where K_e is called back emf constant [Vs/rad] while K_t is referred to as torque constant [Nm/A]. Note that when SI units are used, $K_e = K_t$.

The separately excited DC motor offers the maximum flexibility of torque and speed control. By changing the field winding connection of this motor, one can create a family of DC motors as shown in Fig. B.2. For instance, in DC shunt machine (as illustrated in Fig. B.2a), field winding is in parallel with the armature connection and

thus the simplicity in the power supply compromises the flexibility of the control (and torque generation capability). Similarly, in series motor (Fig. B.2b), the field windings are connected in series with the armature. In compound motor structures (Fig. B.2c and B.2d), two field windings, are utilized. Since the polarity of these windings could be changed, one can create a compound DC motor with opposing (differential) and strengthening (integral) fields. Hence, the torque capability of the machine can be drastically modified.

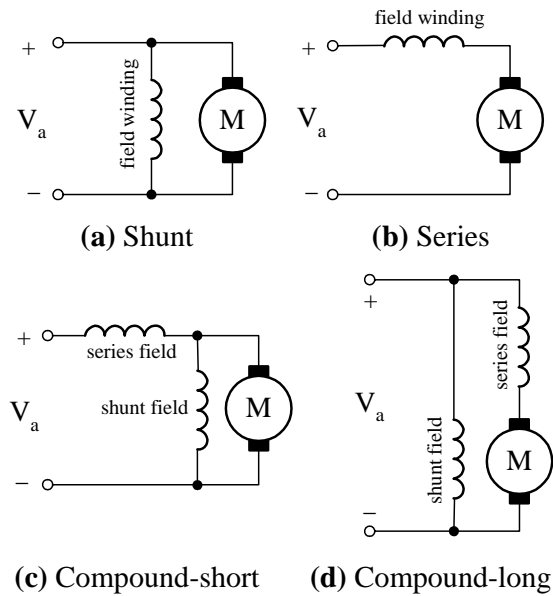


Fig. B.2 DC motor configurations.

B.1.2 Induction Machine

For nearly a century, **induction machines** (IMs) with squirrel-cage rotors have been the workhorse of industry because of their low cost, rugged construction, and reliability. When fed directly from the line, an induction motor with a constant load torque operates at a nearly constant speed. However, by means of power electronics converters, it is possible to vary not only the speed of the motor but also the developed torque. Not surprisingly, the utilization of induction motors in servo-drive

applications has widened rapidly due to the significant developments in power electronics and microprocessors. The emphasis of this article is to present a brief overview of the induction machines so as to illustrate how it is possible to regulate the torque on such machines precisely.

The construction of a squirrel-cage IM is quite simple. The stator consists of three windings that are distributed in the stator slots. These three windings are displaced by 120° apart in space with respect to each other. When excited via a three-phase AC voltage source with constant frequency (f); a balanced set of currents flow through these windings. Thus, a “rotating” magnetic field with constant amplitude is established. The electrical speed of the field, which is known as the synchronous speed, can be expressed as $\omega_e = 2\pi f$ where f is the excitation frequency.

With respect to the rotor side, the squirrel cage rotor includes a stack of insulated (iron) laminations. Furthermore, the rotor has electrically conducting bars inserted through the laminations. These bars, which are very close to the periphery of the rotor in the axial direction, are electrically shorted at the end of the rotor by end rings. Thus, the overall structure resembles a cage. Roughly speaking, the rotating magnetic field (in the stator) induces large currents circulating through these rotor bars. Since a (Lorentz) force develops on the conductors located inside a magnetic field, an overall torque is produced on the rotor. Notice that if the electrical speed of the rotor approaches to the synchronous speed, there will be no relative motion between the (rotating) air-gap magnetic flux and the rotor. Consequently, no rotor currents will be induced to produce any torque. In fact, depending on the motor load, the electrical speed of the rotor (ω_r) is usually lower than ω_e . This difference between ω_r and ω_e is known as the slip speed and often times normalized as

$$s = \frac{\omega_e - \omega_r}{\omega_e} = 1 - \frac{\omega_r}{\omega_e} \quad (\text{B.7})$$

where s is referred to as the “slip.” Note that the shaft speed of the motor (ω_m) is expressed as

$$\omega_m = \frac{\omega_r}{P/2} \quad (\text{B.8})$$

where P refers to (even) number of poles of the IM. In fact, a squirrel cage IM can be visualized as a transformer with moving secondary windings. In this special configuration, the secondary (rotor) windings are short-circuited by its design.

In electrical machinery literature, the steady-state analysis of IM is often times performed using per-phase equivalent circuit as shown in the Fig. B.3. This well-known single phase circuit represents the balanced operation for a three-phase machine. In fact, the circuit ingeniously combines the stator- and rotor circuitries, which are excited at different frequencies.

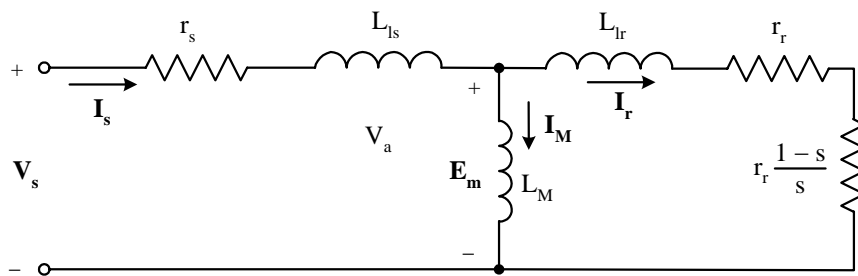


Fig. B.3 Per-phase equivalent circuit of an induction machine.

Here, the electrical power supplied at the stator terminal is converted to magnetic power where r_s and L_{ls} denote the equivalent resistance and the leakage inductance of the stator winding respectively. Notice that L_m (a.k.a. the magnetizing inductance) represents the mutual magnetic coupling between the rotor- and stator windings and simply accounts for the transfer of power across the air gap. In fact, the voltage across the magnetizing inductance is often times called the stator-induced back-EMF per phase. In this circuitry, the slip-dependent equivalent resistance in the rotor stands for the mechanical power delivered at the shaft due to electro-mechanical power conversion. In this part of the circuitry, L_{lr} is the leakage rotor inductance as

reflected to the stator side. Similarly, r_r is the equivalent rotor resistance referred to stator. Hence, the torque developed by the motor can be expressed as

$$T_m = \frac{3P}{2} |I_r|^2 \frac{r_r}{s \omega_e} \quad (\text{B.9})$$

Although the per-phase equivalent does not entirely characterize the dynamics of the motor, it provides a basic understanding of the machine. In literature, a well-known model, which accurately captures not only the steady-state dynamics but also the transient one, is also available. Such a model (in synchronous dq reference frame) could be given as

$$v_{qs}^e = r_s i_{qs}^e + \frac{d\lambda_{qs}^e}{dt} + \omega_e \lambda_{ds}^e \quad (\text{B.10})$$

$$v_{ds}^e = r_s i_{ds}^e + \frac{d\lambda_{ds}^e}{dt} - \omega_e \lambda_{qs}^e \quad (\text{B.11})$$

$$0 = r_r i_{qr}^e + \frac{d\lambda_{qr}^e}{dt} + (\omega_e - \omega_r) \lambda_{dr}^e \quad (\text{B.12})$$

$$0 = r_r i_{dr}^e + \frac{d\lambda_{dr}^e}{dt} - (\omega_e - \omega_r) \lambda_{qr}^e \quad (\text{B.13})$$

where the flux linkage equations are

$$\lambda_{qs}^e = L_{ls} i_{qs}^e + L_m (i_{qs}^e + i_{qr}^e) \quad (\text{B.14})$$

$$\lambda_{ds}^e = L_{ls} i_{ds}^e + L_m (i_{ds}^e + i_{dr}^e) \quad (\text{B.15})$$

$$\lambda_{qr}^e = L_{lr} i_{qr}^e + L_m (i_{qr}^e + i_{qs}^e) \quad (\text{B.16})$$

$$\lambda_{dr}^e = L_{lr} i_{dr}^e + L_m (i_{dr}^e + i_{ds}^e) \quad (\text{B.17})$$

The developed (air gap) torque becomes

$$T_m = \frac{3P}{4} (\lambda_{dr}^e i_{qs}^e - \lambda_{qr}^e i_{ds}^e) \quad (\text{B.18})$$

Note that in dq model of the machine, the actual three-phase machine is transformed into an equivalent two-phase one provided that the windings of the motor are distributed symmetrically and that the actual machine is operated in a balanced fashion. Thus, all physical motor states (such as currents, voltages, flux linkages,

etc.) can be represented in this virtual motor with two phases: direct (d) and quadrature (q). Hence, the corresponding windings of this machine are 90° apart.

B.1.3 Synchronous Machines

Synchronous machines are commonly used in servo-drive applications such as computer peripheral equipment, robotics, CNC machine tools, home appliances, medical equipment etc. For low power applications up to a few kW, permanent magnet synchronous machines are on their way to replace all conventional DC motors. Synchronous motors with wound rotor field are suitable candidates for some HEV applications.

A synchronous machine with wound rotor constitutes two windings: rotor and stator windings. Just like the IM, the three-phase stator windings of a synchronous machine have a sinusoidal distribution in the stator slots. When the stator is supplied with a set of balanced three phase currents, whose frequency is to be controlled by electronic means; a constant amplitude flux rotating at the synchronous speed is produced in the air gap. On the other hand, the field winding on the rotor produces a field flux. Thus, the torque is produced as an interaction between the **magneto-motive-forces** (MMFs) created by these two windings. The developed torque is maximized when the magnetic axis of the rotor field and the corresponding axis of the stator field are mutually orthogonal.

Notice that to excite the rotor windings, the slip rings are needed. Hence, just like conventional DC motors, some wear and tear is unavoidable during the operation of the machine. To avoid slip ring, low power synchronous machines rely on strong permanent magnets to generate the rotor field. Notice that permanent magnet machines can be classified into two categories:

- Permanent Magnet Synchronous Machines with Trapezoidal Windings
- Permanent Magnet Synchronous Machines with Sinusoidal Windings

The descriptions of the machines follow.

B.1.3.1 Permanent Magnet Synchronous Machines with Trapezoidal Windings

These machines are also known as *electronically commutated machines*. Due to concentrated stator windings, the induced (i.e. back EMF) voltages in these machines are trapezoidal in nature. The reason behind the popularity of these machines is the simplicity of control. Only six discrete rotor positions per (electrical) revolution are needed in a three-phase machine to lock the phase of stator currents to those of the back EMF voltage waveforms for effective torque modulation. A set of three Hall-effect sensors, which are placed on the stator 120° apart, face the magnet wheel attached onto the rotor. Hence, they provide information on the orientation of the rotor's magnetic field. Thus, the controller excites the stator windings so that both magnetic fields are mutually orthogonal to each other to produce the highest torque possible. Since the motor, which is controlled via this "electronic commutation" scheme, resembles a conventional DC motor turned inside out, the motor system is also known as brushless DC motor in industry. Note that this control scheme eliminates the need for high-resolution encoder or position sensor required in PMSM with sinusoidal windings. But, the penalty paid in return is in performance. For HEV applications, a high resolution encoder may be necessary for phase advancing at high speeds.

B.1.3.2 Permanent Magnet Synchronous Machines with Sinusoidal Windings

The permanent magnet synchronous machine has a stator with a set of three phase windings similar to those of an IM. A balanced set of applied three-phase voltages create sinusoidal currents in the stator windings which in turn establish a rotating magnetic field across the air gap. The stator currents are regulated using rotor position feedback so that the currents are always in phase with the orientation of the rotor field.

The rotor of the machine constitutes a bunch of permanent magnets which are appropriately designed to yield a sinusoidal rotor flux linkage. There are two common rotor arrangements in literature:

1. Rotor with surface mounted magnets
2. Rotor with buried magnets.

The dq model of a PMSM with sinusoidal windings (in rotor reference frame) is well known in electrical machinery literature and will be given here for sake of discussion. The voltage equations of the machine are

$$v_{qs}^r = r_s i_{qs}^r + \frac{d\lambda_{qs}^r}{dt} + \omega_r \lambda_{ds}^r \quad (\text{B.19})$$

$$v_{ds}^r = r_s i_{ds}^r + \frac{d\lambda_{ds}^r}{dt} - \omega_r \lambda_{qs}^r \quad (\text{B.20})$$

where the relevant flux linkage equations are

$$\lambda_{qs}^r = L_{ls} i_{qs}^r + L_{mq} i_{qs}^r = L_q i_{qs}^r \quad (\text{B.21})$$

$$\lambda_{ds}^r = L_{ls} i_{ds}^r + L_{md} i_{ds}^r + \lambda_f = L_d i_{ds}^r + \lambda_f \quad (\text{B.22})$$

where λ_f corresponds to the constant field flux provided by the permanent magnets. Depending on the design of the rotor, the inductances in the d and q axis may not be the same. Hence, the developed (air gap) torque becomes

$$T_m = \frac{3P}{4} (\lambda_{ds}^r i_{qs}^r - \lambda_{qs}^r i_{ds}^r) \quad (\text{B.23})$$

$$T_m = \frac{3P}{4} [\lambda_f i_{qs}^r + (L_d - L_q) i_{qs}^r i_{ds}^r] \quad (\text{B.24})$$

It is critical to note that in the model above, the damper windings (or damper cage) are not present.

B.2 Motor Drives for HEV Applications

A motor drive consists of a power electronics converter and its controller as illustrated in Fig. B.4. The converter is composed of fast-acting solid-state switching devices and handles the power flow between the battery and the motor. The digital controller processes the command input and the feedback information to generate the switching signals for the power converter switches.

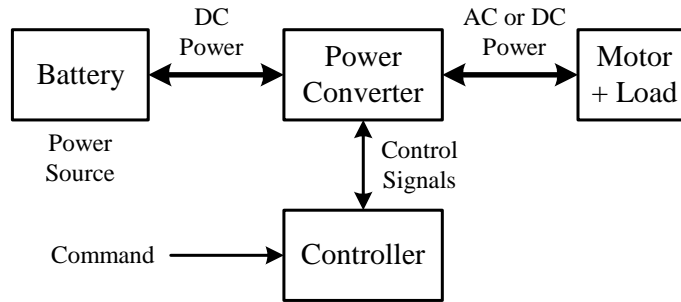


Fig. B.4 Motor drive topology for HEVs.

A modern power converter often times employs a DC voltage source to generate the power (AC or DC) required by the motor. The solid-state devices in a certain converter topology basically function as on/off electronic switches to convert this fixed DC supply voltage (or so called DC bus voltage) to a variable voltage and variable frequency supply. All switching devices have a control terminal so that they can be turned on and off at will according to the command generated by the controller. Fig. B.5 illustrates typical motor driver topologies.

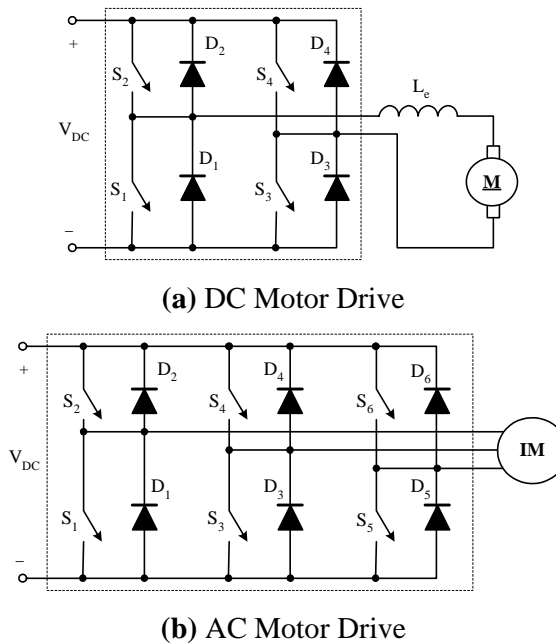


Fig. B.5 Typical motor driver topologies.

B.3 Control of Electrical Machinery

As mentioned in previous section, a modern electrical drive system constitutes a current controlled voltage source inverter. With the utilization of appropriate switching sequences (i.e. commands to the switching devices), the controller can generate any desired voltage waveform across the terminals of the motor.

In contemporary drive systems, the switching frequency is quite high ranging between 20 kHz up to 1 MHz in extreme cases. Hence, the average bandwidth of a modest switch mode inverter is on the order of 10 to 50 kHz. Such high bandwidth frequencies often times yields excellent current (torque) control performance. The following sections discuss the torque control on electrical machinery using switched mode inverters.

B.3.1 Torque Control of Conventional DC Motor

If compared to electronically commutated motors, the torque control of a conventional DC motor is relatively simple owing to the fact that the armature mechanical assembly intrinsically guarantees the maximum torque generation by maintaining the orthogonality between the field flux and the armature MMF.

As indicated by Equation (B.6), the torque produced by the machine is proportional to its armature current if the field flux is held constant. Fig. B.6 shows the torque modulation scheme for a typical DC motor drive. In this configuration, the desired motor torque (T_m^*) is first converted to the corresponding armature current (i_a^*), which is then applied to the current regulator as a command. The current regulator, which is usually a P or PI type analog controller, calculates the deviation of the actual armature current from the reference value and generates a correction signal to the pulse width modulator. The modulator then produces a sequence of switching signals for the converter (a.k.a. the H bridge). Finally, a voltage waveform, which yields the desired armature current, is generated.

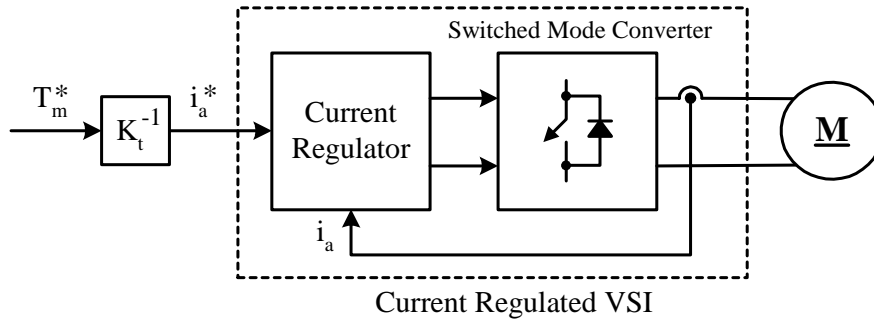


Fig. B.6 Conventional DC servo motor drive.

Similarly, the block diagram of a conventional DC servo-motor drive is illustrated in Fig. B.7. Since the bandwidth of a switched-mode converter (a.k.a. “power amplifier”) is extremely high (a few hundred kHz), it is ideally modeled as a simple gain which in turn implies an amplifier with infinite bandwidth. The current regulator used in this topology is proportional (P) controller. However, PI regulators (with back EMF compensation) are also utilized in advanced drive systems. Notice that in practice, the current regulator along with power amplifier must have a current- and a voltage limiter to protect the motor drive. For the sake of clarity, such nonlinearities are not shown in the diagram.

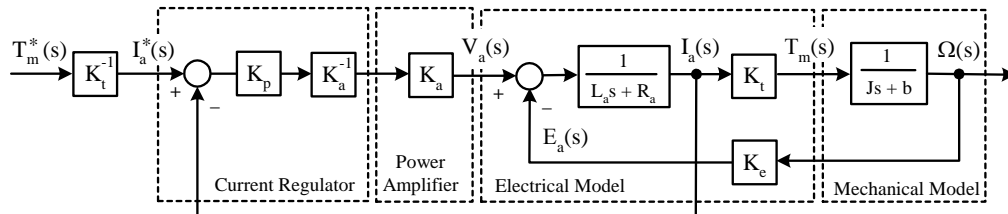


Fig. B.7 Block diagram of a conventional DC servo-motor drive.

B.3.2 Torque Control of Induction Machines

For effective torque modulation, the action of the commutator of a DC machine can be emulated in induction machine drive by orienting the stator current with respect to the rotor flux so as to attain independently controlled flux and torque.

A basic understanding of how this can be accomplished could be attained from the dq model of an induction machine given in the previous section. For the sake of simplicity, the reference frame is chosen as the rotor flux oriented reference frame so that the frame is assumed to be rotating at the speed of the rotor flux vector (ω_{rf}). Hence, the dq model in synchronous frame can be directly utilized by substituting ω_{rf} into the synchronous speed ω_e . In this new reference frame, if λ_{qr}^{rf} is set as 0, the torque equation (B.18) becomes

$$T_m = \frac{3P}{4} \lambda_{dr}^{rf} i_{qs}^{rf} \quad (\text{B.25})$$

The similarity between this expression and the DC motor torque expression (B.4) is quite apparent. When λ_{dr}^{rf} is held constant, the instantaneous control of the q-axis control in the rotor flux oriented reference frame will yield instantaneous response in the motor torque. Since current regulators of modern electrical machines have very high bandwidth frequencies, such operation can be conveniently carried out. Consequently, the rotor voltage and current equations in the rotor flux oriented reference frame take the following form:

$$0 = r_r i_{qr}^{rf} + (\omega_{rf} - \omega_r) \lambda_{dr}^{rf} \quad (\text{B.26})$$

$$0 = r_r i_{dr}^{rf} + \frac{d\lambda_{dr}^{rf}}{dt} \quad (\text{B.27})$$

and the flux linkage equations are

$$\lambda_{qr}^{rf} = L_{lr} i_{qr}^{rf} + L_m (i_{qr}^{rf} + i_{qs}^{rf}) = L_r i_{qr}^{rf} + L_m i_{qs}^{rf} \cong 0 \quad (\text{B.28})$$

$$\lambda_{dr}^{rf} = L_{lr} i_{dr}^{rf} + L_m (i_{dr}^{rf} + i_{ds}^{rf}) = L_r i_{dr}^{rf} + L_m i_{ds}^{rf} \quad (\text{B.29})$$

Hence, from (B.28),

$$i_{qr}^{rf} = -\frac{L_m}{L_r} i_{qs}^{rf} \quad (\text{B.30})$$

A slip relationship can be established using (B.28) as

$$(\omega_{rf} - \omega_r) = s\omega_{rf} = -\frac{r_r}{\lambda_{dr}^{rf}} i_{qr}^{rf} \quad (\text{B.31})$$

Substituting (B.30) into (B.31) yields

$$s\omega_{rf} = \frac{r_r}{L_r} \frac{L_m i_{qs}^{rf}}{\lambda_{dr}^{rf}} \quad (\text{B.32})$$

Combining (B.27) and (B.29) gives

$$\lambda_{dr}^{rf} = \frac{r_r L_m}{r_r + L_r D} i_{ds}^{rf} \quad (\text{B.33})$$

where D corresponds to d/dt operator. Similarly, when (B.33) is substituted in (B.27), we get

$$i_{dr}^{rf} = \frac{L_m D}{r_r + L_r D} i_{ds}^{rf} \quad (\text{B.34})$$

Note that i_{dr}^{rf} exists only when i_{ds}^{rf} changes and is zero in steady state. Similarly, in steady state, the rotor flux boils down to

$$\lambda_{dr}^{rf} = L_m i_{ds}^{rf} \quad (\text{B.35})$$

Fig. B.8 illustrates an implementation of an indirect field oriented IM drive. In this topology, the slip calculation employs (B.33), (B.34), and (B.31) expressions to calculate slip command $s\omega_{rf}^*$. The slip command is integrated once to calculate the change in the rotor flux position. The flux and torque commands are generally computed by taking into account the torque capability of the machine.

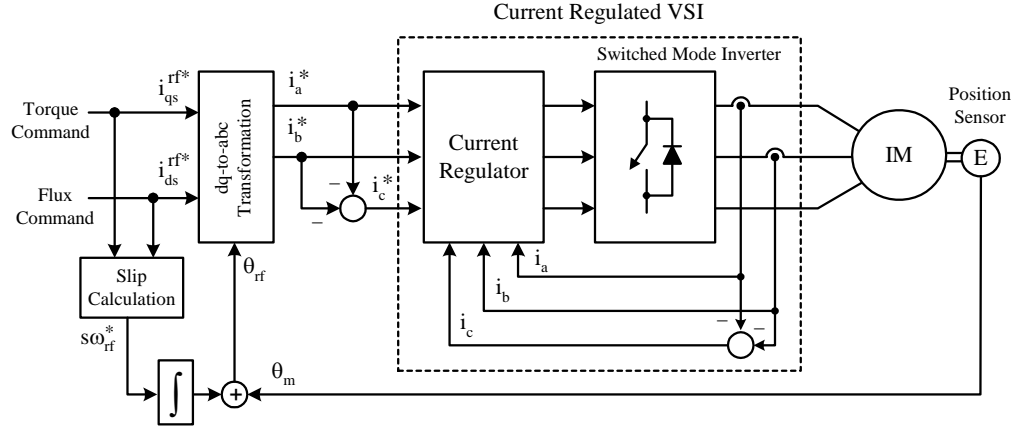


Fig. B.8 Indirect field oriented induction motor drive.

B.3.3 Torque Control of PMSM with Sinusoidal Windings

As discussed in Section B.1.3, the torque developed by PMSM is given by (*). It is obvious that to maximize the torque production of the motor, the direct axis current in the rotor reference frame (i_{ds}^r) has to be set 0. Hence, the corresponding torque equation takes the following form:

$$T_m = \frac{3P}{4} [\lambda_f i_{qs}^r] = \frac{3P\lambda_f}{4} i_{qs}^r = K_t i_{qs}^r \quad (\text{B.36})$$

where K_t is referred to as the motor torque constant. Consequently, in terms of desired motor torque (T_m^*), the corresponding currents in rotor reference frame can be calculated as

$$i_{qs}^{r*} = K_t^{-1} T_m^* \quad (\text{B.37})$$

$$i_{ds}^{r*} = 0 \quad (\text{B.38})$$

The currents expressed in direct and quadrature axes could be transformed into the desired phase currents via Park's equations:

$$\begin{bmatrix} i_a^* \\ i_b^* \\ i_c^* \end{bmatrix} = \begin{bmatrix} \cos(\theta) & \sin(\theta) & 1 \\ \cos(\theta - 120^\circ) & \sin(\theta - 120^\circ) & 1 \\ \cos(\theta - 240^\circ) & \sin(\theta - 240^\circ) & 1 \end{bmatrix} \cdot \begin{bmatrix} i_{qs}^{r*} \\ i_{ds}^{r*} \\ 0 \end{bmatrix} \quad (\text{B.39})$$

Hence,

$$i_a^* = (K_t^{-1} T_m^*) \cos(\theta) \quad (\text{B.40})$$

$$i_b^* = (K_t^{-1} T_m^*) \cos(\theta - 120^\circ) \quad (\text{B.41})$$

$$i_c^* = (K_t^{-1} T_m^*) \cos(\theta - 240^\circ) \quad (\text{B.42})$$

where θ is the electrical angle of the rotor and could be calculated in terms of measured motor position θ_m as

$$\theta = \frac{P}{2} \theta_m \quad (\text{B.43})$$

Here, P refers to number of poles on the motor. Notice that for controlling PMSM, the rotor field position is to be measured by means of an absolute position sensor. The sensor must be initially aligned with the magnetic axis of phase a (or any other reference axis).

With the frequency of the stator currents “locked” to the rotor position, which is continuously measured, there is no possibility of losing synchronism and torque angle remains at its optimal value of 90° . Fig. B.9 shows the block diagram of a PMSM servo drive.

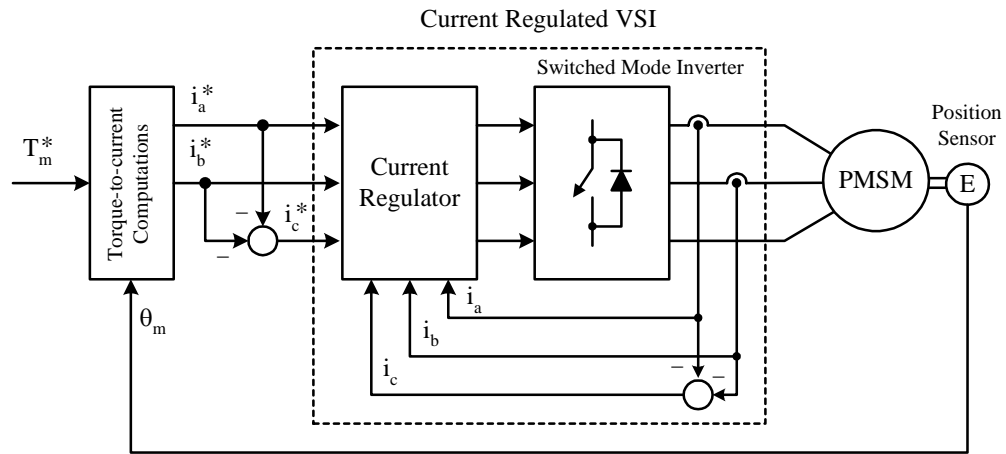


Fig. B.9 Synchronous motor servo drive.

In practice, the current controller dynamically maintains the desired current levels.

When $i_{ds}^r \cong i_{ds}^{r*} \cong 0$, Equations (B.21)-(B.22) boils down to

$$\lambda_{qs}^r = L_q i_{qs}^r \quad (\text{B.44})$$

$$\lambda_{ds}^r = \lambda_f \quad (\text{B.45})$$

Therefore, (B.19) becomes

$$v_{qs}^r = r_s i_{qs}^r + L_q \frac{di_{qs}^r}{dt} + \omega_r \lambda_f \quad (\text{B.46})$$

The electrical speed of rotor (ω_r) can be expressed in terms of motor speed (ω_m):

$$\omega_r = \frac{P}{2} \omega_m \quad (\text{B.47})$$

Hence, the block diagram of the resulting system is as shown in Fig. B.10. Here, the PMSM driver, not surprisingly, resembles a conventional DC servomotor system. Notice that the torque-to-current computations are eliminated for the sake of simplicity and therefore the current regulation is directly performed in the rotor dq reference frame.

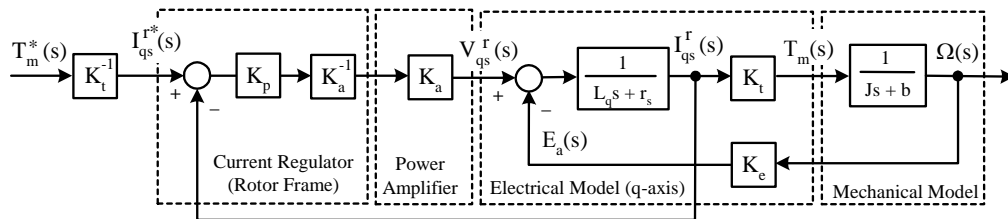


Fig. B.10 Block diagram of a PM synchronous motor drive.

APPENDIX C

DRIVING CYCLES

There exist several standardized driving cycles used by many professional societies including ECE, FUDS, SAE, etc. These driving cycles, which usually include common driving sequences encountered during city as well as highway cruising, are utilized to evaluate the driving performance of test (target) vehicle in this research study. In these driving cycles, many vehicle operating parameters such as emission, acoustic noise emission, fuel consumption, driving comfort, etc. are taken into consideration. In this study, the ECE 15 Urban Cycle (Economic Commission for Europe Test Cycle, Exhaust Emission) is employed. This cycle is an urban driving cycle, also known as UDC and mainly used for the emission certification of light duty vehicles in Europe [EEC Directive 90/C81/01] and represents the city driving conditions. The cycle's velocity profile is shown in the Fig C.1 [52].

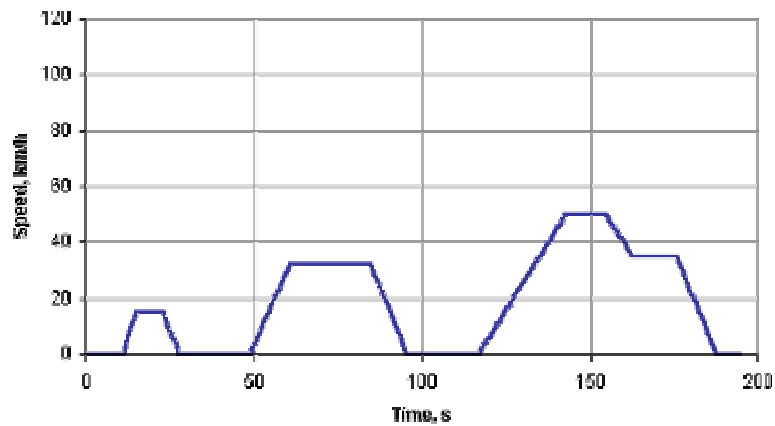


Fig. C.1 ECE 15 Urban Cycle [52].

It should be noted that the ECE-15 Urban Cycle constitutes the following parts:

- Acceleration
- Driving at constant speed
- Deceleration to the full stop
- Deceleration to lower speed
- Idle engine operation

The intervals in that cycle are as follows:

- Idling period [14 s]
- Acceleration up to 15 [km/h] [6 s]
- Constant Speed at 15 [km/h] [8 s]
- Deceleration until stopping [4 s]
- Idling period [32 s]
- Acceleration up to 30 [km/h] [10 s]
- Constant Speed at 30 [km/h] [8 s]
- Deceleration until stopping [6 s]
- Idling period [32 s]
- Acceleration up to 50 [km/h] [22 s]
- Constant Speed at 50 [km/h] [12 s]
- Deceleration until 30 [km/h] [8 s]
- Constant Speed at 30 [km/h] [12 s]
- Deceleration until stopping [12 s]
- Idling period [14 s]

The highway cycle utilized in the study is a high acceleration and deceleration demanding cycle as shown in Fig. C.2.

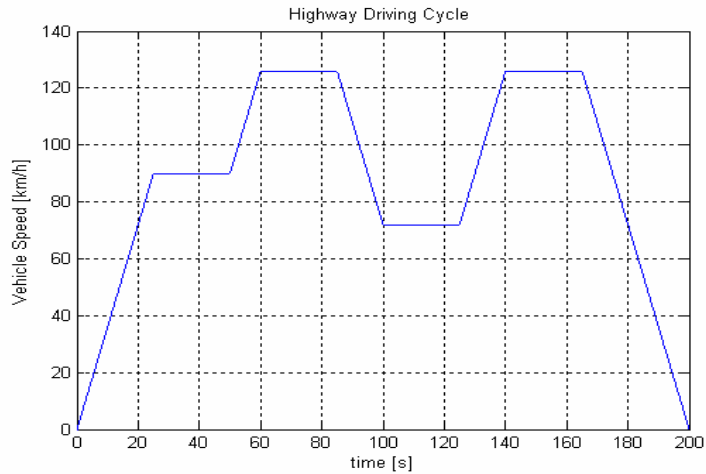


Fig. C.2 Highway Driving Cycle.

Notice that for homologation issues of Ford vehicles, EUDC, which is also called as New European Drive Cycle (NEDC), is utilized. Besides it represents the characteristics of both urban and highway by adding a segment after the fourth ECE cycle to evaluate more aggressive, high speed driving modes. Hence, EUDC is found to be appropriate in order to simulate the HEVs with smart power manager in mixed cruising mode. The maximum speed of the EUDC cycle is 120 km/h as seen if Fig C.3.

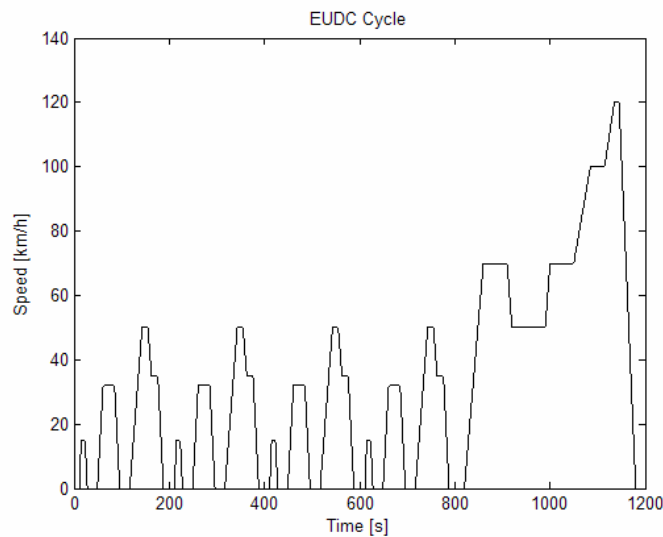


Fig. C.3 Speed of the vehicle in EUDC.